University of North Dakota
UND Scholarly Commons

Theses and Dissertations | Theses, Dissertations, and Senior Projects

January 2016

Design And Implementation Of Co-Operative Control Strategy For Hybrid AC/DC Microgrids

Rasel Mahmud

Follow this and additional works at: https://commons.und.edu/theses

Recommended Citation
Mahmud, Rasel, "Design And Implementation Of Co-Operative Control Strategy For Hybrid AC/DC Microgrids" (2016). *Theses and Dissertations*. 2041.
https://commons.und.edu/theses/2041

This Thesis is brought to you for free and open access by the Theses, Dissertations, and Senior Projects at UND Scholarly Commons. It has been accepted for inclusion in Theses and Dissertations by an authorized administrator of UND Scholarly Commons. For more information, please contact zeineb.yousif@library.und.edu.

www.manaraa.com

DESIGN AND IMPLEMENTATION OF CO-OPERATIVE CONTROL STRATEGY FOR HYBRID AC/DC MICROGRIDS

by

Rasel Mahmud

A Thesis
Submitted to the Graduate Faculty

of the

University of North Dakota

in partial fulfillment of the requirements

for the degree of

Master of Science

Grand Forks, North Dakota

August

2016

www.manaraa.com

This thesis, submitted by Rasel Mahmud in partial fulfillment of the requirements for the Degree of Master of Science from the University of North Dakota, has been read by the Faculty Advisory Committee under whom the work has been done and is hereby approved.

Arash Nejadpak, Chairperson

Hossein Salehfar

Reza Fazel-Rezai

Prakash Ranganathan

Ali Sarikhani

This thesis is being submitted by the appointed advisory committee as having met all of the requirements of the School of Graduate Studies at the University of North Dakota and is hereby approved.

Dr. Grant McGimpsey
Dean of the School of Graduate Studies

July 19, 2016
Date

PERMISSION

Title Design and implementation of co-operative control strategy for hybrid AC/DC microgrids

Department Electrical Engineering

Degree Master of Science

In presenting this thesis in partial fulfillment of the requirements for a graduate degree from the University of North Dakota, I agree that the library of this University shall make it freely available for inspection. I further agree that permission for extensive copying for scholarly purposes may be granted by the professor who supervised my thesis work or, in his absence, by the chairperson of the department or the dean of the Graduate School. It is understood that any copying or publication or other use of this thesis or part thereof for financial gain shall not be allowed without my written permission. It is also understood that due recognition shall be given to me and to the University of North Dakota in any scholarly use which may be made of any material in my thesis.

Signature Paul

Date 07/20/2016

TABLE OF CONTENTS

www.manaraa.com

www.manaraa.com

www.manaraa.com

www.manaraa.com

LIST OF FIGURES

www.manaraa.com

www.manaraa.com

www.manaraa.com

ACKNOWLEDGEMENTS

I would like to thank my thesis advisor, Dr. Arash Nejadpak, for his guidance, generous support, and patience over the course of the last two years. I would also like to thank Dr. Hossein Salehfer, Dr. Reza Fazel-Rezai, Dr. Prakash Ranganathan and Dr. Ali Sarikhani for serving as my thesis committee members.

Special thanks to my wife, parents, sister and brother for their continuous support patience, and encouragement.

www.manaraa.com

ABBREVIATIONS

AC	Alternating Current
ADC	Analog-to-digital converter
CSI	Current source inverters
DC	Direct Current
DCC	Distributed cooperative control
DER	Distributed energy resource
DG	Distributed generator
DNO	Distribution Network Operator
DR	Demand Response
ECU	Electronic control unit
EMS	Energy management system
EPLL	Enhanced phase-locked-loop
EPS	Electric power system
ESS	Energy storage systems
GUI	Graphical user interface
IC	Interfacing converter
MAS	Multi Agent System

www.manaraa.com

MPPT	Maximum Power Point Tracking
PCC	Point of common coupling
PERL	Power Electronics Research Laboratory
PEV	Plug-in-electric-vehicle
PHIL	Power hardware-in-the-loop
PI	Proportional-Integral
PLL	Phase-locked-loop
P-MG	PERL Microgrid
PSC	Post synchronization controller
PV	Photo-voltaic
PWM	Pulse-width-modulation
RAF	Running average filter
RES	Renewable energy source
SITL	System-in-the-loop
SoC	State-of-charge
STS	Static transfer switch
SU	Synchronizer unit
VSC	Voltage source converter

www.manaraa.com

VSI Voltage source converters

www.manaraa.com

ABSTRACT

This thesis is mainly divided in two major sections: 1) Modelling and control of AC microgrid, DC microgrid, Hybrid AC/DC microgrid using distributed co-operative control, and 2) Development of a four bus laboratory prototype of an AC microgrid system. At first, a distributed cooperative control (DCC) for a DC microgrid considering the state-of-charge (SoC) of the batteries in a typical plug-in-electric-vehicle (PEV) is developed. In DC microgrids, this methodology is developed to assist the load sharing amongst the distributed generation units (DGs), according to their ratings with improved voltage regulation. Subsequently, a DCC based control algorithm for AC microgrid is also investigated to improve the performance of AC microgrid in terms of power sharing among the DGs, voltage regulation and frequency deviation. The results validate the advantages of the proposed methodology as compared to traditional droop control of AC microgrid. The DCC-based control methodology for AC microgrid and DC microgrid are further expanded to develop a DCC-based power management algorithm for hybrid AC/DC microgrid. The developed algorithm for hybrid microgrid controls the power flow through the interfacing converter (IC) between the AC and DC microgrids. This will facilitate the power sharing between the DGs according to their power ratings. Moreover, it enables the fixed scheduled power delivery at different operating conditions, while maintaining good voltage regulation and improved frequency profile.

The second section provides a detailed explanation and step-by-step design and development of an AC/DC microgrid testbed. Controllers for the three-phase inverters are designed and tested on different generation units along with their corresponding inductor-capacitor-inductor (LCL) filters to eliminate the switching frequency harmonics. Electric

www.manaraa.com

power distribution line models are developed to form the microgrid network topology. Voltage and current sensors are placed in the proper positions to achieve a full visibility over the microgrid. A running average filter (RAF) based enhanced phase-locked-loop (EPLL) is designed and implemented to extract frequency and phase angle information. A PLL-based synchronizing scheme is also developed to synchronize the DGs to the microgrid. The developed laboratory prototype runs on dSpace platform for real time data acquisition, communication and controller implementation.

www.manaraa.com

Chapter 1

Introduction

A microgrid is a small scale electrical power distribution network which includes a number of distributed generations (DGs), energy storage systems (ESS) serving the local loads. The microgrid can be operated in grid-tied mode or islanded mode depending on the emergency conditions or the planned islanding of the microgrid. Examples of microgrid applications are university campuses, remote island communities, residential complexes, and industrial or commercial facilities. Microgrids are ideal candidates for integrating renewable energy sources (RES) and DGs in power distribution network by minimizing the impact of the stochastic nature of DGs and RESs, such as photovoltaic, and wind energy through effective control strategies [1]-[2]. Other pertinent benefits of the microgrids are reduced transmission and distribution costs, greater reliability, and lower energy losses. Several advantages of DC microgrids over AC microgrids have been reported in the literature in terms of power availability [3]-[4], and loss reduction [5]. Issues of AC power systems such as synchronizations, reactive power flow, and frequency control are not present in DC microgrids [6]. However, AC power systems have matured protection system and standards which DC microgrids lack [7]. In order to take advantage of both of the systems, hybrid microgrids, combining AC and DC microgrids, have been proposed in many research papers [8]–[11].

www.manaraa.com

The presence of different energy sources and ESS with diverse dynamic properties with varied electrical and mechanical properties in microgrids has raised the concerns of safety, efficiency and stability of the system. The operation and control of microgrids become more crucial in islanded mode of operation when there is no support from the utility. The concentration of this work includes the islanded mode of operation and control of AC microgrid, DC microgrid, hybrid AC/DC microgrid and development of a microgrid laboratory prototype testbed.

1.1 Research Objectives and Methodology

This thesis examines the modeling and designing the control of AC/DC microgrids. This work investigates the possibility of improving the voltage profile of both for AC and DC microgrids and the frequency profile (AC microgrid) in steady-state islanded mode of operation while providing accurate control over the power sharing among the DGs connected to the microgrids. The operation of microgrids is further explored in this thesis by developing ***a laboratory prototype of AC/DC microgrid testbed***.

The first objective of this thesis is to investigate the operation of a DC microgrid comprising several DGs connected to the system through DC-DC converters. The conventional method of DC microgrid operation is droop-based where output voltage of each of the DC-DC converters is proportional to the output power of the converter. Though this approach is very simple in operation, the voltage regulation of the microgrid is very poor and power sharing among the converters is not accurate if droop-based control is employed. In order to overcome these issues, a distributed co-operative control

www.manaraa.com

(DCC) strategy is proposed and developed where each DC-DC converter is provided with information from its neighboring converters to improve and properly regulate its output voltage. Specifically, the proposed DCC augments the droop-based control by using the information from the neighboring DGs to improve the voltage regulation of the microgrid and provides accurate power sharing between the converters. The operation of the proposed DCC strategy is extended to include the dynamic behavior of battery charging and discharging of plug-in-electric–vehicles (PEVs). A distributed energy management system (EMS) is also developed for the charging/discharging of PEVs in a DC microgrid.

Currently droop-based control is also mostly used to control the voltage and frequency of the AC microgrids in islanded mode of operation. However, droop controlled AC microgrids also suffer from problems, including poor voltage regulation, large deviation of frequency from nominal value, and poor real power and reactive power sharing. To address these issues, a DCC strategy for the AC microgrid is also investigated in this thesis. Using an estimated average voltage value, delivered real power and reactive power normalized with respect to rated values from the neighboring DGs in an AC microgrid, the controller updates the reference values of voltage and frequency of its own DG to achieve good voltage and frequency profiles while maintaining accurate real power and reactive power sharing.

Hybrid AC/DC microgrids will be the most efficient way to integrate DC and AC energy sources/load in future smart grid architecture. Though power management of individual AC microgrids and DC microgrids has been extensively studied, power management of hybrid AC/DC microgrids has not yet received that much of attention.As

www.manaraa.com

such different modes of operation of AC/DC hybrid microgrids, and power management control strategies for hybrid microgrids using DCC are also investigated in this thesis. Most of the power management strategies for hybrid AC/DC microgrids found in the literature are droop based which exhibit the inherent problems of droop-based controls such as poor voltage regulation and inaccurate power sharing. A DCC-based power management scheme for hybrid microgrid under different mode of operation is proposed and developed in this thesis.

Power electronic interfaced DGs are the main constituents of AC microgrids. That is why the operation and control strategies for AC microgrids are not the same as the conventional AC power systems. Before the control methods are implemented in a real microgrid serving critical loads, they have to be first tested in laboratory based microgrid prototypes in order to ensure their reliability and dependability. One of the major objectives of this thesis is to design and develop a four-bus ***AC/DC microgrid testbed***. Each of the hardware, software, and communication components of the laboratory prototype are designed, built, analyzed, verified and implemented at the Power Electronics Research Laboratory (PERL) at University of North Dakota. Finally, the microgrid testbed is tested under different network topologies and load variations for dynamic and steady-state performance evaluation purposes.

1.2 Outline of the Thesis

The contents of the remaining chapters of the thesis are briefly discussed in this section.

www.manaraa.com

Chapter 2 provides the literature survey on microgrid that are relevant to the investigations carried out in this thesis. The literature survey is broken down into four groups discussing previous works, developments and researches on control strategy for DC microgrids, AC microgrids in islanded mode of operation, control strategy for AC/DC hybrid microgrid power management, and microgrid laboratory prototype developments.

Chapter 3 briefly discusses graph theory which provides the basic mathematical foundation for the DCC based control strategy. The communication graph required for implementing the proposed DCC for DC microgrid is presented in this chapter. Using this communication graph, the development of DCC for DC microgrid is discussed in the next section. Using an optimum control strategy, the State-of-Charge (SoC) of the batteries of PEVs connected to the DC microgrid is analyzed. Furthermore, an energy management system (EMS) for the DC microgrid with PEVs is also presented. The chapter finally includes simulation results to verify the effectiveness of the developed SoC based DCC for the DC microgrid.

Chapter 4 starts with a detailed mathematical model of the AC microgrid and lays the foundation for development of the DCC for AC microgrid. Using the graph theory presented in chapter 3, a communication graph for AC microgrid is developed. DCC for AC microgrid is developed where voltage and frequency references are updated by employing the communication graph for information sharing from neighboring DGs. The performance improvement in terms of voltage profile, frequency profile, and power sharing are demonstrated through simulation at the end of this chapter.

www.manaraa.com

Chapter 5 discusses the different mode of operation and power management strategies for hybrid AC/DC microgrid. The DCC strategy developed for AC and DC microgrids in the previous chapters are investigated to achieve power flow control in AC/DC hybrid microgrids. A DCC based power management control strategy is proposed in this chapter for hybrid AC/DC microgrids. The proposed method is verified through simulation under different operating conditions at the end of this chapter.

Chapter 6 presents the design, development, validation and operation of the microgrid laboratory testbed at PERL, UND. The chapter first elaborates on the design procedures of hardware components such as power supplies, power electronic converters, filters, distribution line models, load models, and the real-time data communication platform used in the laboratory testbed. It then discusses the microgrid software architecture, microgrid power network architecture and microgrid control architecture. Design of the phase-locked-loop (PLL) used for synchronization and inverter control is discussed in this chapter.

Chapter 7 analyzes the experimental data obtained from the laboratory testbed under varying load conditions and topology changes.

Chapter 8 concludes the thesis with an overall discussion about the methods and results obtained through simulations and experiments. This chapter also recommends some future research areas on microgrids that can improve the works done so far at the PERL, UND.

www.manaraa.com

Chapter 2

Literature Review

2.1 Overview

The literatures reviews on microgrids operation, control, and prototype development surveyed during this thesis are briefly discussed in this chapter.

2.2 Microgrid operation and control

2.2.1 DC microgrid with PEV

Plug-in-electric-vehicles (PEVs), with their batteries, can store energy, making them one of the most common sources of distributed energy storage. In distributed storage, PEVs have the potentials to participate in both net metering or "vehicle-to-grid" (V2G) energy outflows, and demand response programs. With the introduction of Distributed Generation (DG) sources, microgrids are becoming a key concept in accommodation of these DGs and energy storage systems [12]. Microgrids are small scale power systems with generation, consumption, and storage all placed in a close physical vicinity [13]. To supply different kind of loads from renewable energy sources, it is necessary to have multiple AC-DC and DC-AC conversions which cause a significant energy wastage before end use [14]. Considering the fact that many of the emerging Renewable Energy Sources (RES), e.g., solar photovoltaics, fuel cells, and energy storage units, e.g.,

www.manaraa.com

batteries, hydrolysers, and ultra-capacitors, produce DC power, DC microgrids have been suggested to reduce cost and avoid redundant conversion stages [12]-[13], [15]. Aside from the great popularity of DC microgrids, the rapid development of Plug-in-Electric-Vehicle (PEV) technology is attracting much attention both in industrial and academic field [16]. In recent years, penetration of PEVs in the market has increased dramatically [17]. However, uncoordinated charging of these PEVs may have serious negative impacts, both technical and economical, on the Grid [18]-[19]. As distributed energy storage units, the batteries of PEVs can offer an attractive solution to the intermittent and random nature of the RESs. PEVs can also contribute significantly to the power flow controls, energy management, and maintaining power quality if the charging/discharging of PEV batteries are properly captured and coordinated [20].

A composite DC microgrid system may be connected to a number of DGs, ESSs, and other resources such as solar photovoltaic units, fuel cells, and PEVs along with local loads. Similar to the control of AC microgrids, hierarchical controls DC microgrid can be adopted with three layers of control, namely primary control, secondary control and tertiary control [12]-[13], [15], [21]. In the primary control, a virtual output-impedance regulates the converter output voltages to reduce the circulating current among parallel converters and reduces the difference between the scheduled power and the actual instantaneous actual power delivered by the converters. One of the drawbacks of primary control or droop control is that it has a poor voltage regulation, i.e., the converter output voltage deviates from the reference voltage. To compensate for this voltage deviation, a secondary controller restores the voltage of the converter to its reference level. The tertiary control regulates the power flow between the DC microgrid with other networks,

www.manaraa.com

such as, AC/DC distribution networks or AC/DC microgrids. The overall objectives of the hierarchical control are to ensure good voltage regulation and proportional load sharing (in per unit) among the converters.

Secondary and tertiary control of DC microgrids can be further categorized into two classes, centralized control structures [22], [23], [24] and decentralized control structures [25]. An energy control center (ECC) regulates the microgrid terminals using extensive communications in the centralized control structure. This type of system suffers heavily from reliability and scalability issues because a single communication link failure may result in the disruption of the microgrid operation. Decentralized control architecture itself may be of two forms, 1) local controller where only local information are used [26], and 2) distributed controller [27] where information from neighboring terminals are used to reach a global consensus which then eliminates the requirement of extensive communications between the central controller and microgrid terminals.

A fuzzy logic power flow controller was used in [19] to control the charging/discharging of PEV batteries in a workplace parking garage within a DC distribution system. Variations of DC link voltage in Photovoltaic (PV) generation systems was used in [28] to develop a smart PEV charging controller. However, both of these controllers are designed assuming grid connection and do not consider isolated microgrid operations. Using radial basis function network (RBFN) technique for forecasting PV generation, and Genetic Algorithm (GA) for the solution of optimization problem, a method for optimal integration of PEVs in microgrids was proposed in [20]. But this method requires a centralized control for Distribution Network Operators

www.manaraa.com

(DNOs). A distributed optimal charging rate control method of PEVs using Multi Agent System (MAS)-based framework and consensus algorithm was presented in [29], though it does not consider the case of PEV discharging. In [26], a double-quadrant state-of-charge (SoC) based droop control method for energy management system (EMS) of energy storage units (ESUs) is proposed. As this method uses only the local SoC estimation, generation capacity of the microgrid has no effect on the PEV battery charging rate.

2.2.2 Islanded mode of operation of AC microgrid

High penetration of renewable energy sources (RESs) into modern electric grid is expected to grow in near future [30] as an alternative to conventional power stations [31]. The concept of microgrid was introduced to accommodate these RESs into power system for better power quality and environment friendliness [32]. Most of the RESs are connected to the microgrid through power electronic converters [33]. The interfacing converters are parallel connected in a microgrid to integrate the RESs. Due to the parallel configuration of the converter connection, output power should be distributed among the converters based on the power ratings of the generation sources[30]. The control objectives of microgrid are almost same as conventional grid. Three objectives must be met for microgrid operation: 1) balance of instantaneous real power generation and demand, 2) frequency regulation & control of interchange power, and 3) generation economic dispatch. All of these objectives have to be met considering the constraints of DGs (generation limit) and power flow network. In a hierarchical control of AC microgrid, droop control acts as primary control and operates instantaneously to match

www.manaraa.com

real power generation and demand. Due to the close proximity of the generation and load in a microgrid, unlike conventional grid where the required reactive power has to be produced or consumed locally, reactive power can be shared by the converters according to the rating of the parallel converters. Droop control also takes care of reactive power sharing. The frequency and voltage are regulated in secondary control to minimize the deviations in these parameters caused by droop control. Another objective of the secondary control is to maintain a proper interchange of power among the DGs in a microgrid and with the utility. Tertiary control is responsible for the optimal generation dispatch in a microgrid to minimize generation cost and network power flow losses.

Droop/primary control is activated using only local information in both conventional grid and microgrid. In traditional grid, secondary and tertiary controls are realized through the centralized energy management System (EMS). However, there is no pre-established control architecture for microgrid. Methods for secondary and tertiary control of AC microgrid reported in literature can be classified into three groups: 1) centralized control [34], 2) Master-slave control [35], and 3) distributed control. Reliance on high speed communication channels for centralized and master-slave controls of AC microgrid lowers the system reliability and increases maintenance cost. With droop control only, decentralized control can be achieved but at the cost of reduced performance in terms of power quality. Hence droop based hierarchical distributed control can offer a much affordable solution with high reliability, low bandwidth and less complex communication networks and plug-play capabilities. With constrained information only from neighboring DGs and local measurements, distributed control architecture can achieve the same

www.manaraa.com

performance of centralized control without any knowledge of number, type or capabilities of other DGs in the microgrid or the communication network [36].

There is a significant effort in microgrid research community on designing control architectures for microgrid operation. A distributed control architecture has been proposed in [36] for frequency regulation and optimal dispatch. However, voltage regulation and power interchange have not been addressed in the paper. The power management strategies have been investigated in [37], and [38], though the strategies are based on centralized control. A distributed model predictive control (MPC) framework is presented in [39] for Automatic Generation Control (AGC) for large power systems, though it does not consider the special case of microgrids. A distributed control strategy for reactive power compensation has been considered in [40] while frequency regulation and power interchanged were not discussed. The status of different hierarchical structures of microgrid control systems has been reviewed in [41]. Effect of the communication delays in the secondary control for frequency regulation was studied in [42] for the stable operation of microgrid. To compensate the voltage unbalance in an islanded microgrid, hierarchical control scheme was proposed in [43] with centralized secondary control.

2.2.3 Power management of hybrid AC/DC microgrid

Though there are several benefits of DC microgrids over AC microgrids, AC system dominates the microgrid area due to the maturity of the technology of AC power systems. Recently the idea of integrating both of the AC and DC microgrids to form AC/DC hybrid microgrids in order to take advantage of both of the systems [44],[9] has drawn the attention of several researchers. A droop control based scheme is presented in [8] in

www.manaraa.com

order to ensure proportional power sharing among the AC sources and DC sources through interlinking converter. A decentralized control algorithm is proposed in [45] for an AC/DC/distributed storage (DS) hybrid microgrid. The authors in [45] realized the decentralized power control by local power sharing for individual AC or DC network, global power sharing for the entire microgrid and storage power sharing for the energy storage system. A two stage modified droop based method is investigated in [46] for the control of interfacing converters (IC) in an AC/DC hybrid microgrid. The controller takes the frequency information from the AC microgrid and voltage measurement from the DC microgrid to generate the power reference for the ICs using the proposed droop characteristics. Authors in [47] proposed an interlinking control scheme for hybrid AC/DC microgrid in order to share real power proportional to the rating of sources, not on the placement of sources. A nonlinear disturbance observer based DC-bus voltage control algorithm for a hybrid microgrid is discussed in [48] to eliminate the requirements of remote measurement with communication. However, this method only improves the transient performance without any contribution to the power management of an AC/DC microgrid.

2.3 Microgrid laboratory prototype development

Increased international awareness and strict regulations to reduce green-house gas emissions have prompted the research on RES integration in academia as well as industry. Microgrids are seen as ideal candidates to increase the RES participation in total energy consumption due to higher efficiency, economy, reliability and better utilization of the locally available energy sources as a result of the recent improvements in power

www.manaraa.com

electronic technology, control methodologies and the availability of fast communication networks. Researches on microgrids are mainly focused on 1) control 2) energy management and 3) microgrid protection [49]. However, a hardware-software integrated microgrid testbed is essential to verify the proposed methods and techniques coming out of these research initiatives.

Recently, a number of microgrid laboratory testbeds have been developed in several universities and research institutions with varying degree of complexities for educational and research purpose. The CERTS microgrid at Columbus, OH was developed to showcase the ease of small energy sources integration into microgrid [50]. The CERTS microgrid concept demonstrates the techniques of seamless transmission between grid-connected mode and islanded mode, microgrid protection and voltage and frequency stability with low-speed communication networks. The inverter-based Microgrid Research Laboratory (MGRL) with hierarchical control at Aalborg University, Denmark was designed to provide a platform for comprehensive studies on Microgrid [51]. An integrated microgrid laboratory system with multi-microgrid structure was presented in [52]. This microgrid was developed with master-slave control architecture and smaller microgrids within the system can form a larger microgrid and the system is capable of running in stand-alone mode or grid-connected mode. The Laboratory based-smart power system at Energy Systems Research Laboratory, Florida International University (FIU) includes implementation of control strategies implementation for generating stations and programmable loads in a laboratory scale with power rating up to 35KW ac power [53]. The smart power system at FIU is capable of conducting automated power system

www.manaraa.com

network operation and control in real-time. A highly flexible and reconfigurable microgrid testbed was reported in [54] which contains distributed generation units and energy storage systems. This microgrid testbed was used for research on microgrids and deriving guidelines for microgrid projects. The laboratory prototype at Applied Power Electronics Laboratory (APEL), IIT-Bombay for hierarchical and re-configurable microgrids has the capability of power network and control layer re-configuration [55]. The microgrid prototype is supported by a hybrid communication layer consisting of CAN, RS-485 and MODBUS protocols. The Microgrid testbed at the University of Texas at Arlington (UTA) uses off the shelf components and has an active control system based on national instruments for the operation of three smaller microgrids jointly or independently [56]. By combining Power hardware-in-the-loop (PHIL) and System-in-the-loop (SITL), the design and development of a hybrid reconfigurable microgrid testbed was described in [57]. In order to emulate different branches in microgrid, the authors in [57] used power electronic circuits, programmable sources, and loads as emulators. The microgrid testbed at Mount Holly, North Carolina by Duke Energy has capability of inter-operability achieved by sharing data among the devices by publish and subscribe message bus protocols via distributed intelligent platform (DIP) [58]. The University of Genoa Smart Polygeneration Microgrid (SPM) produces energy for the university with low emissions and is used for research on development for smart grid components [59]. The SmartGridLab, a lab scale smart grid testbed, uses the 802.15.4 wireless network to emulate the behavior of a smart grid [60].

www.manaraa.com

Chapter 3

DC microgrid with PEV

3.1 Overview

In this chapter, a SoC based distributed cooperative control (DCC) for the charging/discharging of PEV batteries and a distributed Energy Management System for a DC microgrid with PEV are introduced. Using only the information from neighboring DGs and PEVs, not only the PEVs can optimally balance their charging and discharging process, but also the DGs can share the load according to their ratings while keeping the microgrid voltage acceptably close to the reference voltage. By using distributed control, the requirement of centralized control has been eliminated which offers a higher reliability and scalability of the system. The distributed cooperative control of this work is adopted from [13] and is extended to include the management of PEVs charging/discharging based on SoC. The proposed method is computationally less demanding, hence can be used for real time operations in PEVs without the need of installing expensive computing resource.

www.manaraa.com

3.2 SoC Based Distributed Co-operative Control

3.2.1 Description of the microgrid

The configuration of an islanded DC microgrid with PEV is shown in Figure 3.1 where two DGs are connected with two PEVs and five loads through transmission lines. Under normal operation, the DGs would run in Maximum Power Point Tracking (MPPT), supplying the energy demand of PEV charging and loads. However, energy generation from renewable sources is highly intermittent and stochastic in nature and the loads may vary widely pushing the DGs to their maximum capacity. Energy stored in the PEV battery can be used to supply the additional demand from loads when the DGs are unable to supply the required power.

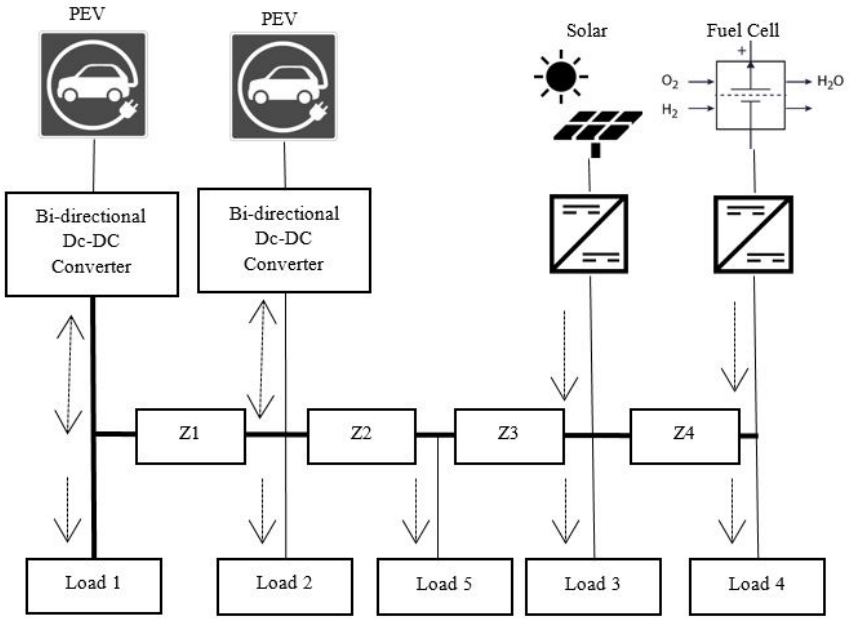

Figure 3.1: DC microgrid System layout with PEVs

www.manaraa.com

Whichever is supplying the energy demand, i.e., DGs, PEVs, the load has to be distributed according to the ratings of the energy suppliers to guarantee that none of them are overloaded. Additional care has to be taken for PEV batteries during charging and discharging process, as available energy from the batteries also depends on their SoC. To prevent the overuse and prolong the life of PEV batteries, SoC of each of the PEV batteries has to be balanced and a power equalization must be maintained during their charging and discharging process [26]. In the discharging mode of the PEVs, batteries with more SoC should supply more power than those with a lower SoC. A PEV disconnects from the microgrid when the SoC of its battery reaches the minimum acceptable limit and waits for a charging signal to commence charging. Meanwhile, during the charging process, a battery with lower SoC should charge faster than that with a higher SoC. When SoC reaches the maximum limit, the corresponding PEV waits for a discharging signal after disconnecting from the microgrid.

3.2.2 Background on graph theory

A directed graph (diagraph) in a communication network can be represented as $G_r = (V_G, E_G, A_G)$, where $V_G = \{v_1^g, v_2^g, \ldots, v_N^g\}$ is a set of nonempty N nodes connected through a set of edges or arcs $E_g \subset V_G \times V_G$ and the associated adjacency matrix $A_G = [a_{ij}] \in R^{N \times N}$. In the communication network of a microgrid, converters are considered as nodes and the communication links are taken as edges. a_{ij} is the weight of the edges in adjacency matrix A_G, where $a_{ij} > 0$ if $(v_i^g, v_j^g) \in E_G$ and $a_{ij} = 0$, otherwise. The sequence of edges connecting the nodes v_i^g and v_j^g is called direct path. If a diagraph has at least one root node from where all other nodes have direct path, then the diagraph is

www.manaraa.com

said to have a spinning tree [61]. The communication network for the microgrid in Figure 3.1 is planned with at least one spanning tree and is also chosen in such a way that in case of any communication link failures the network would contain at least one spanning tree. Figure 3.2 shows the communication network superimposed on the physical network of the microgrid.

3.2.3 Distributed Co-operative Control (DCC)

Each converter *i* transmits a set of data, $\psi = [\overline{v}_i, i_i^{pu}]$, to its neighbors where $\overline{v}_i$ is the estimated average voltage across the microgrid measured at node *i*, and i_i^{pu} is the measured per-unit current at node *i* and $i_i^{pu} \triangleq i_i / i_i^{rated}$ where i_i^{rated} is the rated current of *i*-th converter of a DG and i_i is the instantaneous current at node *i* .

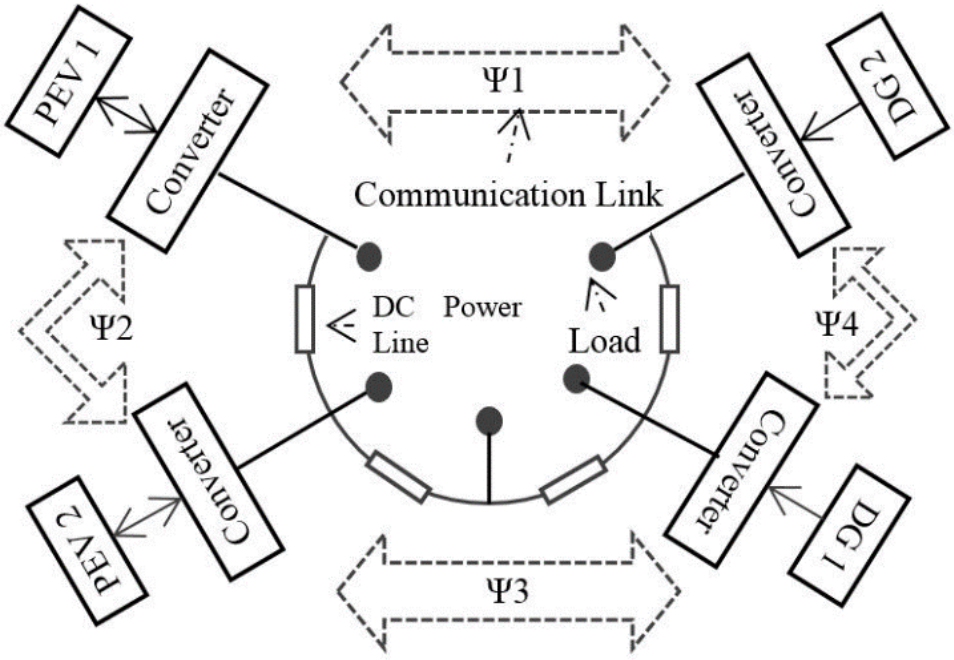

Figure 3.2: Communication network layout over physical network [13]

www.manaraa.com

In the secondary control of the DC microgrid, local and neighbor's information are used to adjust the local voltage set point v_i^* using two correction factor (Δv_1 and Δv_2) [13]:

$$v_i^* = v_i^{ref} - r_i . i_i + \Delta v_1 + \Delta v_2 \tag{3.1}$$

where Δv_1 comes from voltage regulator, Δv_2 comes from current regulator, r_i is the virtual output-impedance, and v_i^{ref} is the reference voltage of the DC microgrid.

The voltage regulator has two parts 1) voltage observer and 2) PI controller. The voltage observer estimates the average voltage $\overline{v_i}$ at node i using the average voltage estimates, $\overline{v_j}$, of its neighboring nodes as shown below.

$$\overline{v_i}(t) = v_i(t) + \int_0^t \sum_{j \in N_j} a_{ij} \left(\overline{v_j}(\tau) - \overline{v_i}(\tau) \right) d\tau \tag{3.2}$$

where $v_i(t)$ is the measured voltage at node i, $N_j$is the number of nodes exchanging information with node i, and a_{ij} is the edge between node i and node j in the communication graph. If all communication links are bi-directional, then $\bar{v}$ converges to the true average value [13]. The PI controller H_i compares v_i^{ref} and $\overline{v_i}$ to produce the Δv_1. The current regulator uses one PI controller to compute Δv_2 from the current mismatch, δ_i which compares i_i^{pu} and the average of neighbor's per-unit current, i_j^{pu}:

$$\delta_i = \sum_{j=N_i} c a_{ij} \left(i_j^{pu} - i_i^{pu} \right) \tag{3.3}$$

www.manaraa.com

where c is the coupling gain. This second correction, Δv_2, factor ensures that the converter's per unit currents become equal so that they share the load in proportion of their ratings.

3.2.4 SoC based Distributed Co-operative Control for PEV charging and discharging

The concept of SoC based droop control introduced in [26] uses only local information for controlling the battery charging and discharging. In the present research work, the availability of generation in the microgrid is also taken as an extra parameter in the droop control by using the distributed cooperative control. The proposed method controls the PEV battery discharging/charging for optimal use of the available generation capacity that exists in the microgrid. The distributed cooperative control of DC microgrid ensures a proportional load sharing among different converters by equalizing the per unit currents of the converters, mathematically in steady state,

$$i_1^{pu} = i_2^{pu} = i_3^{pu} = \ldots = i_m^{pu} \tag{3.4}$$

The per unit current of the *i*-th battery is updated as:

$$i_i^{pu} \triangleq i_i / {i_i}^{cap} \triangleq i_i / ({i_i}^{max} \times SoC_i^n) \tag{3.5}$$

where ${i_i}^{cap}$ is the available current injection capacity of the *i*-th battery and ${i_i}^{max}$ is the maximum current injection capacity of that battery and *n* is the speed regulator for SoC balancing. Combining (3.4) and (3.5) and considering the fact that the voltage drop across the DC microgrid should be within 5% of the reference voltage regardless of the cable length, the power sharing of PEV batteries during discharging mode can be achieved according to the following equation:

www.manaraa.com

$$\frac{p_1}{{P_1}^{max} \times SoC_1^n} = \frac{p_2}{{P_2}^{max} \times SoC_2^n} = \cdots = \frac{p_n}{{P_n}^{max} \times SoC_m^n} \tag{3.6}$$

(3.6) states that by updating the per unit current of *i*-th battery according to (3.5), while in discharging mode, the proposed method not only balances the SoCs of the batteries by faster discharging of the battery with higher SoC but also ensures the distribution of load among the batteries according to their ratings so that none of them are overloaded.

In charging mode, the conventional droop control method is modified to control the speed of charging according to the available generation capacity of the DGs. Conventional droop control method can be expressed as:

$$\mathrm{v}_i^* = \mathrm{v}^{ref} - r_i \times p_i \tag{3.7}$$

where v_i^*, r_i and p_i are output reference voltage under loaded condition, droop coefficient and the charging power respectively. For SoC balancing, the droop coefficient was set to:

$$r_i = r_c SoC_i^n \tag{3.8}$$

where r_c is the constant droop coefficient for battery. With higher value of *n*, charging rate of the battery will be higher [26]. As DCC guarantees that the per unit currents of all the DGs would be same under steady state condition, that per unit current is a good measure of the available power delivery capacity of the DGs. When the per unit current approaches unity, there will be not much power left to meet the demand. So the ideal condition would be to charge the PEVs faster when there is enough power in the DGs and when the DGs are running closer to their maximum capacities, the charging rate

www.manaraa.com

should be slower. This approach will ensure Demand Response (DR) within the microgrid by controlling the charging current of the batteries depending on the availability of power delivery capacity of all the DGs in the microgrid. To achieve DR, the value of *n* was updated dynamically according to following equation:

$$n = k \times \left(1 - i_j^{pu}\right) \tag{3.9}$$

where *k* is the maximum allowable value of *n* and i_j^{pu} is the per unit current of the neighboring *j*-th DG. According to (3.9), the value of *n* decreases when i_j^{pu} increases and vice versa. A higher voltage, v_i^*, from equation (3.7) will cause higher current from the battery. As it is evident from (3.7) and (3.8) that the battery charging rate is higher with higher value of *n*, the battery will charge faster when i_j^{pu} is lower. But lower i_j^{pu} means that microgrid has more power to deliver than the case of higher i_j^{pu}. From (3.4) and (3.7)-(3.9), it can be shown that the charging power of PEV batteries should be controlled using the following formulae to achieve DR:

$$p_1 : p_2 : \ldots : p_m = \frac{1}{SoC_1^{k\times\left(1-i_{j1}^{pu}\right)}} : \frac{1}{SoC_2^{k\times\left(1-i_{j2}^{pu}\right)}} : \ldots : \frac{1}{SoC_m^{k\times\left(1-i_{jm}^{pu}\right)}} \tag{3.10}$$

From (3.10), it is clear that the charging rate of the batteries with lower SoC are higher than those with higher SoC.

Considering the simple equivalent circuit model given by [29] and [62] for a battery, the SoC of the battery can be modelled as:

$$SoC_i(k+1) = SoC_i(k) + \frac{\Delta T}{V_{dc}Q_i} P_i(k) \tag{3.11}$$

www.manaraa.com

where ΔT, Q_i , P_i are the charging time length, battery capacity and charging power of the i-th PEV respectively. In order to meet the demand-generation balance in the microgrid, the DGs and the discharging PEVs have to supply all the load demand and the charging energy for PEVs, as expressed below.

$$P_{DG} + P_{PEV,d} = P_{Load} + P_{PEV,c} \tag{3.12}$$

where P_{DG} , $P_{PEV,d}$ are the power coming from DGs and discharging PEVs, respectively, and $P_{PEV,c}$, P_{Load} are the demand of charging PEVs and loads. From (3.6), (3.10)-(3.12), the following equations can be derived for discharging and charging modes of batteries, respectively.

$$SoC_i(k+1) = SoC_i(k) + \frac{\mathrm{P}_{PEV,d}\Delta T}{V_{dc}Q_i} \times \frac{{P_i}^{max} SoC_i^n}{\sum_{r=1}^{k} {P_r}^{max} SoC_r^n} \tag{3.13}$$

$$SoC_i(k+1) = SoC_i(k) + \frac{\mathrm{P}_{PEV,c}\Delta T}{V_{dc}Q_i} \times \frac{\frac{1}{SoC_r^{k\times\left(1-i_i^{pu}\right)}}}{\sum_{r=1}^{k}\frac{1}{SoC_r^{k\times\left(1-i_r^{pu}\right)}}} \tag{3.14}$$

To illustrate the effect of per unit current on the charging rate, (3.14) was solved for several different per unit current values. Figure 3.3 shows the simulation results and it is clear from the figure that with increasing per unit current the charging rate decreases, thus reducing the total microgrid demand.

www.manaraa.com

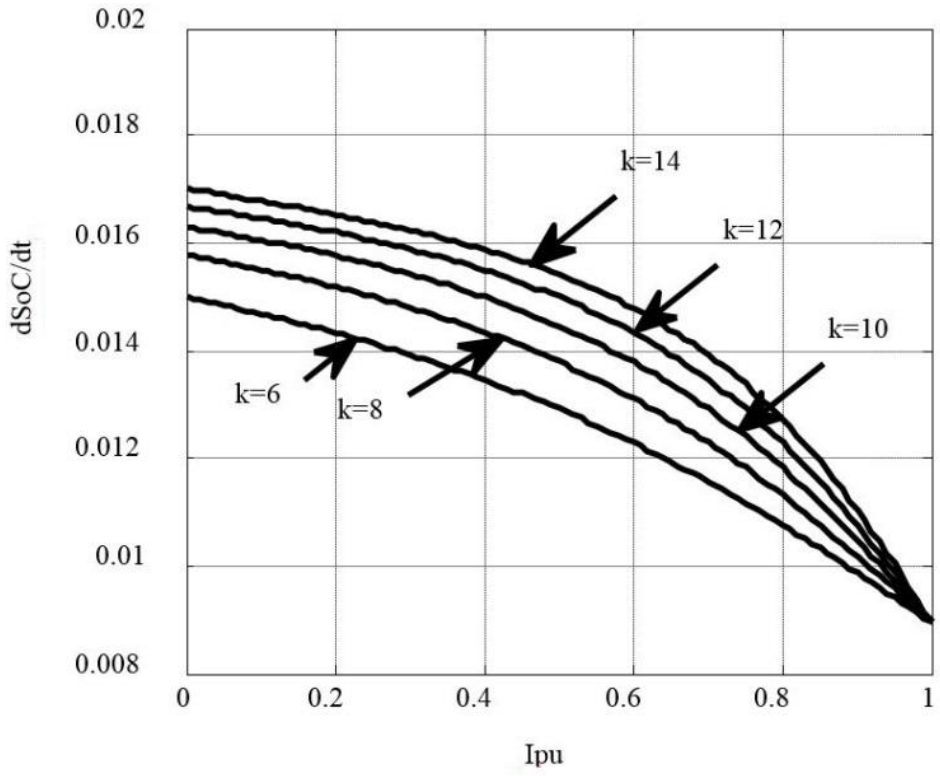

Figure 3.3: Rate of change of SoC decreases as per unit current (Ipu) increases

3.2.5 Distributed Energy Management System (EMS)

As the per unit current, under steady state conditions, effectively indicates the available capacity of the microgrid, the optimal charging and discharging decision for PEVs can be made without any central supervisory controller. Figure 3.4 depicts the charging/discharging decision flowchart with an SoC based DCC. When a PEV is plugged into the microgrid, it will first check the per unit current, i_j^{pu}, of the neighboring DGs. If all $i_j^{pu} \approx 1$, then the DGs are running at almost full capacity. Under this condition, the PEV will not try to charge; rather it will check its own SoC. If its own SoC is above minimum value, the PEV will start discharging. While in discharging mode, when the per unit current of the PEV approaches unity, the PEV transits from voltage

www.manaraa.com

control mode to power control mode delivering maximum available power without controlling the voltage.

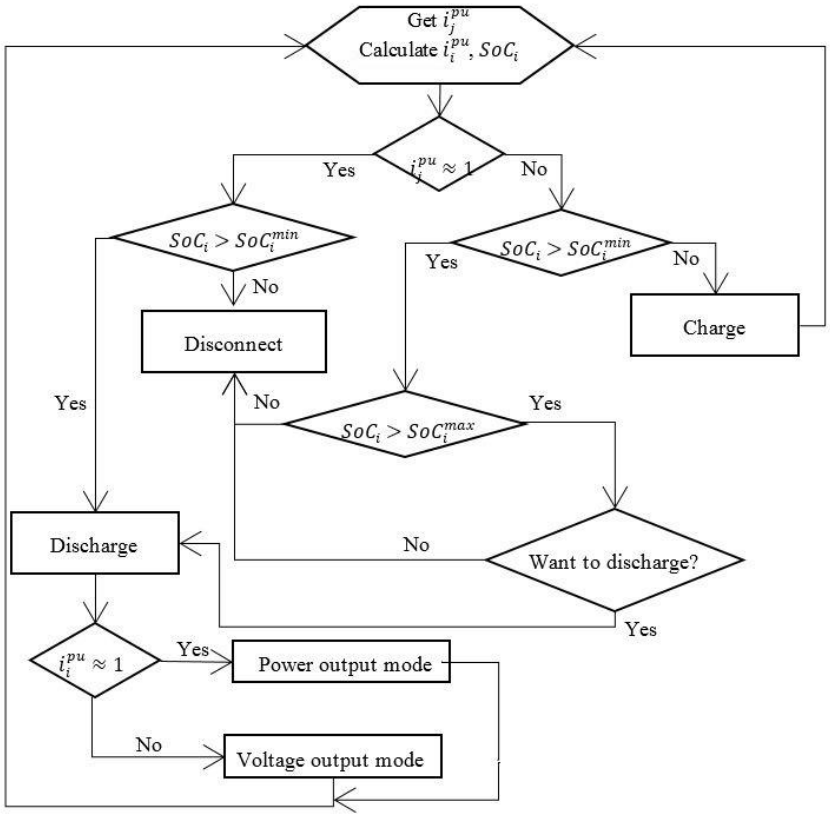

Figure 3.4: Charging/discharging decision flowchart for PEV

However, if $SoC_i < SoC_i^{min}$, the PEV will be disconnected from the microgrid and will wait for further signals. On the other hand, when the per unit current for all the DGs in the microgrid, i_i^{pu}, is much less than unity, the PEV will check its own SoC for a charging decision. If $SoC_i < SoC_i^{min}$, the PEV will start charging otherwise if $SoC_i > SoC_i^{max}$, the PEV will be ready to discharge. If the PEV owner opts for discharging while all conditions are met, the PEV will start discharging. In this way, the battery will deliver power to the microgrid when there is a shortage of available generation capacity and the

www.manaraa.com

battery will store energy when there is enough generation capacity. This scenario is ideal for microgrids with renewable energy sources.

3.3 Case Studies

A Matlab/Simulink based model of Figure 3.1 was simulated to verify the effectiveness of the proposed method. Figure 3.2 shows the Simulink model the simulated DC microgrid. The DC microgrid reference voltage was chosen as 48V and the ratings of the two converter for the DGs were assumed to be [20, 20] Amps. The batteries for the PEVs were considered to be Lithiam-ion batteries with initial SoC for PEV 1 as 80% and for PEV 2 as 65%. For both of the batteries of PEV 1 and PEV 2, maximum available discharging current at 48V was considered as 10 Amps (480 watt).

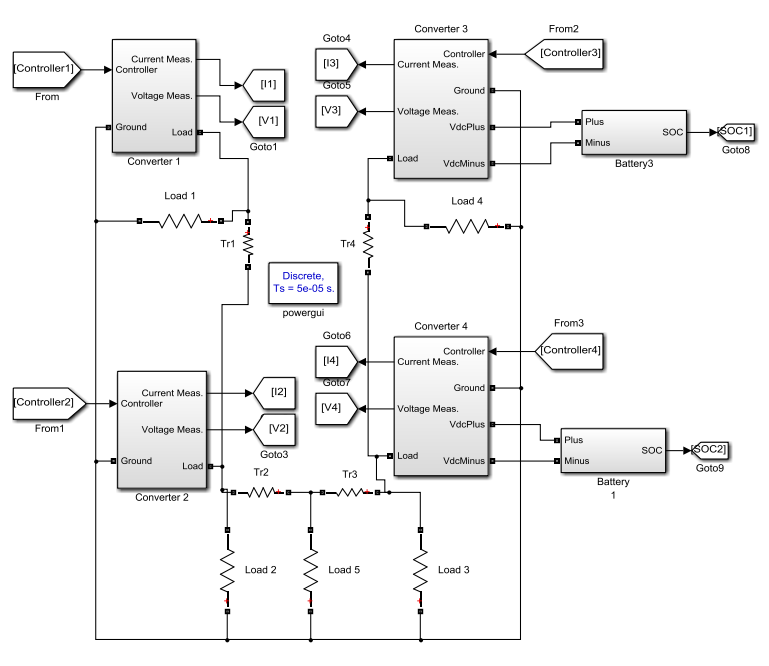

Figure 3.5: Simulink model of the DC microgrid

www.manaraa.com

3.3.1 All the PEVs are discharging

To verify the performance of the SoC based distributed cooperative controller, the PEVs were put in discharging mode sharing the load with solar and fuel cell DGs. As it can be seen in Figure 3.6(a), output voltages of the DGs and PEVs are very close to the reference voltage while in Figure 3.6(b), the load is being shared among the DGs and the PEVs according to their ratings. Also the discharging rate of PEV 1 with higher SoC is more than the discharging rate of PEV 2 which has a lower SoC.

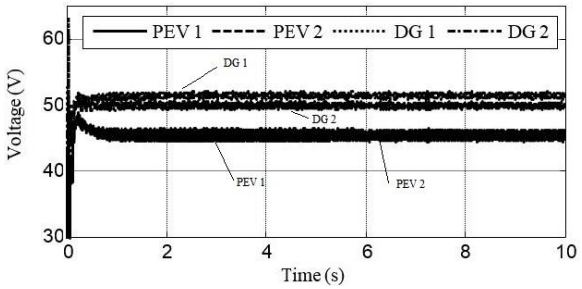

(a)

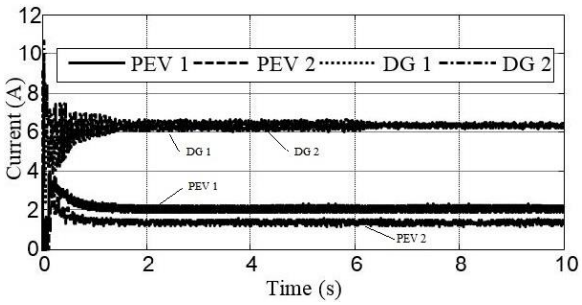

(b)

www.manaraa.com

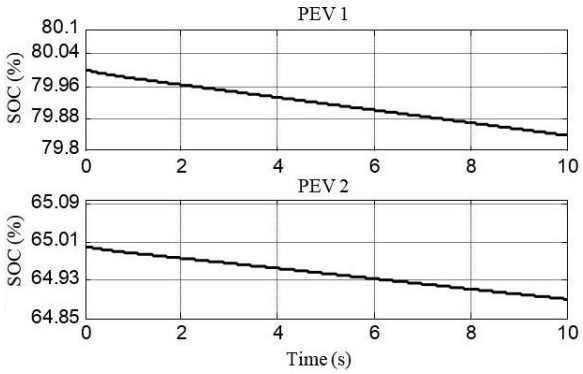

(c)

Figure 3.6: Both of the PEVs are discharging. a) Voltage profile b) Load sharing among the DGs and the PEVs c) SoC of the PEV batteries.

3.3.2 All the PEVs are charging while DGs are supplying demand

In this test, both of the PEVs were put in their charging mode while the DGs were the only source of energy. The proposed method successfully distributed the load equally among the DGs as it can be seen in figure 3.7 (b). PEV 2 was charging with a higher rate compared to PEV 1 as the former has a lower initial SoC. The voltage profile the DGs are again very close to the reference voltage which is evident from figure 3.7(a).

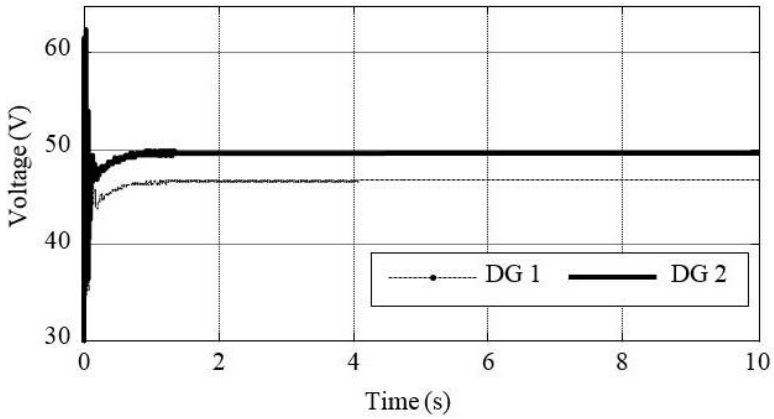

(a)

www.manaraa.com

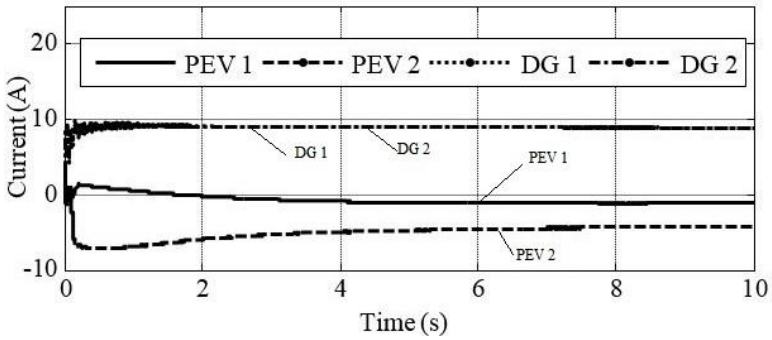

(b)

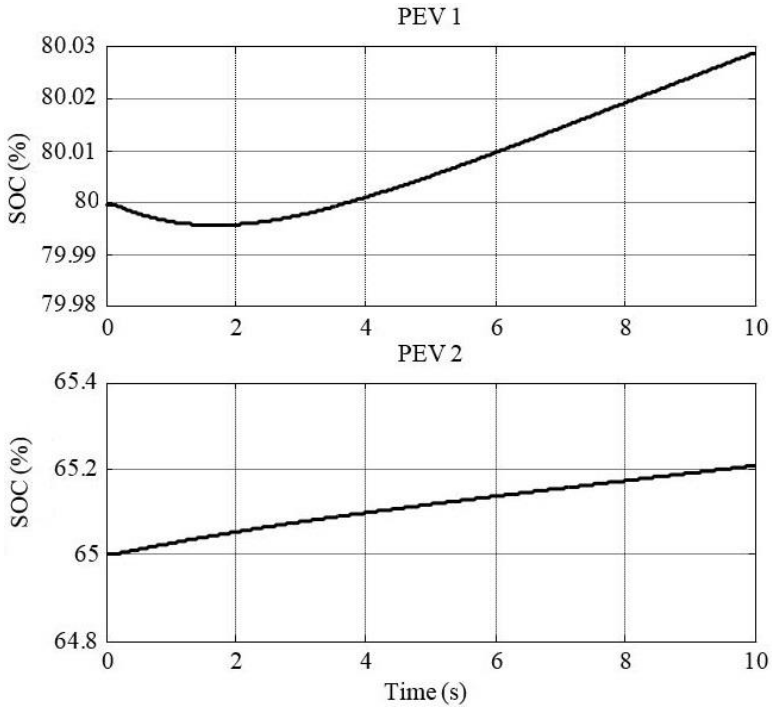

(c)

Figure 3.7: Both of the PEVs are charging a) Voltage profile b) Load sharing among the DGs and the PEVs charging currents c) SoC of the PEV batteries.

www.manaraa.com

3.3.3 Transient performance of the proposed method

In order to verify the transient performance of the proposed method, both of the PEVs were switched from discharging mode to charging mode at t=10.0 s. Figure 3.8 shows the simulation results where it is seen that there is a smooth transition from discharging mode to charging mode.

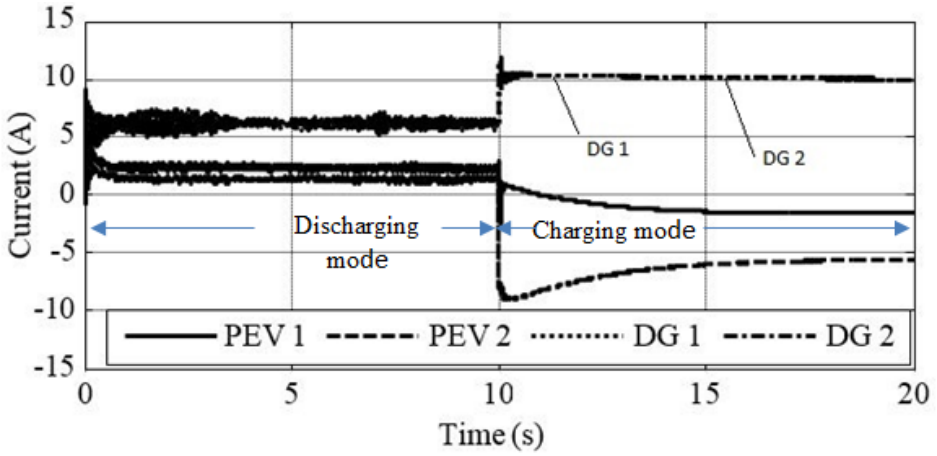

Figure 3.8: Transient performance of the proposed method when both of the PEVs were switched from discharging mode to charging.

3.3.4 Performance of the control scheme under varying load

The load R5 was changed at t=4s from 4Ω to 20Ω and again at t=8.0s from 20Ω to 4Ω in order to verify transient performance of the proposed method. Figure 3.9 shows the simulation results. As can be seen in figure 3.9, the SoC based distributed cooperative control returns all the converter terminal voltages close to the reference voltage after 0.3s of a load change. Under varying load, the proposed method effectively distributes the load among the DGs and the PEVs according to their ratings and initial SoCs.

www.manaraa.com

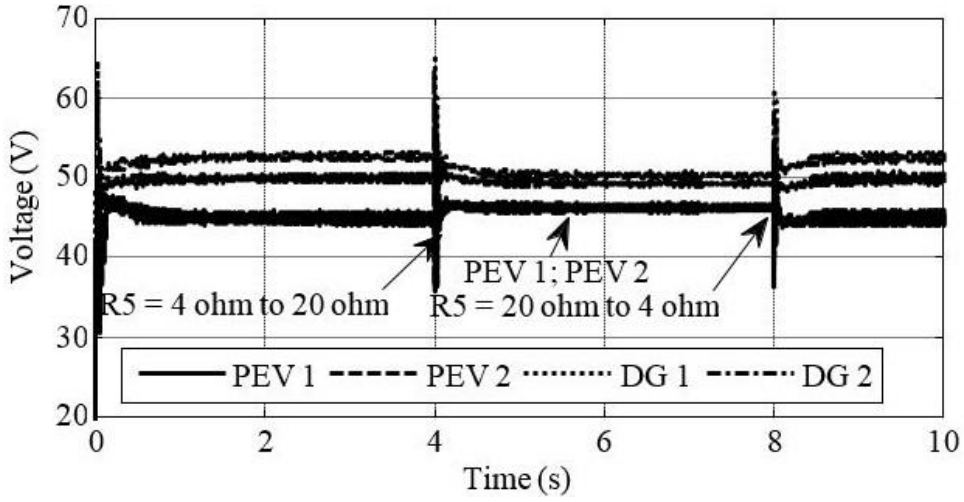

(a)

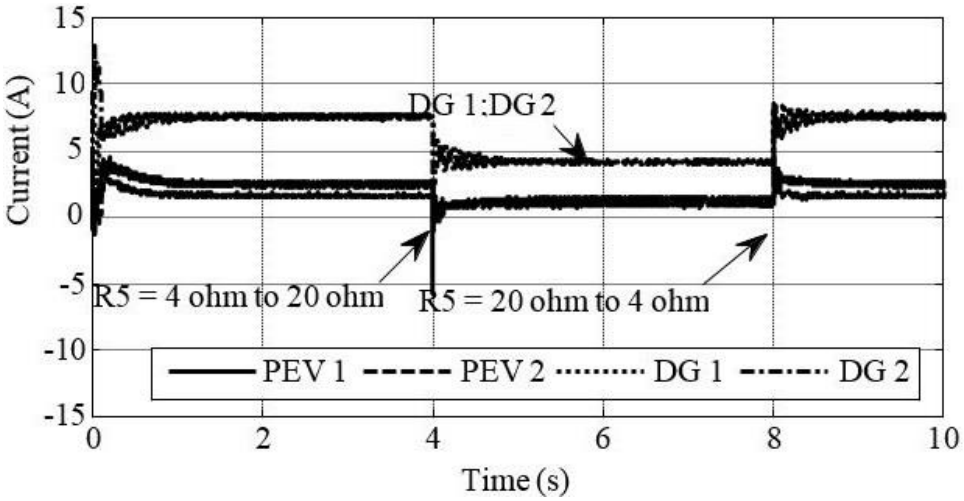

(b)

Figure 3.9: Transient performance of the control scheme under varying load when both of the PEVs are discharging a) Voltage profile b) Load sharing among the DGs and the PEVs.

3.3.5 Performance comparison between droop control and DCC

In this study, the performance of droop control and DCC were compared. Both of the batteries were assumed to have 100% SoC for simplicity. Initially the DGs and PEVs

www.manaraa.com

were put in droop control mode of operation to share the load. At t=1.0s, DCC was enabled replacing droop control. After initial transients, when the microgrid reached steady-state, the performance improvements are clearly visible in figure 3.10. The droop control exhibits poor voltage regulation, while the DCC exhibits superior voltage regulation. Accurate power sharing was also achieved with DCC strategy.

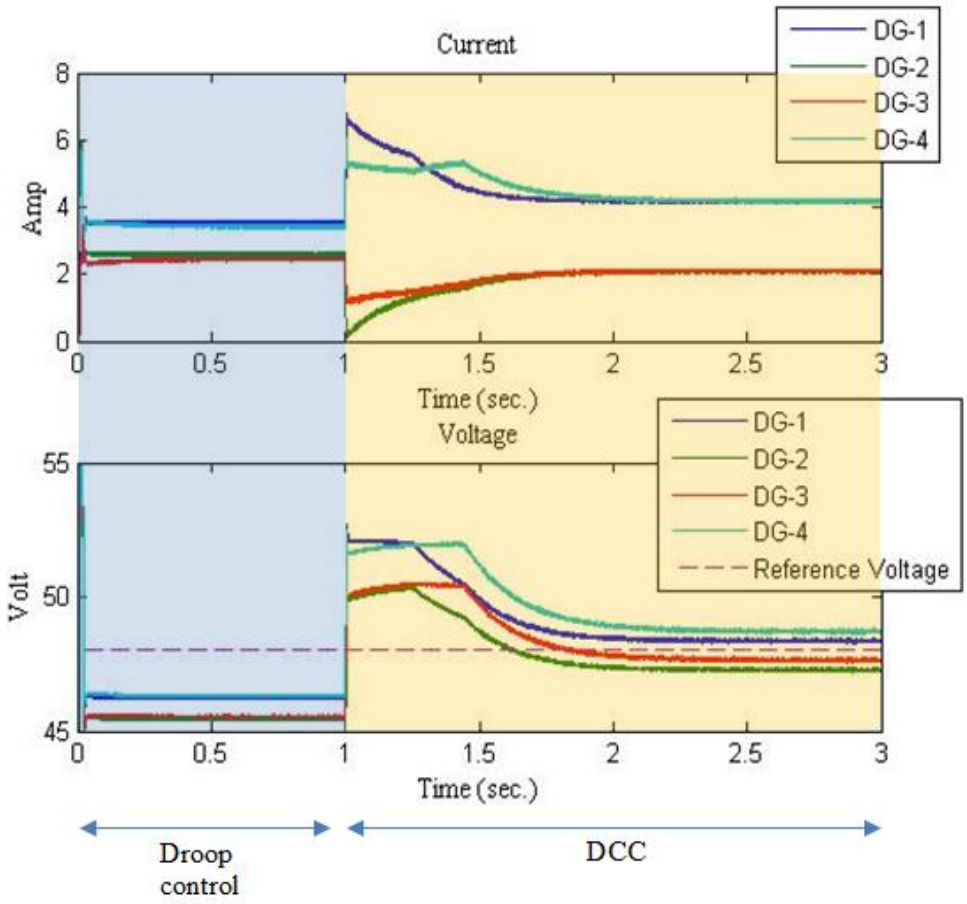

Figure 3.10: Performance comparison between droop control and DCC

www.manaraa.com

3.4 Conclusion

In this chapter, a SoC based distributed cooperative control has been proposed for PEV charging and discharging in an isolated DC microgrid. Available generation capacity of the microgrid was estimated using DCC without requiring a central control mechanism. This estimation was used to control the charging rate of PEVs to reduce the burden on the power generation units, i.e., DGs and discharging PEVs. The proposed method ensures a proportional load sharing among the DGs and discharging PEVs according to their ratings. While in discharging mode, the SoC balancing is also considered. Finally, a distributed EMS was proposed to coordinate the charging/discharging decisions using information only from the neighboring DGs or PEVs. Simulation results were presented to illustrate the effectiveness of the proposed method.

www.manaraa.com

Chapter 4

Control of AC microgrid in islanded mode of operation

4.1 Overview

In This chapter models for each distributed energy resource (DER) and the AC microgrid where the DERs are connected are presented. A Simplified model of the three-phase inverter in synchronous reference frame (d-q frame) and droop control for AC microgrid and DCC for AC microgrid in islanded mode are presented.

4.2 Dynamic Model of Inverter based DGs

Each DG is connected to the microgrid through an impedance $Z = X + R$ with δ_{DG} is the phase angle difference between voltages of DG bus, V_{DG}, and the Point of Common Coupling, V_{PCC}. Then the real and reactive powers shared by each DG with the microgrid is given by,

$$P = \frac{V_{DG}}{R^2+X^2}(XV_{PCC}\sin\delta_{DG} + R(V_{DG} - V_{PCC}\cos\delta_{DG})) \quad (4.1)$$

$$Q = \frac{V_{DG}}{R^2+X^2}(RV_{PCC}\sin\delta_{DG} + X(V_{DG} - V_{PCC}\cos\delta_{DG})) \quad (4.2)$$

(4.1) and (4.2) indicate that for a highly inductive line, real power is mostly determined by voltage angle, δ_{DG} and reactive power is determined by the amplitude of voltage source converter (VSC) voltage. Thus real power can be shared by the DGs in a

www.manaraa.com

microgrid by inserting an artificial droop in the DG frequency and reactive power can be shared by inserting an artificial droop in DG voltage magnitude as in (4.3) and (4.4),

$$\omega = \omega_0 - m_i P_i \tag{4.3}$$

$$V_{i,d} = V_{i,d}^{ref} - n_i Q_i \tag{4.4}$$

$$V_{i,q} = 0 \tag{4.5}$$

where $V_{i,d}, V_{i,q}, V_{i,d}^{ref}, \omega_0, \omega, m_i, n_i$ are d-axis inverter voltage, q-axis inverter voltage, reference voltage for the inverter, reference angular frequency, angular frequency, real power droop gain and reactive power droop gain, respectively. The voltage control of VSC in synchronous reference frame can be achieved by two cascaded inner controllers, voltage controller and current controller, as shown in Figure 4.1. Details of these controllers are depicted in Figure 4.2.

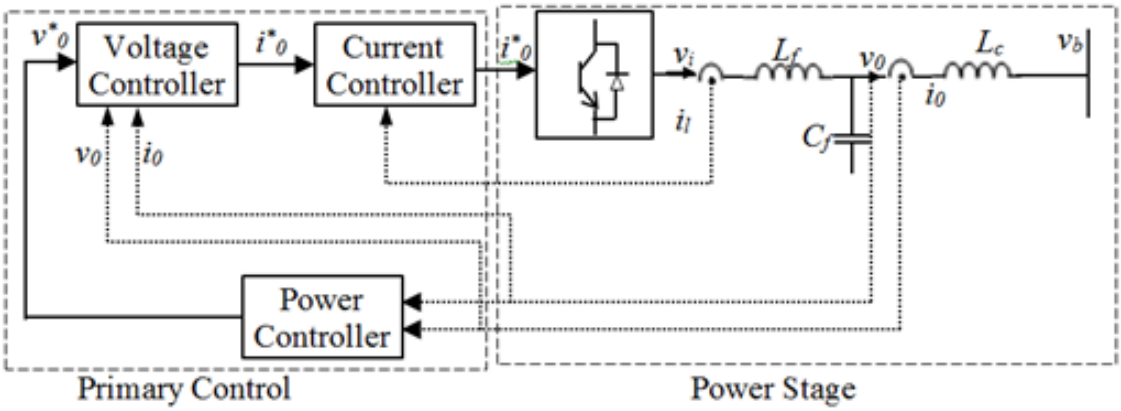

Figure 4.1: Control of three-phase inverter [68]

www.manaraa.com

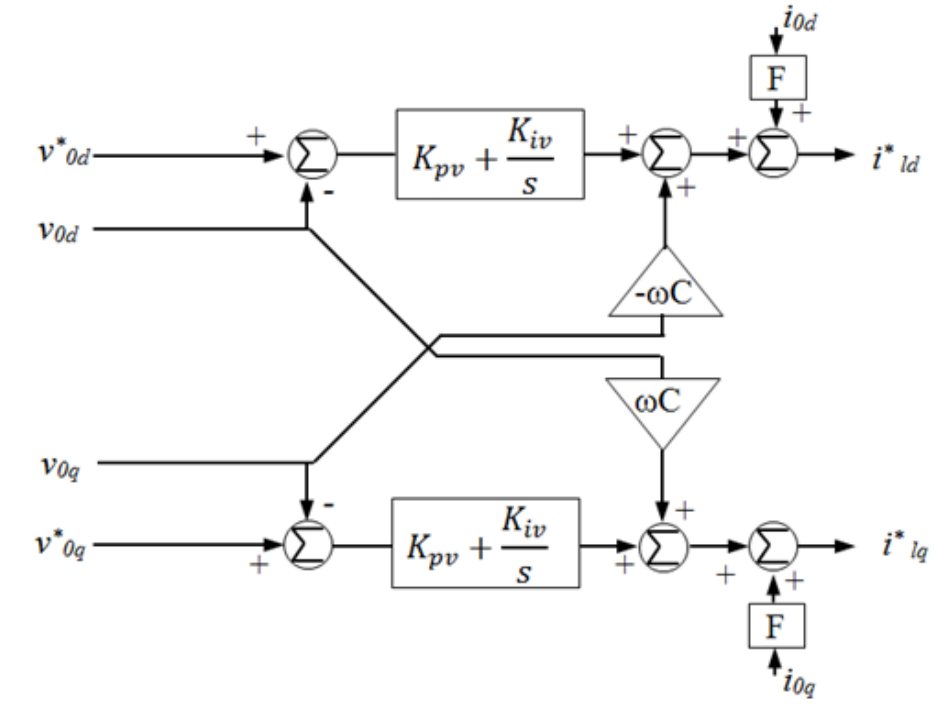

(a)

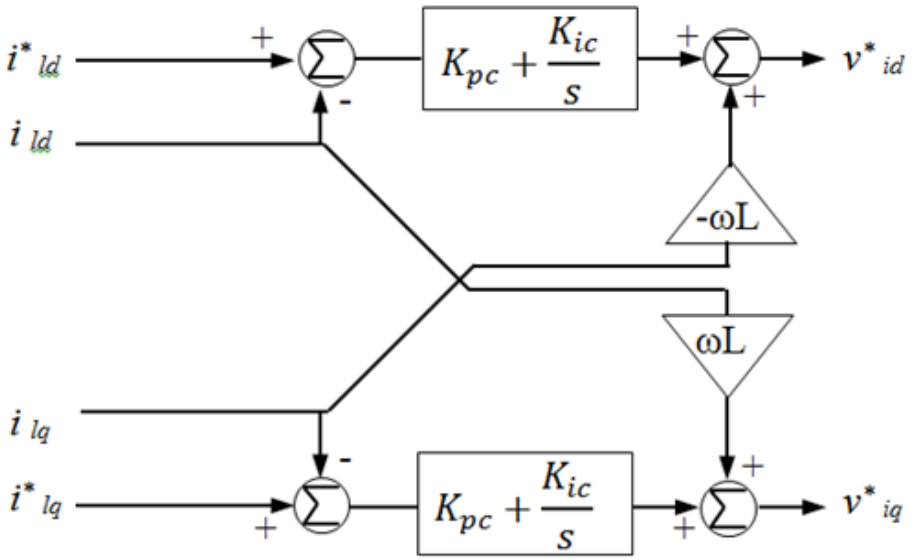

(b)

Figure 4.2: Control block diagram of VSC voltage control, a) Voltage controller, b) Current controller [68]

www.manaraa.com

The droop gains are calculated based on the maximum allowable change of frequency and voltage as in (4.6)-(4.7)

$$m_i = \frac{\omega_{max} - \omega_{min}}{P_{max}} \tag{4.6}$$

$$n_i = \frac{V_{DG,max} - V_{DG,min}}{Q_{max}} \tag{4.7}$$

By increasing the droop gain coefficients m_i and n_i, real and reactive power sharing accuracy among the DGs in a microgrid can be improved, but this will adversely affect the frequency and voltage regulation [63]-[64]. High values of droop gains can also lead to system instability and a poor transient response [65]. As the phase angle of voltage source converter (VSC) can be changed instantaneously, phase angle can be drooped instead of frequency drooping for real power sharing as follows:

$$\delta_i = \delta_i^{ref} - d_i P_i \tag{4.8}$$

The benefit of the above approach is the operation in constant frequency. However, when the load angle is large, this approach suffers from lower stability margins [65],[66],[67]. A centralized control approach may be adopted as in [64] to mitigate this stability problem. But centralized control system is not only costlier but also susceptible to collapse in case of any communication link failures. Figure 4.3 shows a schematic diagram of four bus AC microgrid where each bus is connected to a DG through an interfacing VSC, in this case inverters, and associated LCL filters.

www.manaraa.com

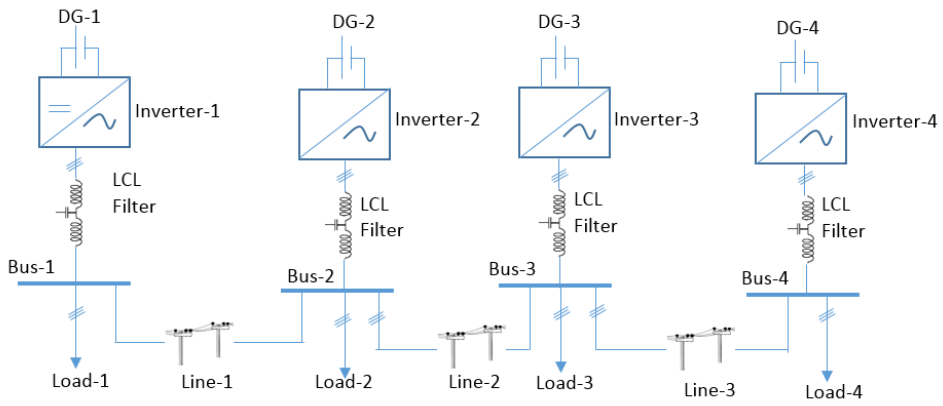

Figure 4.3: Schematic diagram of an AC microgrid

The control of AC microgrid lies in the control of the VSCs that connect the RESs to the AC microgrid. Voltage control of VSCs in synchronous reference frame has two inner controllers 1) inner voltage controller, and 2) inner current controller as it can be seen in Figure 4.1. Though the inner voltage controller is enough to control the output voltage of the VSCs, the inner current controller provides protection against high transient current. Figure 4.2 shows the structure of the inner controllers in synchronous reference frame where figure 4.2(a) depicts the inner voltage controller and figure 4.2(b) shows the inner current controller. The algebraic equations of the voltage controller are [68]:

$$\frac{d\zeta_{i,d}}{dt} = v_{i,d}^{*} - v_{0i,d} \tag{4.9}$$

$$\frac{d\zeta_{i,q}}{dt} = -v_{0i,q} \tag{4.10}$$

$$i_{lid}^{*} = Fi_{0d} - \omega_n C_f v_{0i,q} + k_{PV}\frac{d\zeta_{i,d}}{dt} + K_{IV}\zeta_{i,d} \tag{4.11}$$

$$i_{liq}^{*} = Fi_{0q} + \omega_n C_f v_{0i,d} + k_{PV}\frac{d\zeta_{i,q}}{dt} + K_{IV}\zeta_{i,q} \tag{4.12}$$

www.manaraa.com

The algebraic equations of the current controller are [68]:

$$\frac{d\Theta_{i,d}}{dt} = i_{li,d}^{*} - i_{li,d} \tag{4.13}$$

$$\frac{d\Theta_{i,q}}{dt} = i_{li,q}^{*} - i_{li,q} \tag{4.14}$$

$$v_{id}^{*} = -\omega_n L_f i_{i,q} + k_{PI}\frac{d\Theta_{i,d}}{dt} + K_{II}\Theta_{i,d} \tag{4.15}$$

$$v_{iq}^{*} = \omega_n L_f i_{i,d} + k_{PI}\frac{d\Theta_{i,q}}{dt} + K_{II}\Theta_{i,q} \tag{4.16}$$

The algebraic equations of the output LC filter and the coupling inductance in Figure 4.1 are [68]:

$$\frac{di_{ld}}{dt} = -\frac{r_f}{L_f}i_{ld} + \omega i_{lq} + \frac{1}{L_f}(v_{td} - v_{id}) \tag{4.17}$$

$$\frac{di_{lq}}{dt} = -\frac{r_f}{L_f}i_{lq} + \omega i_{ld} + \frac{1}{L_f}\left(v_{tq} - v_{iq}\right) \tag{4.18}$$

$$\frac{dv_{id}}{dt} = \omega v_{iq} + \frac{1}{C_f}(i_{ld} - i_{id}) \tag{4.19}$$

$$\frac{dv_{iq}}{dt} = \omega v_{id} + \frac{1}{C_f}\left(i_{lq} - i_{iq}\right) \tag{4.20}$$

The large signal dynamic model of an inverter based DG can be described by equations (4.3) to (4.20). In compact form, the large signal dynamic model is as follows [69]:

$$\dot{x}_\iota = f_i(x_i) + k_i(x_i)D_i + g_i(x_i)u_i \tag{4.21}$$

www.manaraa.com

$$y_i = h_i(x_i) \tag{4.22}$$

The state vector in (4.21) and (4.22) is defined as:

$$x_i = \left[\delta_i\ P_i\ Q_i\ \zeta_{i,d}\ \zeta_{i,q}\ \Theta_{i,d}\ \Theta_{i,q}\ i_{ld}\ i_{lq}\ \ v_{id}\ v_{iq}\ i_{id}\ i_{iq}\right]^T \tag{4.23}$$

D_i is considered as a known disturbance and is given by $D_i = [\omega_0\ v_{gd}\ v_{gq}]$. The other functions of $f_i(x_i)$, $k_i(x_i)$, $g_i(x_i)$ can be synthesized from equations (4.3) to (4.20).

Figure 4.4 and Figure 4.5 show strategies to implement the droop control using relation between frequency vs real power and voltage vs reactive power and show the importance of secondary and tertiary controls to mitigate the frequency and voltage deviations caused by droop control.

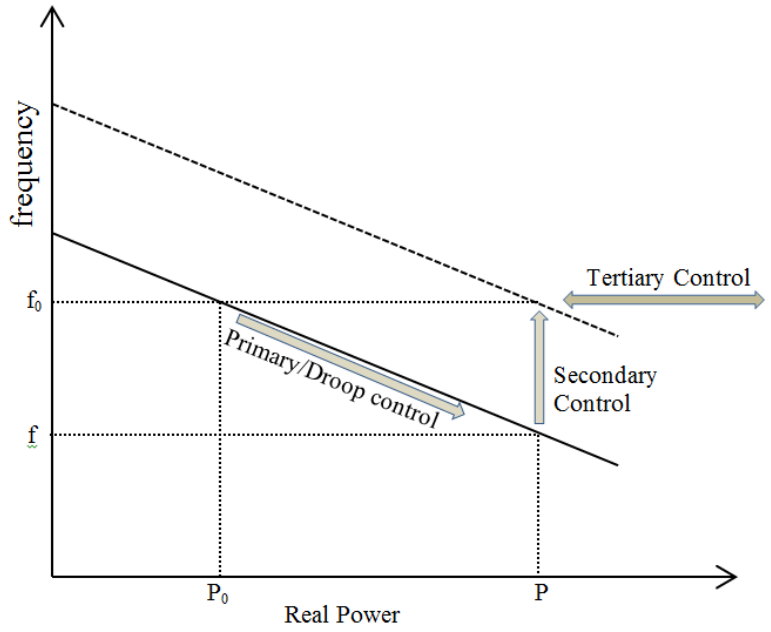

Figure 4.4: Frequency vs real power droop

www.manaraa.com

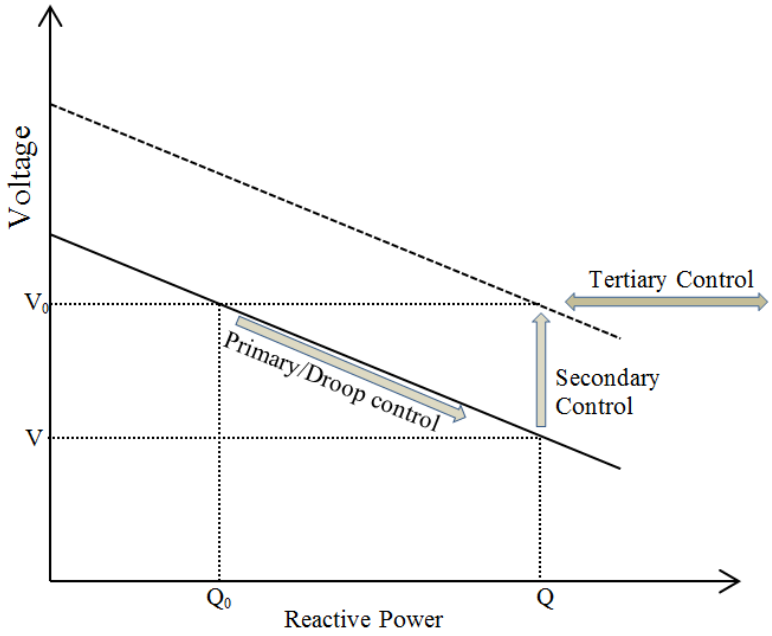

Figure 4.5: Voltage vs reactive power Droop

Figure 4.6 shows the simulink layout of a four-bus AC microgrid where four DGs are connected to each of the buses.

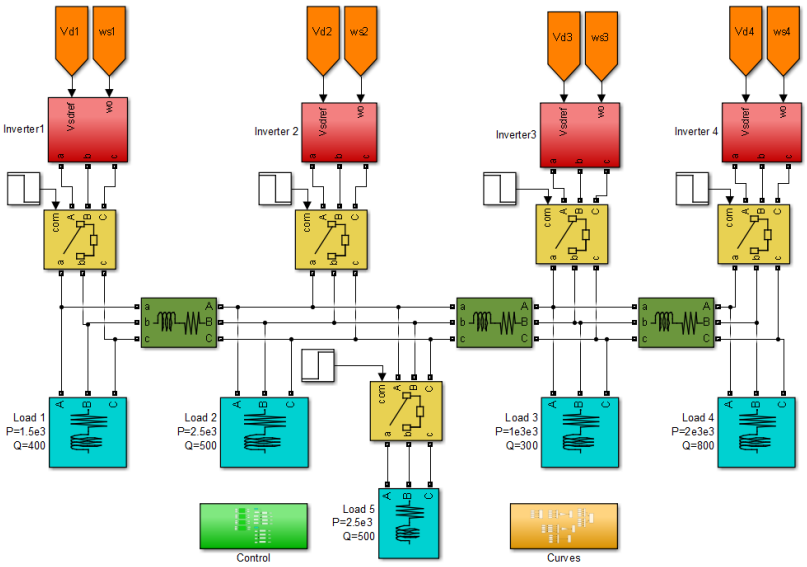

Figure 4.6: Simulink model of the AC microgrid

www.manaraa.com

The inverters in Figure 4.6 are representing the DGs. DG-1 and DG-3 have real power rating of 1000Watt and reactive power rating of 500Var whereas DG-2 and DG-4 have real power rating of 500Watt and reactive power rating of 250Var. The DGs are supplying the power consumed by the loads.

Figure 4.7 shows the outputs of the microgrid when the DGs were running in droop control mode. DG-1 and DG-3 have same rating which is higher than the rating of DG-2 and DG-4. The real power sharing by DGs were following their rating accurately as it can be seen in Figure 4.7 (c). However, there is some difference in reactive power sharing when the microgrid is running in droop control (Figure 4.7 (d)). When only droop control is employed, the voltage and frequency will always deviate from the nominal values as is evident from figure 4.7 (a) and (b). In order to show the performance of the droop control under a varying load, load-4 was disconnected from the microgrid at t=3.5 second. Though the DGs are tracking the varying load, poor voltage regulation and frequency deviations are still present.

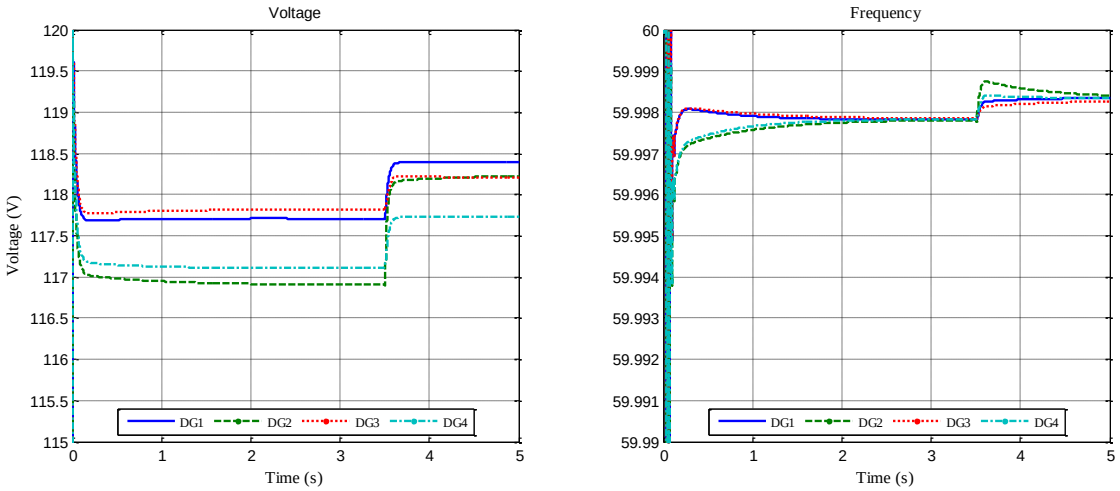

www.manaraa.com

(a) (b)

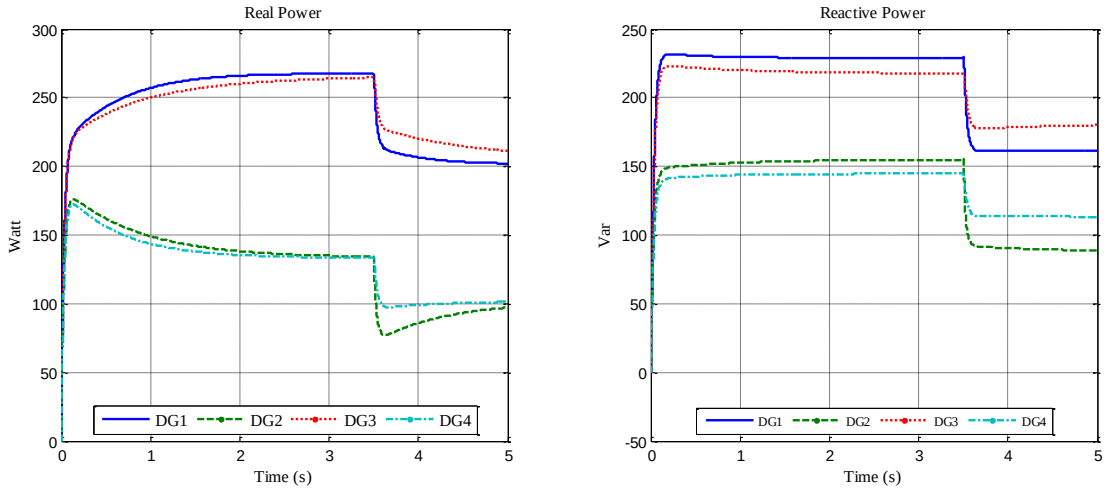

(c) (d)

Figure 4.7: Performance of droop control a) Voltage profile b) frequency c) real power sharing, and d) reactive power sharing

4.3 Beyond droop control

Droop control acting as primary control provides real and reactive power sharing in AC microgrids. However, droop control is unable to recover the rated frequency and voltage of the inverters. In grid-tied mode, grid voltage and frequency are imposed on the microgrid, but in islanded mode of operation, secondary control is required to restore the rated frequency and voltage [70]. Secondary control can be implemented in two ways: 1) centralized control and 2) co-operative control. In centralized control, the requirement of dense communication networks poses a threat to the microgrid operation in terms of reliability since any failure in the communication links may lead to the controller failure

www.manaraa.com

while and at the same time implementation of centralized controllers is costly. Distributed co-operative controller gets an upper hand with respect to centralized controller because of the requirement of lower number of communication links, resiliency and robustness to communication link failures.

4.3.1 Distributed co-operative control (DCC) for AC microgrid:

In order to implement the DCC for an AC microgrid, a communication graph with adjacency matrix $A_G = [a_{ij}] \in \mathcal{R}^{N \times N}$ is required. The communication graph should have the following characteristics:

- Must contain at least one spanning tree
- The graph should have balanced Laplacian matrix
- The graph should carry minimum redundancy

Each DG, considered as a node in a communication graph, shares a set of information from its neighboring DGs. The information set shared by the DGs is expressed as $\psi_i \in \{\overline{v_i}, P_i^{p.u.}, Q_i^{p.u.}\}$, where $\overline{v_i}$ is the overall estimated average voltage magnitude for the whole microgrid calculated at node i, $P_i^{p.u.}$ is the normalized delivered real power by DG_i and is calculated as $P_i^{p.u.} = \frac{P_i}{P_{rated}}$, and $Q_i^{p.u.}$ is the normalized delivered reactive power by DG_i and is calculated as $Q_i^{p.u.} = \frac{Q_i}{Q_{rated}}$. Using this set of information from neighboring DGs, the DCC tries to achieve 1) a nominal voltage at all buses 2) nominal frequency for the microgrid 3) sharing of the real power and reactive power of the DGs according to their ratings.

www.manaraa.com

Figure 4.8 shows the DCC for AC microgrid with the required communication graph.

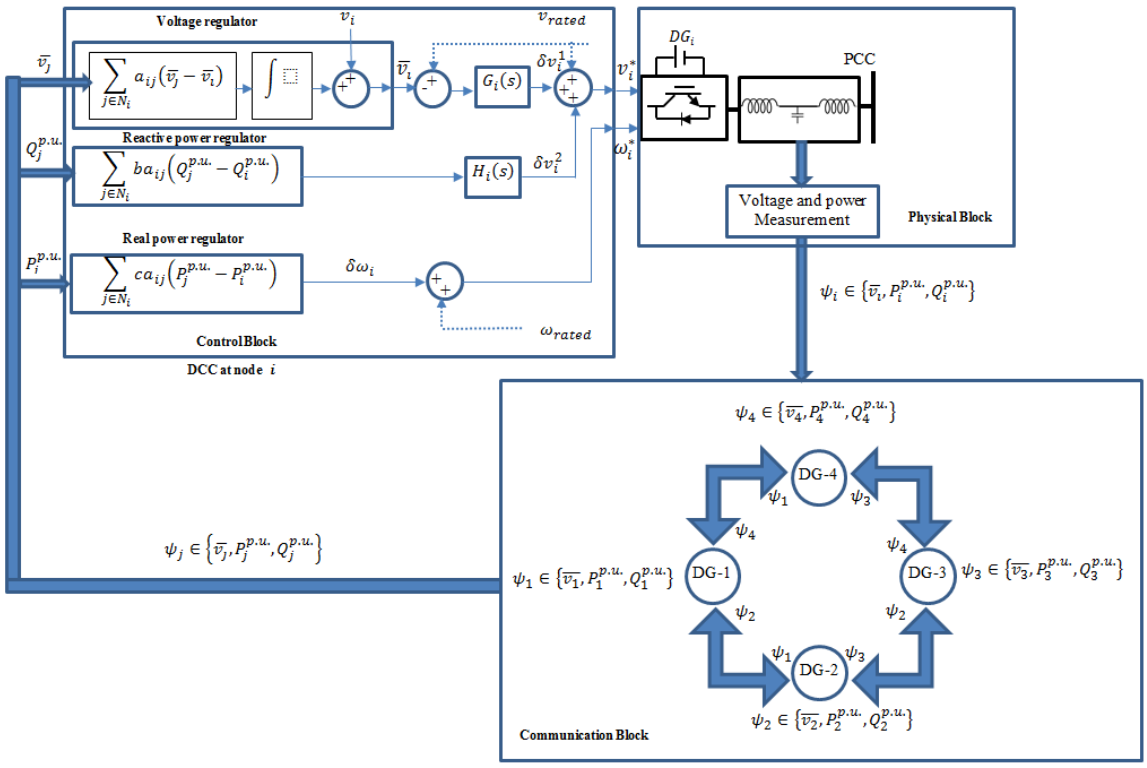

Figure 4.8: Control block and communication graph for DCC of AC microgrid [71]

The DCC has three main parts to control the inverters in the AC microgrid: 1) voltage regulator, 2) reactive power regulator and 3) real power regulator. Two voltage correction factors (Δv_i^1, Δv_i^2), one coming from voltage regulator (Δv_i^1) and the other coming from reactive power regulator (Δv_i^2), are added to the rated voltage reference set point for DG i [71]:

$$v_i^* = v_{rated} + \Delta v_i^1 + \Delta v_i^2 \tag{4.24}$$

The voltage regulator has one voltage estimator that calculates the average voltage across the microgrid using the average voltage estimate information from neighboring

www.manaraa.com

DGs and its own average voltage estimate. The equation for the average voltage estimation is:

$$\overline{v_i}(t) = v_i(t) + \int_0^t \sum_{j \in N_i} a_{ij} \left(\overline{v_j}(\tau) - \overline{v_i}(\tau) \right) d\tau \tag{4.25}$$

The voltage regulator compares this estimated average voltage for the microgrid with the rated voltage; the resultant difference is passed through a PI controller, $G_i(s)$, to produce a voltage correction factor, Δv_i^1, for the DG i. The voltage regulator collectively regulates the microgrid voltage in order to keep the voltage close to the nominal value. The second correction factor for the voltage reference of DG i comes from the reactive power regulator. The normalized per unit reactive power regulator calculates the reactive power loading mismatch of the DGs in the microgrid with the following equation:

$$mq_i = \sum_{j \in N_i} ba_{ij} \left(Q_j^{p.u.} - Q_i^{p.u.} \right) \tag{4.26}$$

The per unit reactive power loading mismatch is then processed with PI controller, $H_i(s)$, to produce the second voltage correction factor, Δv_i^2. The second voltage correction factor, Δv_i^2, introduces a small deviation of voltage from nominal value in steady-state condition, but that deviation is necessary to maintain desired reactive power sharing from the DGs.

The real power regulator compares the real power in per unit shared by the DGs with the following equation:

$$\delta\omega_i = \sum_{j \in N_i} ca_{ij} \left(P_j^{p.u.} - P_i^{p.u.} \right) \tag{4.27}$$

www.manaraa.com

$\delta\omega_i$ is added to the rated frequency to achieve an accurate real power sharing while maintaining the microgrid frequency at rated value. Figure 4.9 shows the performance improvement of the AC microgrid operation when DCC is used.

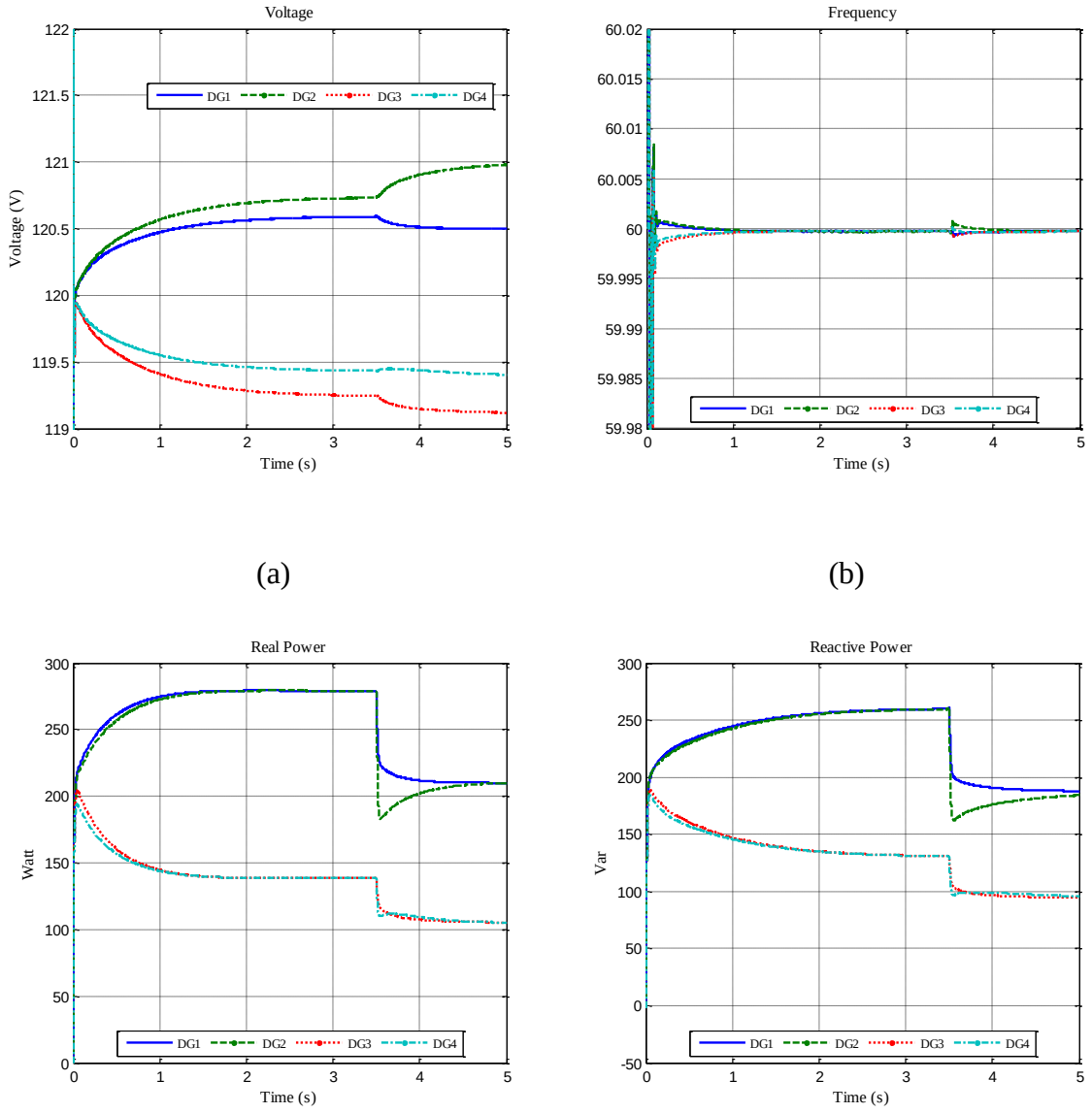

Figure 4.9: Performance of DCC a) Voltage profile b) frequency c) real power sharing d) reactive power sharing

www.manaraa.com

The AC microgrid simulated to verify the DCC is same as the microgrid that was tested for droop control AC microgrid. In this case, DG1 and DG 2 are assumed to have same real power and reactive power rating and DG3 and DG4 are also assumed to have same ratings. However, the DG-1 & 2 have twice the power rating than that of DG-3 & 4. Figure 4.9(c) and (d) clearly show that DGs are sharing real power and reactive power exactly according to their rating. The voltage profile of the microgrid, as it can be seen in Figure 4.9(a), shows superior performance than the of the droop control. Except during transients, the microgrid frequency is also very close to its nominal value. In order to verify the transient performance of the controller, the load-4 was disconnected from the microgrid at t=3.5s. From the curves in Figure 4.9(a)-Figure 4.9(d), it is clear that the controller is able to track the changes in the load accurately while maintaining the voltage and frequency close to their nominal values.

www.manaraa.com

Chapter 5

Co-operative control for AC/DC hybrid microgrid

5.1 Overview

Both the AC and DC microgrids have some advantages and disadvantages of their own. Hybrid AC/DC microgrids have been proposed to take advantage of these two types of microgrid in order to provide a better platform for integration of DGs in power system. Hybrid AC/DC microgrids use interfacing converters (IC) to link the AC and DC subgrids within the hybrid microgrid. The power management control of hybrid AC/DC microgrids then focuses on the control of this IC. When the hybrid system is running in an islanded mode of operation, the IC considers one subgrid as the source of energy while the other subgrid is considered to be the load. In this chapter, a DCC for the hybrid AC/DC microgrid realized through controlling the IC is proposed. A flexible hybrid microgrid architecture has been considered where all the DGs and loads are conveniently placed in either AC subgrid or DC subgrid depending on their AC or DC characteristics. Overall system integration cost can be decreased and efficiency can be increased as this flexible hybrid microgrid architecture reduces the number of various power conversion stages such as AC-DC or DC-AC converters.

www.manaraa.com

5.2 Hybrid microgrid architecture and mode of operations

Figure 5.1 shows a simple flexible structure of hybrid AC/DC microgrid which is formed by one AC microgrid and one DC microgrid connected together through an interfacing converter (IC). The subgrids in the hybrid system are serving their local loads. The IC provides bi-directional power flow between the two subgrids depending on the demand-supply constraints in the individual subgrids. Moreover, the hybrid microgrid can be connected with the utility from the AC subgrid side by a static transfer switch (STS). Under grid connected mode of operation, STS will remain closed and utility will determine the overall dynamics of the hybrid system as the utility can be considered as an infinite bus. The voltage and frequency of AC subgrid under grid connected mode will be controlled by utility and the role of IC will be mainly to control the voltage of the DC subgrid along with power sharing from the DC bus. The RESs connected in both of the subgrids will mainly operate in maximum power point tracking (MPPT) mode to harness the maximum power from the sources. In the islanded mode of operation, the DGs in both of the subgrids will participate in power balancing as well as system stability. The following section describes the performance requirements for both of these modes of operation.

5.2.1 Grid-connected mode of operation for hybrid microgrid:

During grid connected mode, the voltage and frequency of the AC subgrid is controlled by the utility. The voltage of the DC subgrid is controlled by the utility through the IC. However, DGs connected to the AC subgrid will be responsible for generating fixed real/reactive power or vary their real/reactive power by a small amount

www.manaraa.com

around some fixed value to provide voltage support and other ancillary services. The DGs connected to the DC subgrid will generate real power following MPPT in case of renewable energy or can be put on stand-by to be used later in case of dispatchable DGs. Considering these constraints, the grid connected hybrid AC/DC microgrid can be described by the following power balance equations:

$$P_{IC} = \sum_{i \in N_{DG,DC}} P_{DC,i}^{Gen} - \sum_{i \in N_{Load,DC}} P_{DC,i}^{Load} \quad (5.1)$$

$$P_{grid} = \sum_{i \in N_{DG,AC}} P_{AC,i}^{Gen} + P_{IC} - \sum_{i \in N_{Load,AC}} P_{AC,i}^{Load} \quad (5.2)$$

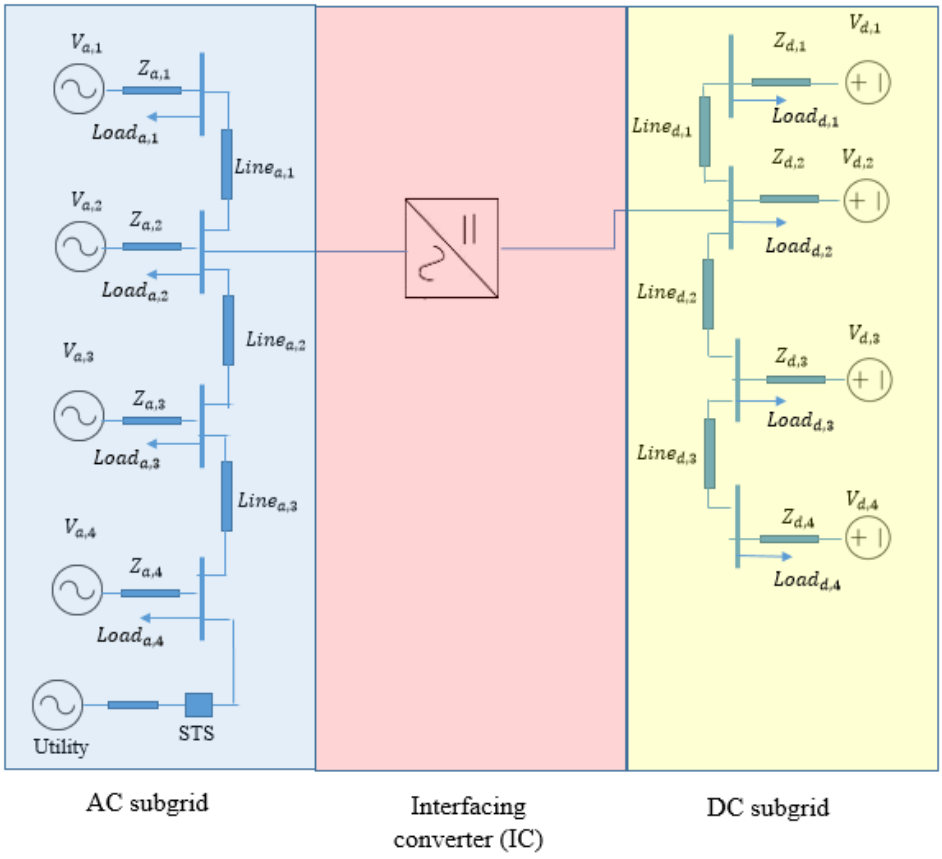

Figure 5.1: Structure of the AC/DC hybrid microgrid

www.manaraa.com

5.2.2 Islanded mode of operation for hybrid microgrid:

Control of hybrid microgrid in islanded mode of operation is more critical since total load of the hybrid microgrid should be shared by the DGs in both of the subgrids autonomously while keeping the voltage and frequency of the hybrid system at acceptable limits. A DCC based control strategy for the IC power management of hybrid microgrid is presented here. In order to fully comprehend the operating conditions that can occur in a hybrid microgrid in islanded mode of operation, the following states in terms of the IC power flow management are identified:

Fixed scheduled power through IC

During the light load conditions, the power demand in each of the subgrids is much less than the generation capacity of individual subgrids. The DGs in the AC subgrid will regulate their own voltage and frequency, and will supply their own loads while DGs in the DC subgrid will supply the DC loads and will maintain an acceptable voltage level in the DC subgrid. Under this situation, the power flow through the IC will be a fixed scheduled power; the value of scheduled power may be determined by the operators of the subgrid. This scenario can be described by the following equations:

$$P_{IC} = P_{IC}^{sch} \tag{5.3}$$

$$P_{grid} = 0 \tag{5.4}$$

$$\sum_{i \in N_{DG,DC}} P_{DC,i}^{Gen} \geq \sum_{i \in N_{Load,DC}} P_{DC,i}^{Load} \tag{5.5}$$

www.manaraa.com

$$\sum_{i\in N_{DG,AC}} P_{AC,i}^{Gen} \geq \sum_{i\in N_{Load,AC}} P_{AC,i}^{Load} \quad (5.6)$$

Power balance in the subgrids through the IC

This situation will occur when there is surplus power in one subgrid and the other subgrid is experiencing a power deficiency. In order to serve all the loads without power interruption, the subgrid with a surplus power can export power to the power deficient subgrid through the IC. The IC will play a crucial role in maintaining the stability of the subgrid that is receiving power. There are a numbers of ways to share the power under this situation. But if the total load in the hybrid microgrid is divided among all the DGs according to their power ratings in both of the subgrids, none of the DGs will be overstressed. In that case the power flow management algorithm for the IC will try to match the normalized power of all the DGs in both of the subgrids to the same per unit power. This situation is mathematically presented by the following equations:

$$P_{grid} = 0 \quad (5.7)$$

$$P_{IC} = \sum_{i\in N_{DG,DC}} P_{DC,i}^{Gen} - \sum_{i\in N_{DG,AC}} P_{AC,i}^{Gen} - \sum_{i\in N_{Load,DC}} P_{DC,i}^{Load} + \sum_{i\in N_{Load,AC}} P_{AC,i}^{Load} \quad (5.8)$$

$$P_{DC,1}^{Gen,p.u} = P_{DC,2}^{Gen,p.u} = \cdots = P_{DC,N_{DG,DC}}^{Gen,p.u} = P_{AC,1}^{Gen,p.u} = P_{AC,2}^{Gen,p.u} = \cdots = P_{AC,N_{DG,AC}}^{Gen,p.u} \quad (5.9)$$

$$P_i^{Gen,p.u} = \frac{P_i^{Gen}}{P_i^{Gen,rated}} \quad (5.10)$$

www.manaraa.com

Load shedding

In the islanded mode of operation when the total load demand in the hybrid microgrid is greater than the combined capacity of the DGs in both of the subgrids, there is no way to serve all the loads. In this extreme case, there has to be some load shedding scheme to serve the critical loads by curtailing less important loads in the microgrid. This situation can be expressed as:

$$P_{grid} = 0 \tag{5.11}$$

$$\sum_{i \in N_{DG,DC}} P_{DC,i}^{Gen} + \sum_{i \in N_{DG,AC}} P_{AC,i}^{Gen} < \sum_{i \in N_{Load,DC}} P_{DC,i}^{Load} + \sum_{i \in N_{Load,AC}} P_{AC,i}^{Load} \tag{5.12}$$

5.2.3 Proposed DCC for hybrid AC/DC microgrid

Controls of individual AC and DC microgrids using DCC were discussed in the previous chapters. In order to make the operation of the hybrid microgrid smooth, not only a power control strategy inside each of the subgrids is required, but the power management strategy through the IC is also required. The power management of the IC is different from the power control strategy of the individual microgrids as the IC is required to provide a bi-directional power flow in order to facilitate the flow of power to and from of both of the AC and DC subgrids. This difficult situation can be dealt with by appropriately designing a communication graph for the IC, transferring adequate information to the DCC controller of the IC. The DCC should be able to handle the scenarios that can arise in the operation of the hybrid microgrid discussed in previous section. Keeping these conditions in mind, the following communication graph and DCC for IC power management is proposed.

www.manaraa.com

The communication graph developed for the DCC of a hybrid AC/DC microgrid is presented in Figure 5.2. The graph contains all the characteristics that were required for the DCC of individual AC and DC microgrids. For the case of hybrid AC/DC microgrid, in addition to the communication graphs for individual subgrids, the IC also get information from AC and DC subgrids in order to implement the DCC for power management. The type of information shared by the AC and DC subgrids with the IC is depicted in Figure 5.2. The IC does not exchange information about the reactive power as the AC and DC subgrids do not share any reactive power.

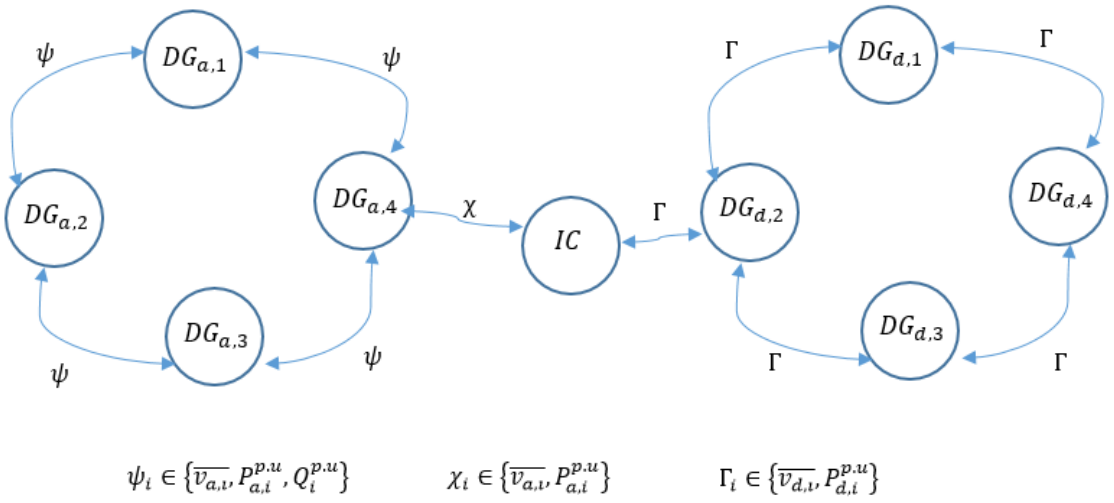

Figure 5.2: Communication graph for DCC of hybrid AC/DC microgrid

The first two cases in the previous section (fixed scheduled power through the IC and power balance in the subgrids through the IC) require power management control for the IC, but the third case (load shedding) does not require any power management for the IC as there is not enough generation in either subgrids to meet the load of the hybrid microgrid. For the first two cases, power may flow either to the DC subgrid or to the AC

www.manaraa.com

subgrid through the IC. When power is flowing to the DC subgrid, DCC controls the DC side voltage of IC in order to achieve the objectives of power sharing and voltage regulation. The output voltage of the IC is controlled by equation 5.13:

$$v_{DC}^{IC} = V_{rated} + \Delta v_1^{IC} + \Delta v_2^{IC} \tag{5.13}$$

Two correction factors (Δv_1^{IC} and Δv_2^{IC}) are added to the rated voltage level for the IC. The first correction factor looks after the average voltage deviation across the microgrid from the rated value. It calculates the average voltage of the microgrid by taking the information about the estimated average DC subgrid voltage from the DGs in the DC subgrid that are connected to the IC by the communication graph. The average voltage is then estimated by the following equation:

$$\overline{V_{IC}} = V_{IC} + \sum_{j \in N_{DC}} a_j \left(\overline{V_J} - \overline{V_{IC}}\right) \tag{5.14}$$

where a_j is the edge of the communication graph connecting the IC with other DGs, V_{IC} is the output voltage of the IC, and $\overline{V_{IC}}$, $\overline{V_J}$ are the estimated average voltage at the IC and the neighboring DGs in the DC subgrid, respectively. The difference between $\overline{V_{IC}}$ and V_{rated} is then passed through a PI controller to get the first correction factor (Δv_1^{IC}) of equation 5.13. This correction factor ensures the voltage of the IC output to be equal to the rated value.

The second correction factor (Δv_2^{IC}) in the equation 5.13 is responsible to maintain the scheduled power through the IC or maintaining the same per unit power sharing by all the DGs in the hybrid microgrid. When the IC is maintaining a fixed scheduled power,

www.manaraa.com

the difference between the actual delivered power and scheduled power is passed through a PI controller to get the second correction factor. The DCC in each individual subgrid ensures that the DGs are the sharing same per unit power in their respective grid. This realization is exploited in the case when the IC is maintaining the same per unit power for all the DGs in the hybrid microgrid. The difference between the per unit powers in DC subgrid and the AC subgrid is processed by a PI controller to get the second correction factor. Due to this correction factor, a small deviation in the IC output voltage from the rated value is observed. But this deviation is necessary in order to achieve the stated objectives. The update protocol for the second correction factor is described illustratively in Figure 5.3.

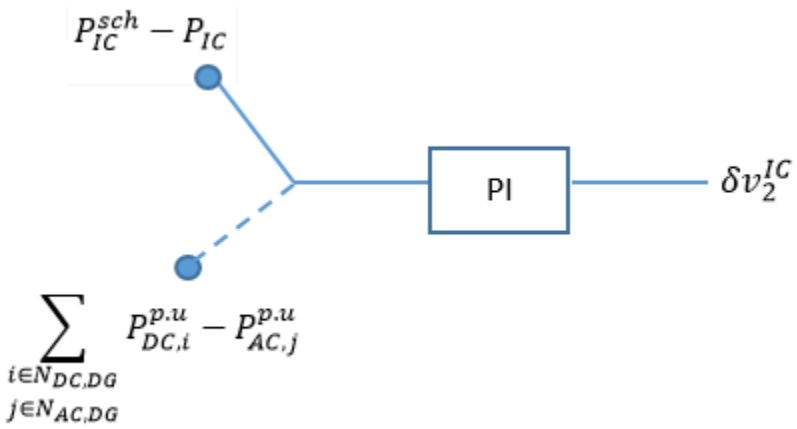

Figure 5.3: Calculation of second correction factor

When the IC is injecting power from the DC subgrid to AC subgrid, the reference frequency is updated according to the following equation to achieve the objectives for power management through IC:

$$\omega^* = \omega^{rated} + \delta v_2^{IC} \tag{5.15}$$

www.manaraa.com

Where δv_2^{IC} is calculated the same way it was calculated for the case of power flowing to the DC subgrid from the AC subgrid.

5.3 Simulation results:

In order to validate the proposed method, an AC/DC hybrid microgrid similar to the microgrid in Figure 5.1 was simulated in Matlab/Simulink. The hybrid microgrid has one AC subgrid and one DC subgrid and the subgrids are connected to each other through an IC. Each of the subgrids contains four DGs and local loads and the topology of the DC and AC subgrid are the same as the microgrids studied earlier in chapter 3 and chapter 4, respectively. The subgrids are controlled by DCC while the power management through the IC was done by the proposed method. Figure 5.4 shows the simulink model of the hybrid AC/DC microgrid. The following two case studies were considered to validate the proposed method:

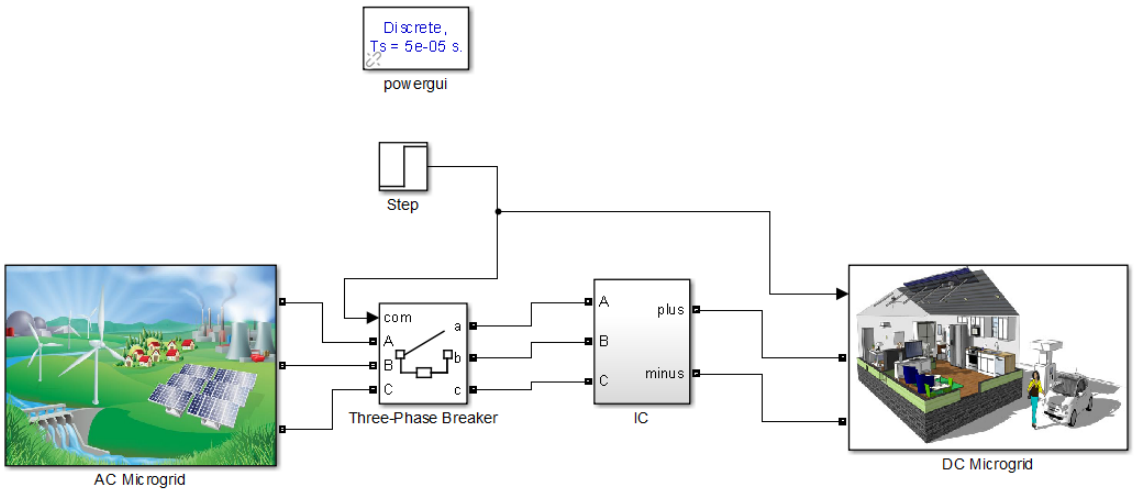

Figure 5.4: Simulink model of the AC/DC hybrid microgrid

www.manaraa.com

5.3.1 Case 1:

In this case, the hybrid AC/DC microgrid is assumed to be operating with the condition that a fixed scheduled power should flow through the IC. Figure 5.5 shows the performance of the proposed method. Initially the AC subgrid and DC subgrid were running separately and isolated from each other when the three-phase breaker was open. At t=1.5s, the breaker was closed, and a fixed 80 W power was scheduled to flow through the IC from the AC subgrid to the DC subgrid. It can be seen from Figure 5.5 (a) that the power through the IC changes to fixed 80 watt at t=1.5s without any severe transient. The power delivered by the DGs in the DC subgrid changes (Figure 5.5 (b)) as the DC subgrid is receiving extra power from the AC subgrid. The voltage profile of the DC subgrid remains at an acceptable limit which is evident from the Figure 5.5(b). The power delivered by the DGs at AC subgrid also changes in order to generate this extra 80 W power. At t=4s, an extra 200 W load was added in the DC subgrid to evaluate the dynamic performance of the controller. From the curves in Figure 5.5, it is clear that though there is an increase in the DC load, the power flow through the IC does not change.

www.manaraa.com

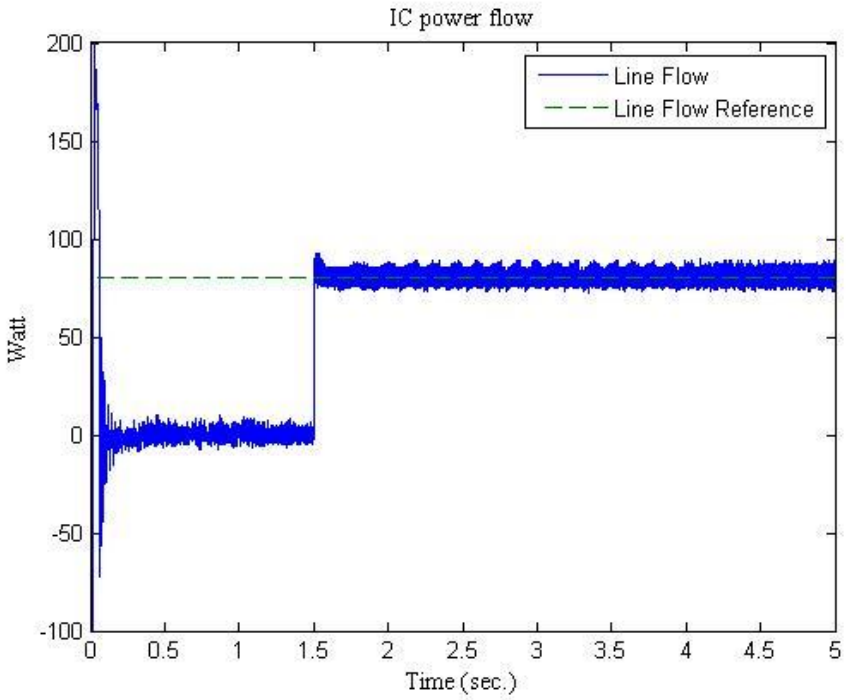

(a)

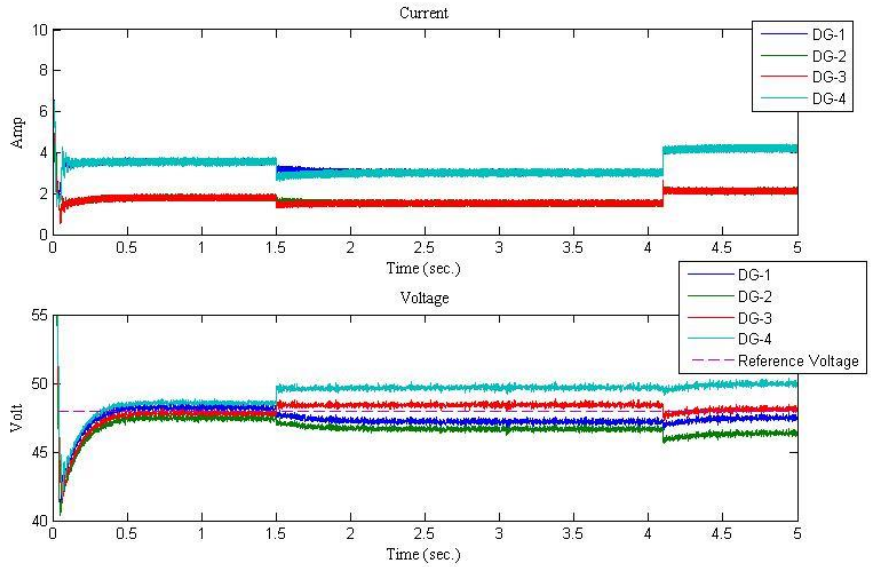

(b)

www.manaraa.com

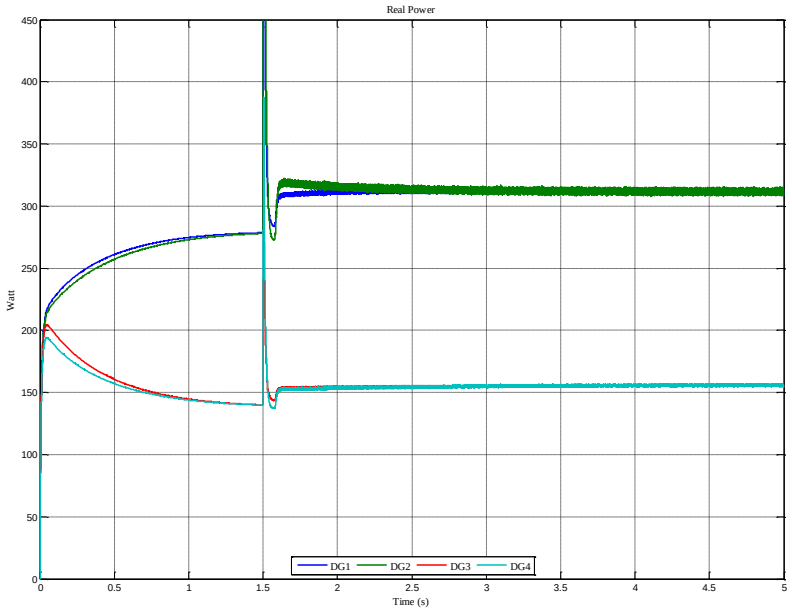

(c)

Figure 5.5: Performance of the controller under the condition of fixed scheduled power through the IC

5.3.2 Case 2

This case simulates the scenario where all the DGs in the hybrid AC/DC microgrid share the power according to their ratings. The DGs in the AC subgrid and DC subgrid have different ratings and the subgrids were loaded with different local loads. Figure 5.6 (a) shows the per unit power delivered by the DGs connected at the DC subgrid and Figure 5.6(b) shows the per unit power delivered by the DGs connected to the AC subgrid. From these curves, it is clear that the DGs are sharing the same per unit power irrespective of their location. At t=2s, an extra 200 W load was added in the DC subgrid in order to verify the dynamic performance of the controller. From the curves, it can be seen that the increased load was equally shared by all the DGs. Figure 5.5(c) shows the

www.manaraa.com

power flow through the IC under a varying load when the DGs were sharing power proportional to their ratings.

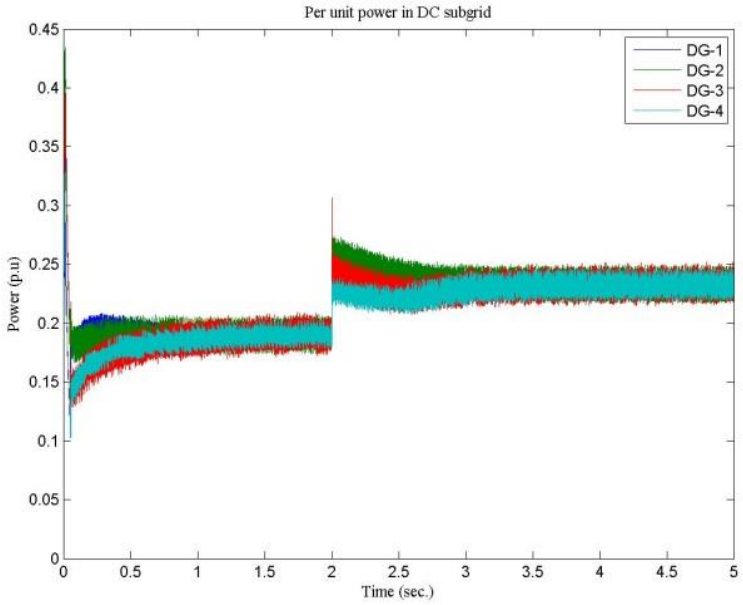

(a)

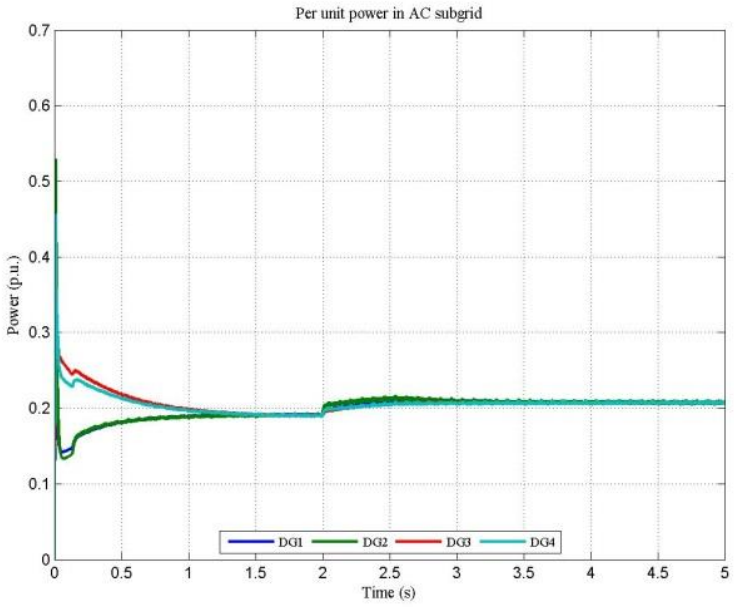

www.manaraa.com

(b)

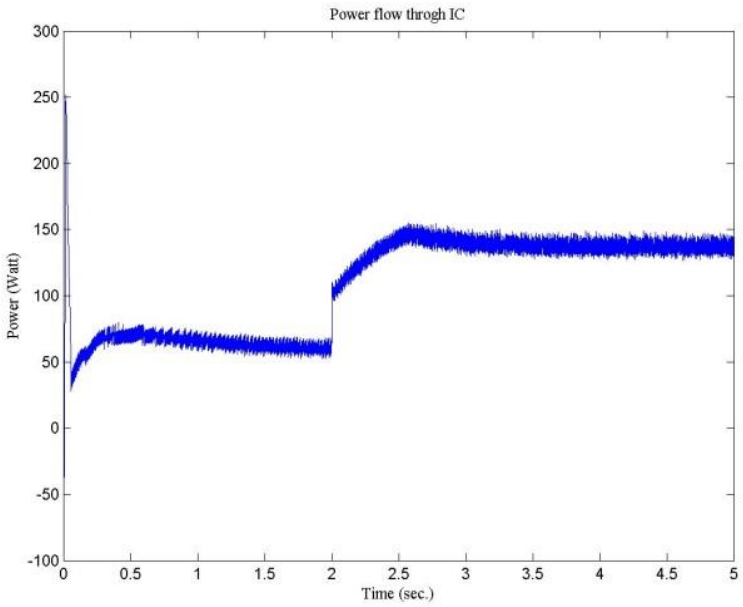

(c)

Figure 5.6: Performance of the controller to share the load among the DGs in a hybrid microgrid according to the power rating

www.manaraa.com

Chapter 6

Microgrid Laboratory Prototype

6.1 Overview

The types of hardware and their configurations in most of the Microgrid testbeds are often fixed and require a good amount of work and time to change or upgrade the hardware setup. These fixed-hardware microgrid testbeds are suitable for a limited number of experiments; and cannot provide the platform to carry on a wide variety of studies. The interactions between distributed generators (DGs) in a microgrid and the grid can be very complex. The microgrid testbeds to study grid-connected mode of operation are mostly connected with the utility. This approach also limits the number of plausible grid condition scenarios that can happen under different conditions. In order to address the aforementioned issues about laboratory scale microgrid testbeds, as a part of the present research work, a highly flexible, scalable multifunctional microgrid testbed is developed at the Power Electronic Research Laboratory (PERL), University of North Dakota (UND). The PERL Microgrid (P-MG) offers a platform for Microgrid research with the following characteristics:

- A flexible, scalable design for the power network components and communication network.

www.manaraa.com

- Programmable AC/DC sources and loads to emulate a wide range of DGs and load profiles.
- Integration and verification facility for new control algorithms, and energy management systems (EMS).
- Verification platform for practical issues related to islanded mode of operation.
- Development and verification platform for new hardware solutions for microgrid/smart grid.
- Verification platform to test and enhance microgrid standards.

6.2 Overview of the components in the PERL-Microgrid (P-MG)

The P-MG was developed to conduct integrated hardware-software research in a laboratory environment on renewable energy integration, microgrid operation and control of smart grid applications. Though an integrated hardware-software research on microgrid requires full access to both the hardware and software components of the testbed, most of the microgrid facilities reported in the literature provide limited access to the hardware components. A unique characteristic of the P-MG testbed is that many of the components of the testbed were designed and built in house at the PERL laboratory and provide a high degree of accessibility. This section describes the design and development steps of all of the hardware components of the P-MG. Figure 6.1 shows partial view of the implemented AC microgrid and Figure 6.2 shows the implemented DC microgrid in the P-MG.

www.manaraa.com

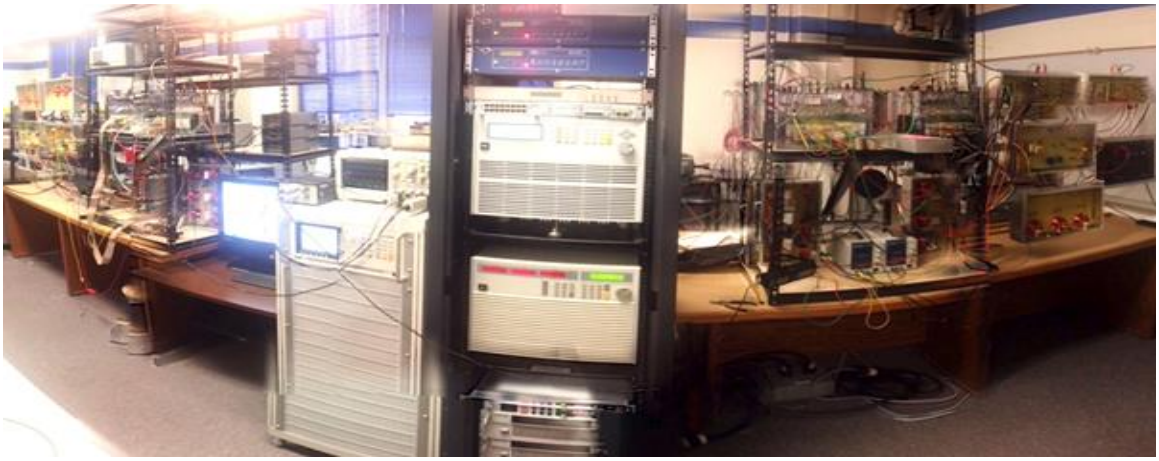

Figure 6.1: Hardware side of AC microgrid in the P-MG showing the inverters, filters, lines and power sources. The controller computers are located on the other side.

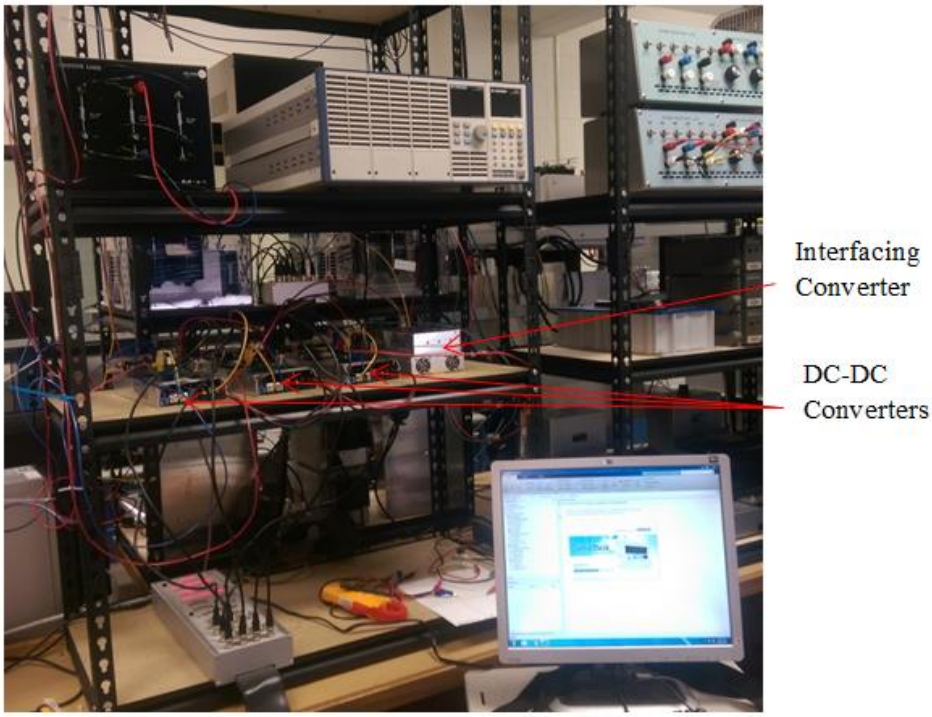

Figure 6. 2: P-MG DC microgrid showing the interfacing converter, DC-DC converter and the dSPACE to control the DC microgrid

www.manaraa.com

6.2.1 Renewable energy source models:

The P-MG testbed provides the platform for testing techniques for integrating hybrid renewable energy sources into microgrids. Programmable DC power supplies and AC power supplies were used for emulating various renewable energy sources in the P-MG. Programmable power supplies that are used in P-MG in order to emulate the renewable energy sources are: two SL-series (Model No. SL200-13/208+GPIB) magna-power programmable DC power supplies [72], one XANTREX (Model No. XDC 60-100) digital DC power supply [73] and one Chroma programmable AC power source (model no. 61612) [74]. The magna power supplies can produce voltages up to 200VDC with a maximum current of 13Amps. They come with external 37-pin I/O isolated analog and digital controls which can map all the monitoring and programming functions in a standard DG-37 connector arrangement. An IEEE-488 GPIB communication interface is also present for communicating with the remote interface software. The XANTREX power supply can be remotely controlled using 0-5V or 0-10V signals via a remote analog programming interface or a remote terminal using RS-232 and IEEE 488.2 (GPIB) protocols. The voltage rating of the XANTREX power supply is 0-60VDC and the current rating is 0-100A with a 6KW power rating. The Chroma programmable AC power supply can deliver up to 300V AC with output frequencies from 15Hz to 1500Hz with power a rating of 18KVA. The power supply can be used to compose different harmonic components to synthesize various harmonic distorted waveforms. The AC power supply comes with IEEE 488.2 GPIB, RS-232, USB and Ethernet interfaces in order to control the power supply remotely. Renewable energy sources in the P-MG are

www.manaraa.com

solar photovoltaic, wind, and fuel-cell technologies. Details of these emulators are described below:

6.2.2 Photovoltaics (PV) simulator

There are numerous photovoltaics power systems in the market each having its own dynamics and steady-state characteristics. Testing actual solar power systems is costly and highly dependent on weather conditions [75]. That is why a simulator which can confidently emulate the behavior of different photovoltaics power systems is a more attractive choice for a microgrid testbed facility such as P-MG.

The Magna-power and XANTREX DC power supplies are used for emulating the current and voltage characteristics of PV panels. A lookup table in a data memory [76][77] or equations describing the semiconductor physics can be used to simulate the behavior of PV panels [78]. The following $I-V$ chareacteristic equation is used at P-MG for PV emulation representing a practical PV array [79]:

$$I = I_{PV} - I_0\left[e^{\frac{V+R_S I}{V_t a}} - 1\right] - \frac{V+R_S I}{R_p} \tag{6.1}$$

where I_{PV} and I_0 are the panel and saturation currents of the PV array, respectively. The thermal voltage of the array when N_s cells are connected in series is defined by $V_t = \frac{N_s kT}{q}$, q is the electron charge, k is Boltzmann constant, T is temperature in Kelvin, R_s is the equivalent series resistance of the array, and R_p is the equivalent parallel resistance. The DC power supplies can reliably produce the static and dynamic behavior

www.manaraa.com

of arrays of solar cells with different configurations under varying weather and load conditions.

6.2.3 Energy storage systems (ESS) simulator

Since ESSs are relatively expensive, using real ESSs for testing different charging/discharging algorithms and circuits is uneconomical [80]. Equations 2 to 4 were used to emulate the $I-V$ characteristic of an ESS such as batteries [81] with the programmable DC power supplies:

$$SoC(t) = SoC_{initial} - \frac{1}{C_{max}}\left[\int i_{cell}(t)\,dt + C_{unav}(t)\right] \tag{6.2}$$

$$V_{oc}[SoC(t)] = a_0 e^{-a_1 SoC(t)} + a_2 + a_3 SoC(t) - a_2 SoC^2(t) + a_5 SoC^3(t) \tag{6.3}$$

$$V_{cell}(t) = V_{oc}[SoC(t)] - i_{cell}(t).R_{series} - V_{trans}(t) \tag{6.4}$$

where $SoC(t)$ and $SoC_{initial}$ are the present and initial state of charge (SoC) of the battery, $V_{oc}[SoC(t)]$ is the SoC dependent open circuit voltage, V_{cell} is the terminal voltage of the ESS, i_{cell} is the battery current, C_{max} and C_{unav} are maximum and unavailable capacity of the ESS. The battery model updates the output voltage by taking measurements of load current to reflect the charging/discharging mode of the emulated battery. The ESS emulator can successfully mimic the behavior of ESS at different age, temperature and state-of-charge (SoC) conditions reducing the development cost and preventing safety hazards.

www.manaraa.com

6.2.4 Fuel Cell system emulator:

The static voltage-current relationship of proton exchange membrane (PEM) fuel cell system was defined as [82][83]:

$$V = f(I) = \beta_3 I^3 + \beta_2 I^2 + \beta_1 I + \alpha_{\beta 0} \tag{6.5}$$

where V is the fuel cell output voltage, I is the fuel cell output current and $\beta_3 - \beta_0$ are the co-efficient of the static $V - I$ relationship. The fuel cell simulator describes the static and dynamic characteristics of a PEM fuel cell. The $I - V$ characteristic model is implemented with the programmable DC power supplies.

6.2.5 Wind energy system simulator and grid simulator

The Chroma programmable AC power supply is used to simulate grid [84] and variable frequency wind energy systems. As the Chroma power supply can produce AC power with variable frequency and voltage amplitude, it can be programmed to emulate wind power system for a wide variety of weather condition. The ability of the Chroma power supply to generate fixed frequency and voltage AC power makes it suitable for grid emulators as for most practical purpose the grid is assumed to be an infinite bus. Furthermore, predefined harmonics can be added to the AC power from the Chroma power supply when presence of harmonics is required for the experimental purpose.

www.manaraa.com

6.3 Power electronic Converter

All the emulated DGs in P-MG are connected to the microgrid through power electronic interfaces. The power generated by the PV, fuel-cell and ESS emulators is converted from DC to AC by DC-AC inverters before being connected with the AC network. The DC loads connected in the AC microgrid are fed by AC-DC rectifiers. There are four Semikron 3-phase converters in P-MG that can be used as both DC-AC controllable inverter and AC-DC controllable rectifiers. The converters also come with integrated three phase AC-DC diode rectifiers as can be seen in Figure 6.3(b). The maximum current rating for the converters is 30A for both the rectifier and inverter operation, maximum allowable DC rectifier output voltage is 600V DC and allowable AC IGBT inverter output is 400VAC [85]. The control algorithms for inverter operation are implemented in ControlDesk software for dSPACE to produce the required PWM signals. The PWM gate drive signals for the inverters are generated by dSPACE which produces the gate drive signals in the range of 0-5V but the voltage requirement for the Semikron inverter gate signal is 0-15V. In order to match the voltage requirement for the gate drive signal, a Gate-drive circuit, shown in Figure 6.4, was built at P-MG to amplify the signal coming from dSPACE. Opto-couplers (FOD 3120) were used to amplify the gating signals coming from dSPACE. The optocouplers also provides over-current protection for the dSPACE by electrical isolation. In order to test the MPPT algorithms on the renewable energy source output, the P-MG also has some DC-DC buck converters and DC-DC boost converters.

www.manaraa.com

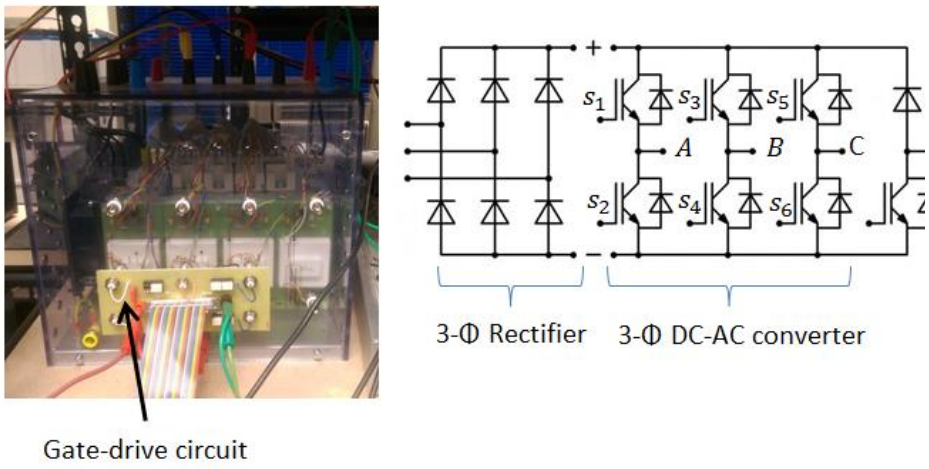

Figure 6.3: Semikron AC-DC converter used in P-MG and its internal power stage a) Semikron converter with custom built gate-drive circuit, b) diode-rectifier and DC-AC converter power stage

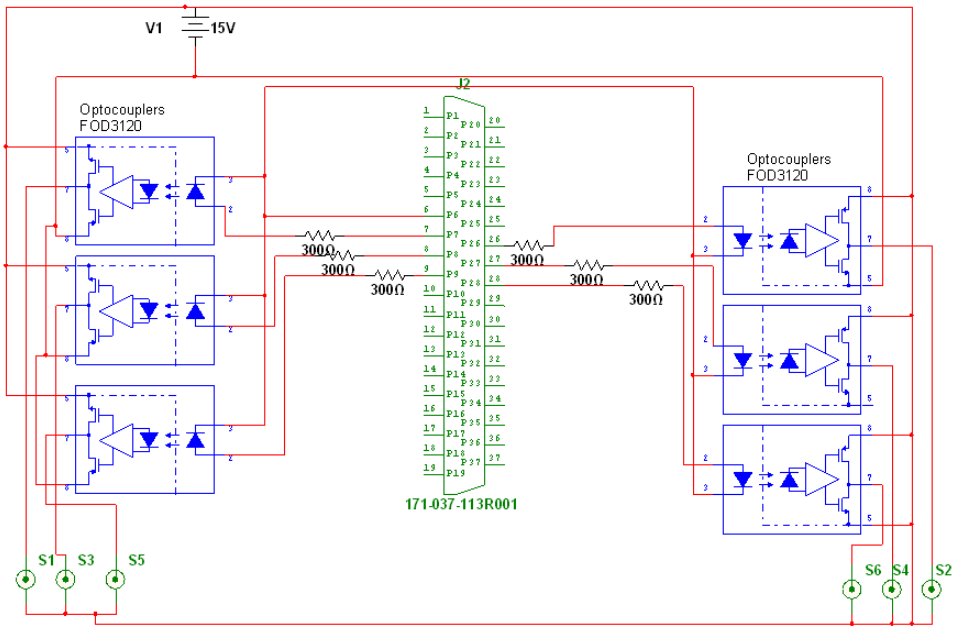

Figure 6.4: Gate drive signal amplifier circuit for the Semikron inverters

www.manaraa.com

6.4 Filters

Pulse-width-modulated (PWM) front-end voltage source inverters (VSIs) and current source inverters (CSI) are used in the AC Microgrid testbed to integrate RESs which are DC source in nature. An inductor is the simplest form of a filter that can be used between the PWM VSIs and the Microgrid to eliminate the switching harmonics. Size, cost of the inductance, and the maximum allowable DC voltage are some of the factors that prohibit one from the use of pure inductive filters [86]. An LCL filter is a better solution for this kind of applications as it offers a lower cost, size and higher harmonic attenuation in the lower switching frequency range. The parameters for the LCL filter used in this Microgrid was designed following the design steps described in [87]. Air-core inductors were chosen for the filter for better heat dissipation while eliminating hysteresis and any type of saturation distortions [88]. Polypropylene capacitors were selected for good high frequency and high voltage capabilities. The whole filter was soldered on a perforated prototype board. Hall effect transducers from LEM (LA 25-NP for current and LV-25-p for voltage) were used in the filter for the measurement of current and voltage. The assembled filter with measurement sensors is mounted on an aluminum box with plastic spacers for electrical clearance. This filter-box, shown in Figure 6.5(a), can easily be placed in the microgrid or can be replaced by another filter with different parameters. Figure 6.5(b) shows the response of the designed filter to eliminate the 10K Hz PWM switching frequency harmonics of the VSIs.

www.manaraa.com

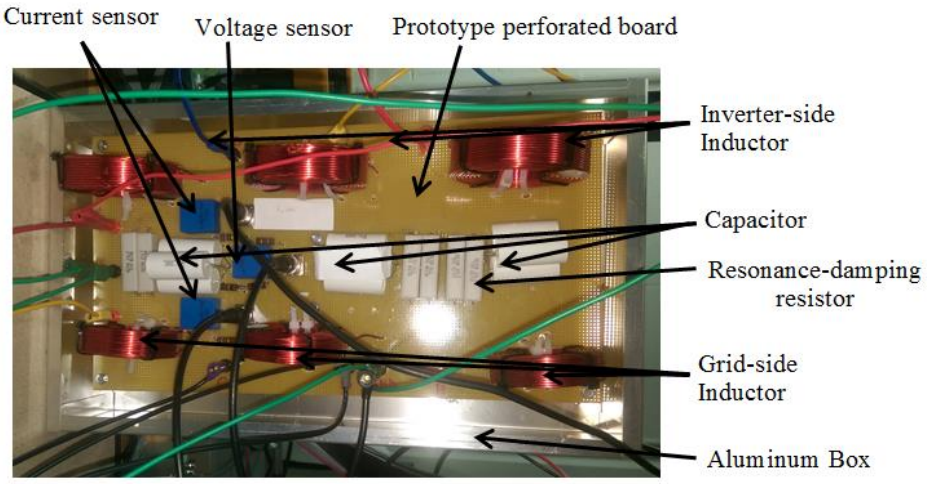

(a)

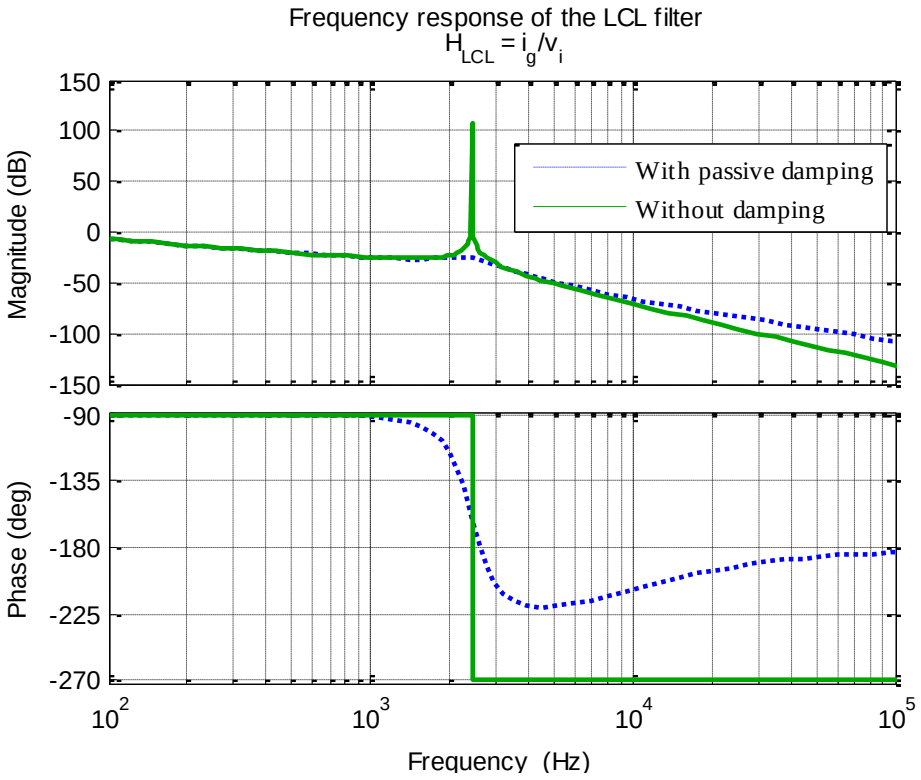

(b)

Figure 6.5: LCL filter used in P_MG a) close view of the filter built at P-MG b) Frequency response of the filter.

www.manaraa.com

6.5 Microgrid distribution network model

One of the main objectives of the P-MG testbed is to perform experiments on different Microgrid network topologies. In order to achieve that objective, three phase distribution line models having appropriate X/R ratios were designed. Each of the phases of the distribution line model contains 1-mH inductor with X/R ratio close to an actual distribution network [89]. Over-current protection for each of the phases of the distribution line models is achieved by fuses. Moreover, remotely controllable three-phase electromagnetic relays are used to close or open the lines in order to control the power flow of the microgrid and the topology modification. The lines are terminated with 1-nF capacitances on both ends essentially forming a π-model to be more realistic. The distribution line models and their protection systems are soldered on perforated prototype boards and the assembled lines and protection systems are mounted on aluminum boxes as can be seen in Figure 6.6. This arrangement of the distribution lines provides a high degree of reconfiguration capabilities.

www.manaraa.com

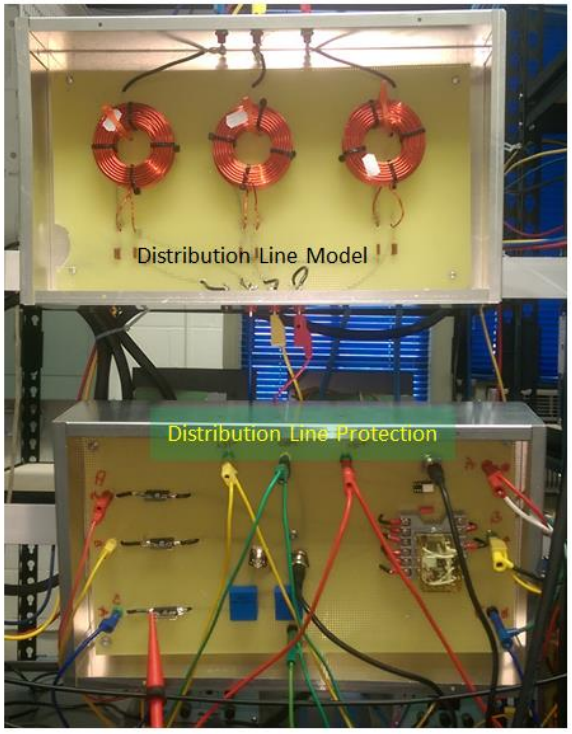

Figure 6.6: The distribution lines built for P-MG following pi-model. The top box contains a line model and the bottom box contains the fuses and electromagnetic relays for protection.

6.6 Load model

The P-MG has different types of loads to test different scenarios as those in actual Microgrids. The loads used in the Microgrid can be grouped into two categories: 1) passive loads, and 2) active loads. Figure 6.7 shows the loads that are being used in P-MG. The active load modules consist of one Chroma High Power DC Electronic Load (model 63203), BK precision DC electronic load (MDL305), one Chroma AC/DC Electronic Load (model 63803) and two induction motor-generator sets. The voltage range for the Chroma AC/DC electronic load is 50V~350Vrms with a power rating of 3.6KW. They can be put in parallel or 3-phase configuration. The DC loading of the AC/DC loads can be constant current (CC), constant impedance (CR), constant voltage

www.manaraa.com

(CV) and constant Power (CP) while in AC loading mode, they can operate in constant power and rectified load modes [90]. The loads can be controlled by a computer programmatically through GPIB and RS-232 interfaces. The high power DC Electronic Load has a rating of 2.6KW, 0~80V and up to 1KA. This load can be tested with CC, CR, CV and CP load modes. For testing of dynamic loadings, there are two induction motor-generator sets whose load can be changed dynamically.

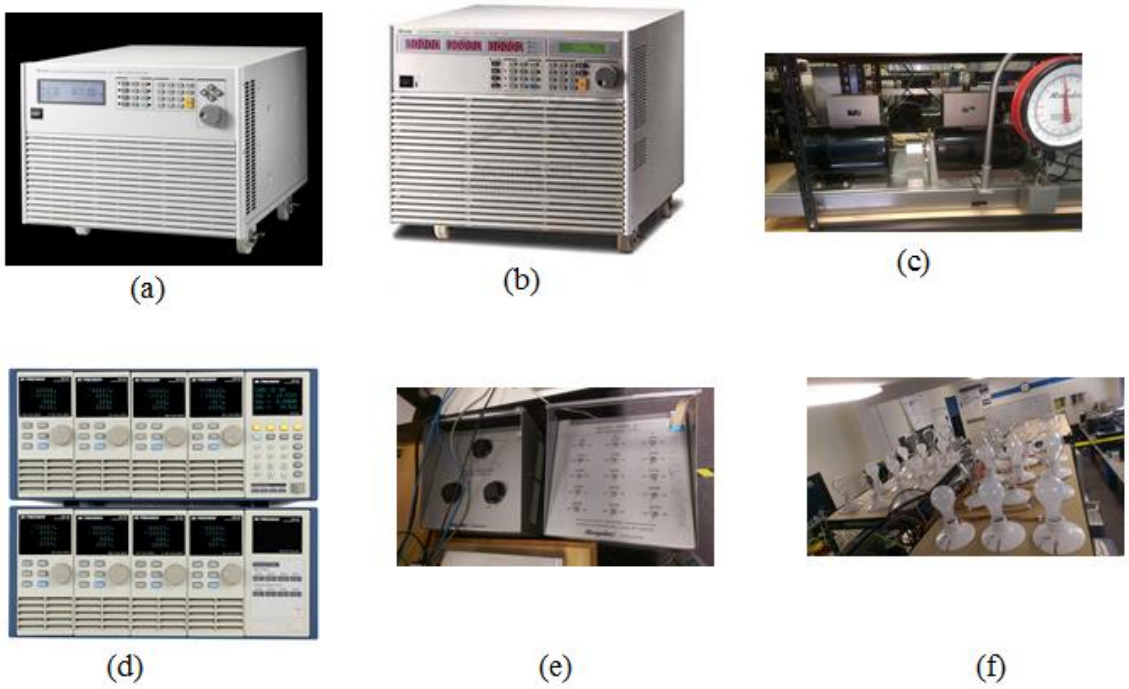

Figure 6.7: Active and passive loads used in P-MG. a) Chroma AC/DC Electronic Load (model 63803) b) Chroma High Power DC Electronic Load (model 63203) c) induction motor-generator set d) BK precision DC electronic load (MDL305) e) three-phase resistive load bank f) lighting load bank

In addition to the active loads, passive three-phase resistive load banks and inductive load banks are also available in the laboratory to test varying loading conditions. A resistive load can vary from 50W to 1.05KW at various steps while the inductive load bank can be varied from 75 mH to 550mH. Additional lighting loads were designed and

www.manaraa.com

built in the laboratory; the lighting loads can be turned on or off sequentially to mimic the behavior of actual loads.

6.7 Real-time data communication control platform

Real-time data acquisition and control of the inverters in the Microgrid are done by the dSAPCE DS1103 PPC controller board and DS1104 R&D Controller Board as shown in Figure 6.8. The controller boards have real-time interfaces and are fully programmable with Matlab/Simulink. The DS1103 board has 36 A/D channels, 8 D/A channels, internal PWM signal generator and a DSP controller unit built around Texas Instruments' TM320F240 [91]. A PWM signal amplifier designed in the P-MG amplifies the PWM signals coming from the dSPACE and provides the required firing signals to gates of the inverters. Closed loop (compensated) hall effect transducers [92]-[93] are used for voltage and current measurements. The transducers provide very good linearity and an excellent accuracy. An additional PCI6024e card from National Instrument (NI) is used to visualize the topology of the Microgrid in real time. PCI6024e card collects the connection status of the DGs in the Microgrid and updates the topology mapping of the Microgrid in real time. PCI6024e is a low cost data acquisition device having 16 analog inputs at up to 200KS/s, 2 analog outputs, 8 digital I/Os and is ideal for high speed data logging in control applications [94].

www.manaraa.com

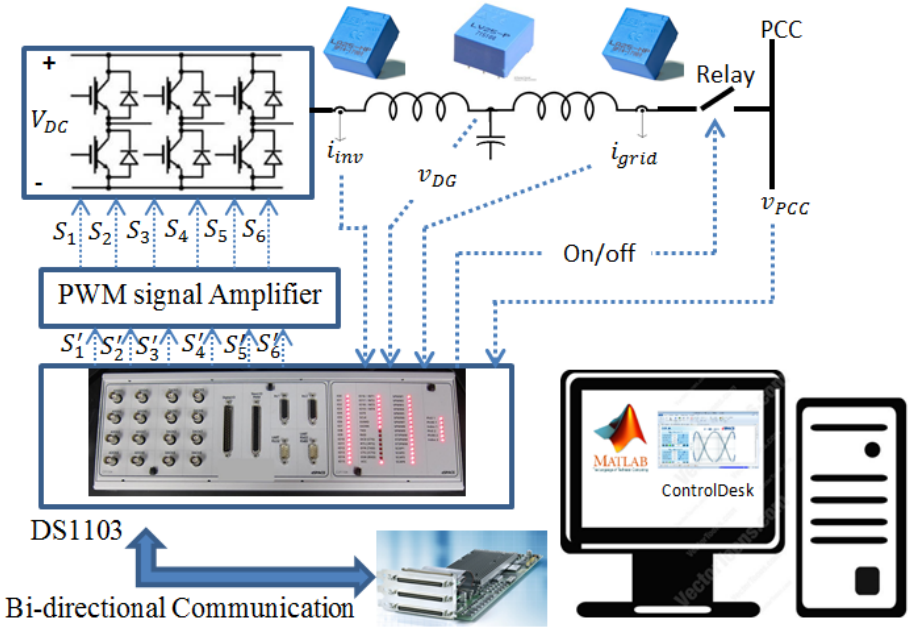

Figure 6.8: Real-time data communication for control and monitoring using dSPACE ds1103.

6.8 Microgrid software architecture

The Microgrid has three layer of controllers for its operation and control. Different controllers (discussed in detail in the following section) of the Microgrid were implemented using different software platforms. The DG emulators used in the Microgrid are essentially programmable AC/DC power supplies which can be programmed to emulate a wide variety of DG sources. The capability of the TI's Labview in its graphical programming syntax for visualization, creating and coding engineering systems [95], availability of Labview drivers for Magna-Power DC power supplies [96] and Labview drivers for Chroma ATE chr616xx Power Supply [97] made Labview an ideal candidate for the software development platform of P-MG to control the DG emulators. Complex voltage-current relations as described in section 6.2 were implemented in Labview to

www.manaraa.com

mimic the behavior of DG sources. Separate Graphical User Interfaces (GUIs) were developed for each of the DGs. The initial design, tuning and verification of the controllers for the inverters were done in Matlab/Simulink environment with off-line simulation. Then the designed controllers were converted to C-programming code which was then compiled and built in order to be compatible with ControlDesk of dSPACE. ControlDesk is the dSPACE's modular experimental and instrumentation software for electronic control unit (ECU) development [98]. Using the DS 1103 or DS 1104 boards for data acquisition, ControlDesk performs real-time computations on the developed controller, computes the necessary control signals and transmits again the computed control signals in real-time to the physical systems. A graphical user interface (GUI) built around ControlDesk allows the user to run the inverters in standalone, set reference values, log the measured and calculated data and tune the control parameters. Software, called Remote Monitor (RM), is also developed to remotely monitor the performance and topology of the Microgrid. The RM program can take relay status, different analog values in real time from different sources and then update the topology mapping of the Microgrid accordingly. RM was developed in the Labview environment. A summary of the software architecture developed for the P-MG can be seen in Figure 6.9.

www.manaraa.com

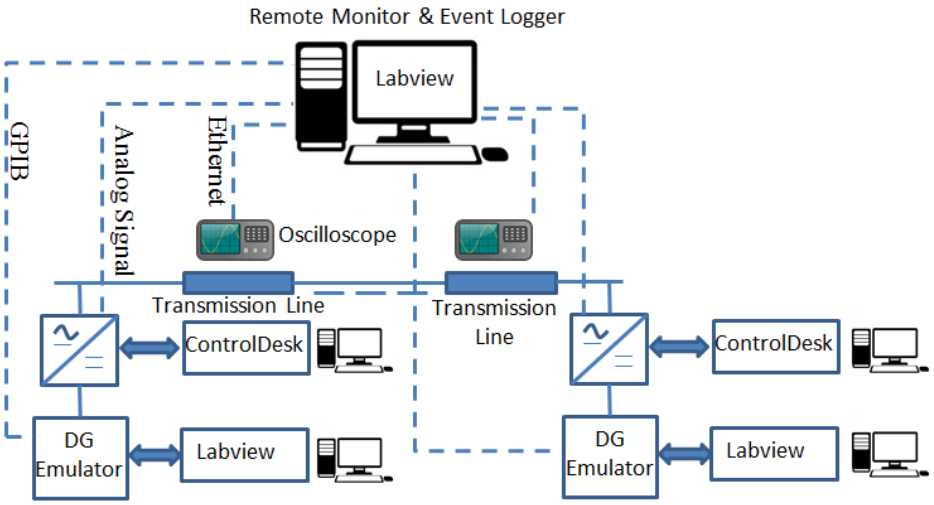

Figure 6.9: Software platforms used in P-MG to developed different application software

6.9 Microgrid Power Network architecture

P-MG is designed to study hybrid renewable energy sources supplying power through power electronics converters. Connecting the DGs with the Microgrid through Power Electronics converters has several benefits, such as control of active and reactive power, ride-through capability in low voltage networks and reactive power injections during fault conditions [51]. Four Semikron inverters are used for the AC Microgrid to connect different sources. The DG emulators described in section 6.2 can be connected to the DC sides of the inverters as power sources or real DGs, i.e., PV, wind, and fuel cells can be directly connected to the DC side. On the AC side, each of the inverters is followed by an LCL filter to eliminate switching harmonics. For greater flexibility of operation and topology configuration of the Microgrid, the inverter-LCL filter set has one synchronizer unit (SU) with the required measurement sensors and electromagnetic

www.manaraa.com

relays. SU provides the options for easily connecting and disconnecting each of the DGs to the Microgrid; thus different topologies are realizable for the Microgrid. Figure 6.10 shows a typical power network topology used in the P-MG.

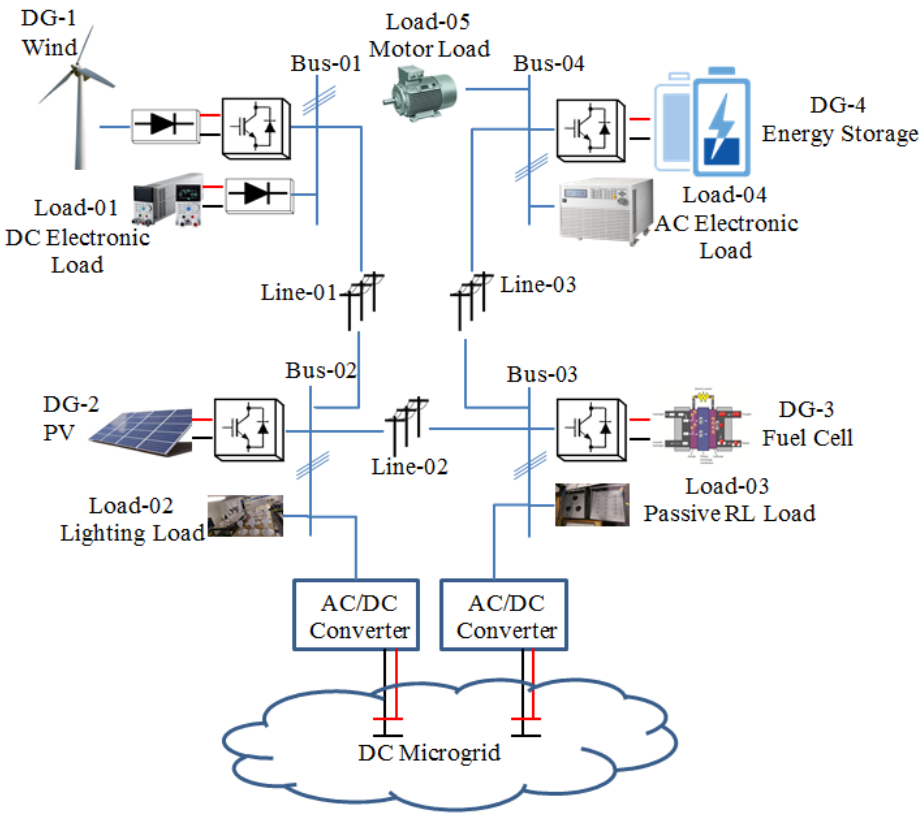

Figure 6.10: A typical multi-bus power architecture of P-MG with different DGs and loads connected at different buses.

Physical models of distribution lines developed at P-MG Microgrid add another configurability of the system. The line models can be easily modified to represent actual varying length of distribution lines; thus experiments done on the Microgrid can be very close to a Microgrid in real world. The modularity of each component in the Microgrid offers options to experiment with a variety of topologies. The DGs can be connected to the system in a single bus topology or multi-bus topology as depicted in Figure 6.9 which

www.manaraa.com

is the typical power architecture for the P-MG. This approach also allows to study Microgrid clusters where each Microgrid can share power with their neighboring Microgrid depending on the shortage or surplus of power [99] while maintaining its own voltage and frequency. In order to perform studies on hybrid AC/DC microgrid systems, a DC microgrid development program has been initiated at the P-MG laboratory.

6.10 Microgrid control architecture

Microgrids are small scale power systems having the capability of operating in grid connected modes or islanded modes with DGs, and ESS as power sources which are connected to the loads distributed in a small geographical area through distribution lines [100]-[101]. One of the future electric power system (EPS) requirements will be to ensure Microgrids can operate in an islanded mode from the main grid powering the islanded EPSs [102]. The P-MG is designed to study plausible scenarios that can occur in a real situation of future EPSs. The following section describes the control algorithms used for operation of the converters and the microgrid.

6.10.1 Control of the converters

There are three modes of operation for the converters in a P-MG: 1) grid forming, 2) grid feeding, and 3) grid supporting [103]. Grid forming converters are more like ideal voltage sources with low output impedance with controllable output voltages and frequencies. Grid forming converters are essential for islanded mode of operation. Several grid forming inverters can operate in parallel, such as in droop control described later in this section, or one grid forming converter can be used to set the reference voltage

www.manaraa.com

and frequency for rest of the Microgrid such as in master-slave mode of operation. The grid feeding inverters are current sources with high parallel output impedance. These inverters can inject pre-specified real and reactive powers into the Microgrid with no control over the voltage and frequency. Hence they cannot operate in stand-alone mode and require at least one grid-forming inverter in the microgrid. The operation of grid-supporting inverters is basically in-between the grid-forming inverters and grid-feeding inverters. They act like current sources to supply active and reactive powers with voltage and frequency regulatory functions. They can adjust their real and reactive power set point to support the voltage and frequency of the Microgrid.

Low level controllers such as voltage controllers and current controllers described in Chapter 4 are responsible for controlling the local output variables, i.e., voltage, current and frequency. These controllers have high bandwidths and fast response times. Higher level controllers are required to maintain stability of the system as well as proper power sharing of the DGs.

6.10.2 Control of the Microgrid

Large percentage of renewable energy source integration into a system requires an accurate control of voltage and frequency for reliability and stability purpose[104]. Proper sharing of real and reactive powers among DGs connected to the Microgrid is one of the major objectives of the Microgrid operation. The controllers that can achieve that objective can be classified into three groups: droop control, centralized control, and distributed control. Droop control is the most popular controller used for Microgrid operation due to the benefits of higher reliability and no requirements of communication

www.manaraa.com

networks. The primary power sharing controller used in P-MG is the droop-based controller described in Chapter 4. Voltage-Var droop control ensures that the more a DG supplies reactive power to the network, the more the voltage set point for that DG is reduced. Properly selected droop parameter also reduces the circulating current among the parallel DGs connected to the Microgrid [104]. The real power-frequency droop enables the DGs to share real power proportional to the frequency-active power droop parameter.

6.10.3 Phase-locked-loop (PLL) and Synchronization

Synchronization is an important aspect in the accurate operation of Microgrids both in grid-connected mode and islanded mode. The controllers for the grid-feeding and grid-supporting inverters require accurate information about the voltage and frequency of the Microgrid or the grid in order to inject power to the system. Connection and disconnection of the inverters from the grid also demand precise information on the grid. During a synchronization process, the voltage, frequency and voltage angle of the incoming inverter are slowly changed to synchronize with the point of common coupling (PCC). A running-average filter (RAF) based enhanced phase-locked loop (E-PLL) was developed for the synchronizer used in P-MG. Figure 6.11 shows the details of the designed E-PLL.

www.manaraa.com

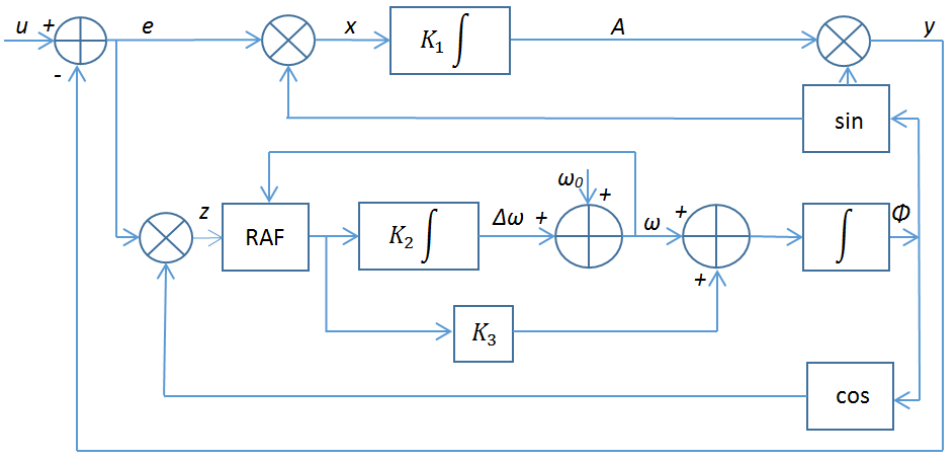

Figure 6.11: Running average filter (RAF) based enhanced PLL (E-PLL)

The DGs used in the Microgrid can be running in stand-alone mode or can be a part of a larger network. Connecting the DG at PCC of the network without synchronization of voltage, frequency and phase angle of the DG and PCC will result in high transients, i.e., sudden voltage and current changes [105]. The synchronization strategy adopted in the P-MG is described by Figure 6.12. The connection and disconnection of a DG from the network is done by a relay which acts as a static transfer switch (STS). The voltage at the both ends of STS is measured and transferred to the synchronization controller by a low bandwidth communication link provided by the analog-to-digital converter (ADC) of dSPACE. When the synchronizer is activated, it adds corrective components to the voltage and frequency reference values that are coming from the post synchronization controller (PSC) to make the differences between voltage, frequency and phase angle limits of the DG output and PCC acceptable. A synchronization check block monitors the measured values at PCC and DG output and sends a closing signal to the relay once the conditions of equation (6.6) are met; at the same time K_1, K_2, K_3 and K_4 switches are

www.manaraa.com

opened. The synchronization criteria described by equation (6.6) was adopted from the IEEE Standard 1547-2003.

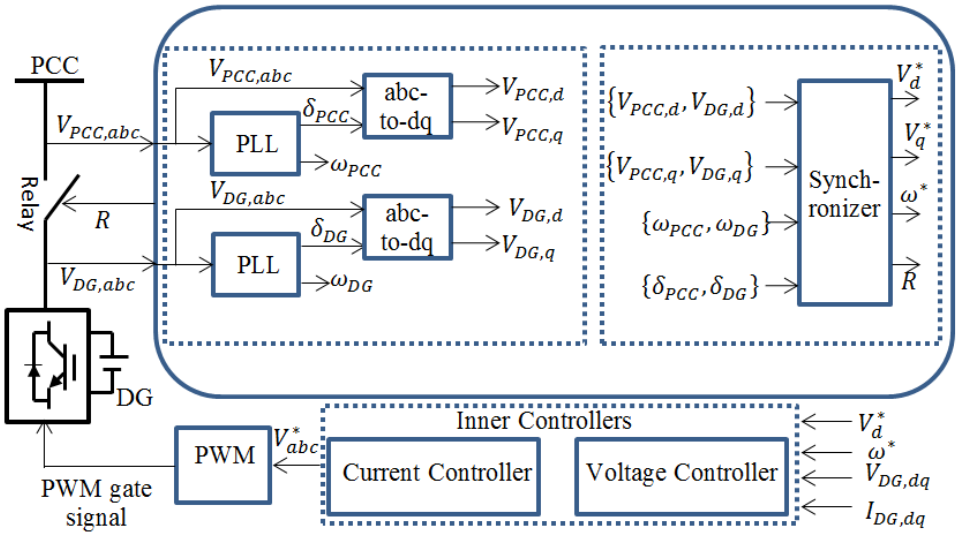

(a)

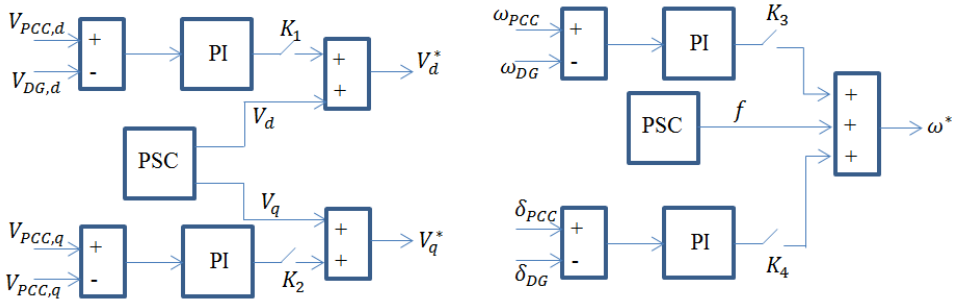

(b)

Figure 6.12: Details of the synchronization scheme used in P-MG a) shows the information flow from and to different blocks in the synchronization scheme b) voltage, frequency and phase angle adjustment approach used in the synchronizer

$$\begin{cases} |V_{PCC,d} - V_{DG,d}| \le 0.1 \times V_{PCC,d} \\ |V_{PCC,q} - V_{DG,q}| \le 0.1 \times V_{PCC,q} \\ |\omega_{PCC} - \omega_{DG}| \le 1.9 \\ |\delta_{PCC} - \delta_{DG}| \le 10^0 \end{cases} \quad (6.6)$$

www.manaraa.com

where $V_{PCC,d}$, $V_{DG,d}$, $V_{PCC,q}$, $V_{DG,q}$ are the d-axis voltage at PCC, d-axis voltage of the DG, q-axis voltage of PCC, q-axis voltage of the DG, respectively. ω_{PCC} and ω_{DG} are the frequency of the voltage at PCC and the frequency of DG output voltage, respectively. And $\delta_{PCC}, \delta_{DG}$ are the phase angle of the voltage at PCC and the phase angle of DG output voltage respectively.

www.manaraa.com

Chapter 7

Experimental Verification

The purpose of the P-MG is to study various aspects of renewable energy integration through power electronic interfaces, microgrid operation under various scenarios and energy management of microgrid. The high degree of reconfiguration capabilities and easy access to almost all hardware and software components of the system make the P-MG setup an ideal platform for control strategy verification, microgrid optimization algorithm evaluation and microgrid topology planning. To demonstrate that the designed P-MG can perform these tasks, several experimental tests were performed on the microgrid. Figure 7.1 shows the ring-bus topology of the microgrid that was used to carry out several experiments:

www.manaraa.com

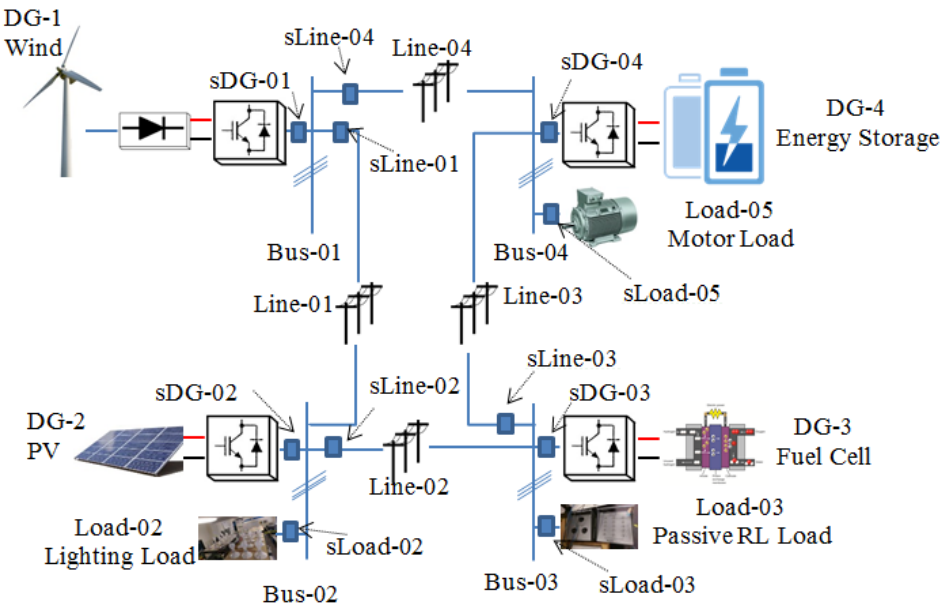

Figure 7.1: Experimental topology

7.1 Case 1: System start-up and steady-state operation

The topology in Figure 7.1 was selected for this study. The experiment was divided into two steps. First, all the DGs were started individually with no connection from other DGs. This scenario can be observed over the duration of T1 in Figure 7.2. The DGs are supplying their own local loads during T1 period. The outputs of the PLLs are oscillating around their last measured values if there are no input signals for the PLLs. For this reason, there is some noise in the frequency when the respective DGs are not started. The voltage values are shown in per unit for better clarity. The DGs have different voltage set points close to their nominal value when they are not connected to each other. After T2 interval, DG-1 and DG-2 are synchronized, they were put in a droop controlled mode and their droop parameters were set to be equal so that they share the same power. Similarly,

www.manaraa.com

at the end of T3, DG-3 was synchronized and at the end of T4, DG-4 was synchronized. All the DGs had the same droop co-efficients so that they share an equal power. During the duration of T5, the Microgrid is in steady-state mode with all the DGs synchronized to same frequency while the voltage droop was chosen differently so that they have the same voltage level close to nominal value.

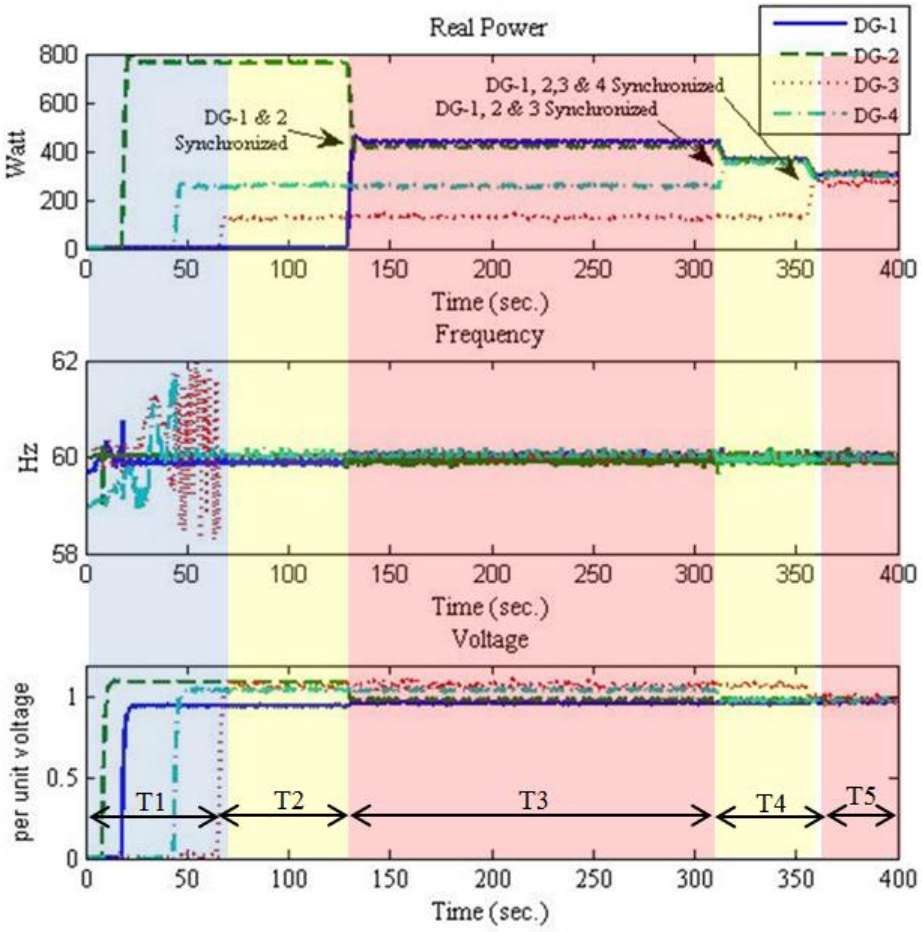

Figure 7.2: Start-up of the DGs and synchronization of the DGs in the Microgrid

www.manaraa.com

7.2 Case 2: Change of load share

One of the important aspects of the Microgrid operation is to share the load among DGs in an appropriate manner. The power sharing ratio could be determined by the ratings of the DGs or by an energy management system (EMS) sitting on top of the hierarchical control of Microgrids. In this study, the performance of changing of load sharing among the DGs under droop control mode was verified. During the duration of T1 in Figure 7.3, the Microgrid was operating in steady state with each DG sharing load almost close to each other. At the end of the duration T1, load shared by DG-1 was decreased to the value which is half of its previous shared load. Consequently, other DGs adjusted their shared load to supply the total demand. A similar change was applied to DG-2 at the end of T2. After the duration of T2, DG-1 and DG-2 were supplying half of the load than the combined load supplied by DG-3 and DG-4. Voltage and frequency of the Microgrid during the whole time remained close to the nominal value without showing significant deviations from the nominal values.

www.manaraa.com

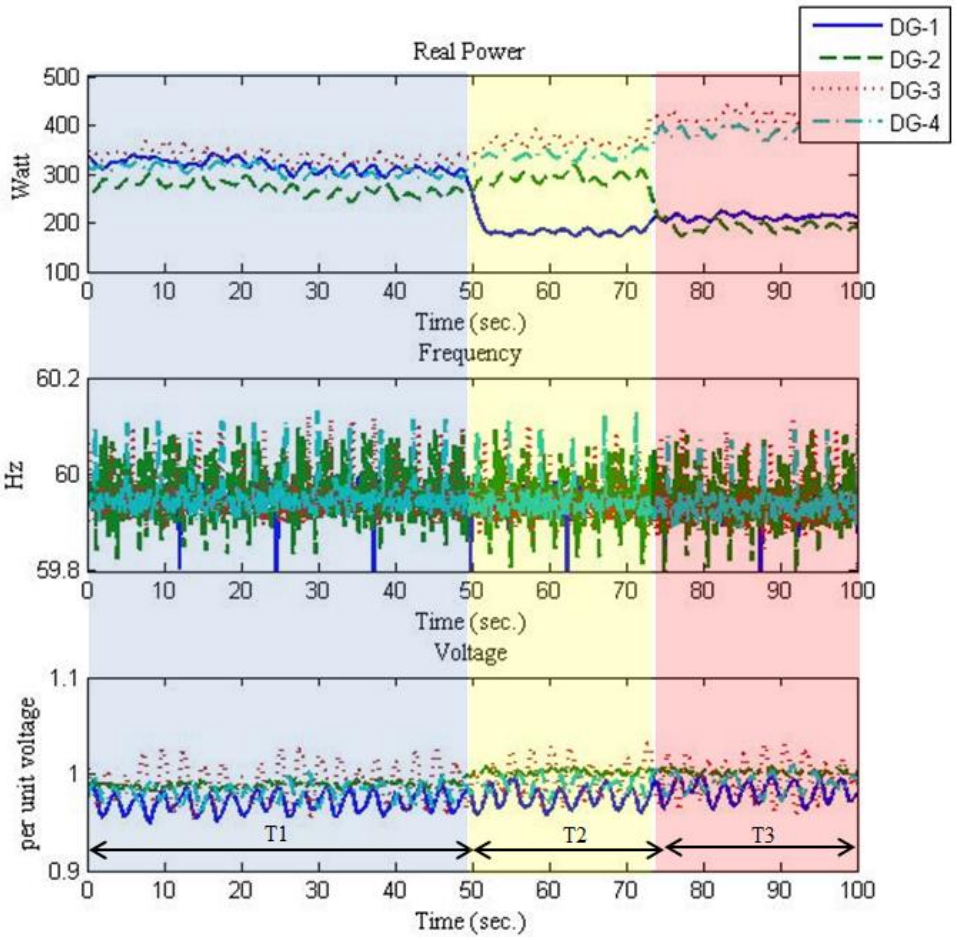

Figure 7.3: Effect of changing the droop parameters

7.3 Case 3: Load dynamics

In this experiment, the performance of the Microgrid under repetitive load changes was studied. During T1, in Figure 7.4, DG-1 and DG-2 were supplying the same load while DG-3 and DG-4 were supplying a slightly different load than DG-1 and DG-2. At the end of T1, the load was suddenly changed to a lower value.

www.manaraa.com

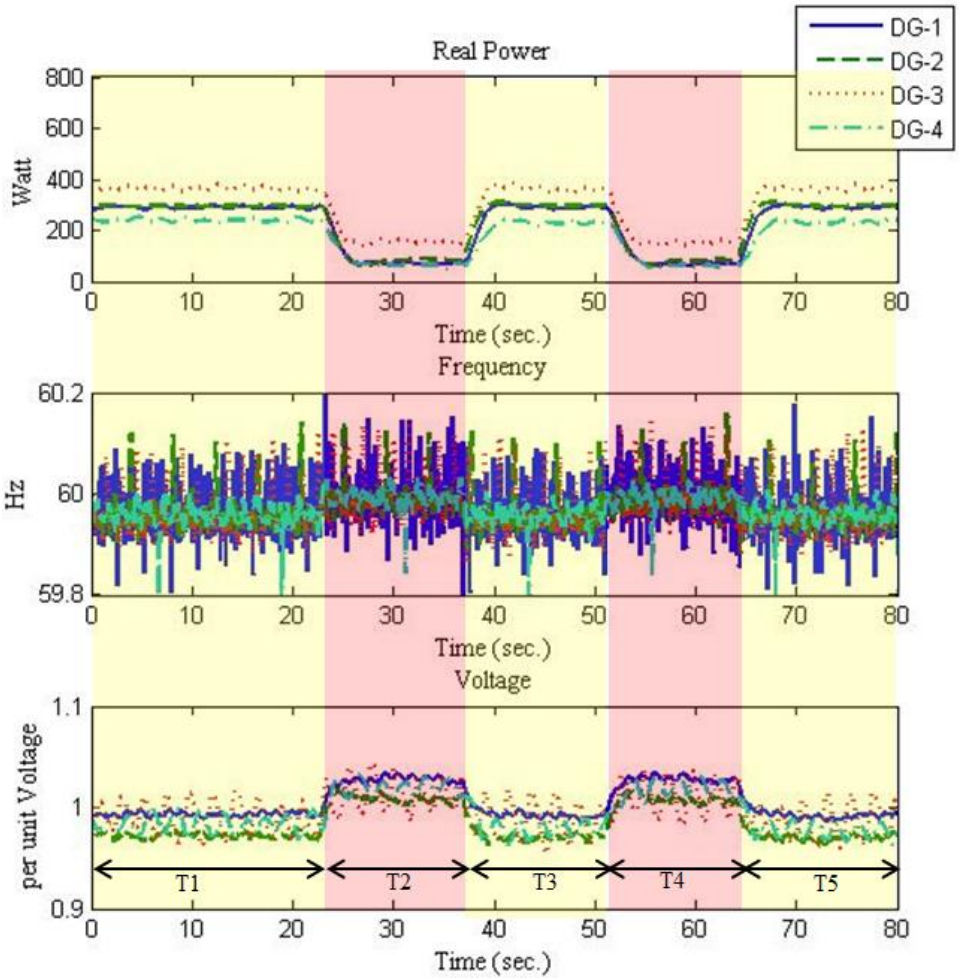

Figure 7.4: Repetitive Load change effects on the microgrid operation

All the DGs simultaneously tracked the load change and reached the steady state position within 2s. As a result of this load change, there was a change in system frequency which moved closer to the nominal value. But as a whole, total deviation of the frequency from nominal value was very low. Same thing can be said for the voltage profile which exhibited some changes after the change in the load but did not deviate from the nominal value too much. The load was brought back to its previous value at the end of T2. Again, all the DGs tracked the load change smoothly and within 2s reached the steady state value. The load was repetitively lowered and raised several times to

www.manaraa.com

verify that the Microgrid can handle such changes. This experiment shows the load tracking capability of the P-MG without significant deviation in the voltage and frequency profiles. Another important observation from this study is that though the load was changed to different values repetitively, the power sharing ratio of the DGs in the microgrid did not change. The DGs successfully tracked the load changes while maintaining their power sharing ratio.

7.4 Case 4: De-synchronization of the DGs

DGs connected in a Microgrid can be disconnected from the system for a variety of reasons. The requirement for disconnection may arise from a fault in the network, loss of prime energy source or simply for maintenance work. Keeping that in mind, the microgrid should be able to disconnect the DGs smoothly without any unacceptable transients. This experiment was designed to see the effect of disconnection of the DGs under various conditions. During T1 in Figure 7.5, the microgrid was running in steady-state with DG1 and DG2 supplying the same load and DG-3 and DG-4 supplying a slightly different load when all the DGs were synchronized together. At the end of T1, DG-3 was disconnected from the system and it was put in a stand-alone mode supplying its own load. It can be seen from the plots that the remaining DGs which were synchronized together adjusted their system frequency and power sharing according to their droop settings in response to the change.

www.manaraa.com

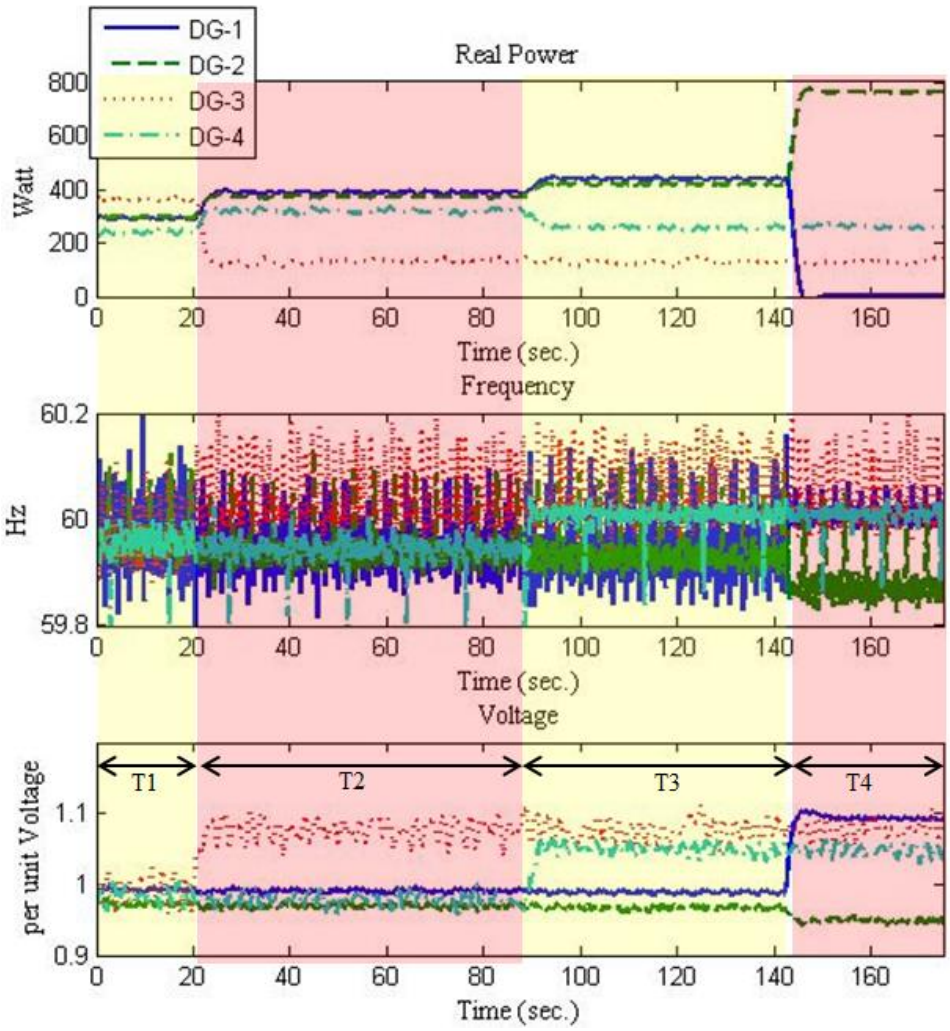

Figure 7.5: De-synchronization of the DGs in P-MG

The voltage of DG-3 was set to 1.07 p.u. in stand-alone mode and its frequency was set to 60Hz. After de-synchronization, the voltage and frequency of DG-3 changed back to the values which were set for the stand-alone mode. After T2, DG-4 was disconnected from the Microgrid and was put in the stand-alone mode supplying its own local load. From that time, the remaining DG-1 and DG-2 running in droop controlled mode started sharing their combined load together. After de-synchronization, the voltage of DG-4 was 1.05 p.u. and frequency was set to 60Hz. Again after T3, DG-1 was disconnected from

www.manaraa.com

the Microgrid. DG-1 does not have its local load, so its output power was reduced to zero, output voltage was 1.08 and output frequency was 60Hz after the de-synchronization. From that point on, DG-2 was supplying the load in droop mode. Hence, there is a frequency deviation coming from the droop setting for DG-2 after T4.

7.5 Case 5: Power network topology Reconfiguration

In a practical microgrid operation, power network topology should be reconfigurable to serve loads from different sources through different power network branches under various conditions. In this experiment, topology reconfiguration was considered which demonstrates the high degree of flexibility and re-configurability of P-MG. Initially the microgrid was running in radial bus formation by opening the switch sLine-01 (Figure 7.1). Duration T1 Figure 7.6 shows the current flowing through line-04 under this radial configuration. The network topology was then changed to a ring bus formation at the end of T1 by closing the switch sLine-01. Both lines Line-01 and Line-04 connect BUS-01 to the system and there is no local load connected to the BUS-01. Hence current through Line-04 was reduced when the topology was changed from radial network to ring bus network formation as some of the power from DG-1 was being delivered through Line-01. This scenario is evident from Figure 7.6 during T2. At this time, current through Line-04 was less than that of the case during T1. At the end of T2, sLine-01 switch was again openned to form the radial network. As a result of this topology change the current through Line-04 increased during T3.

www.manaraa.com

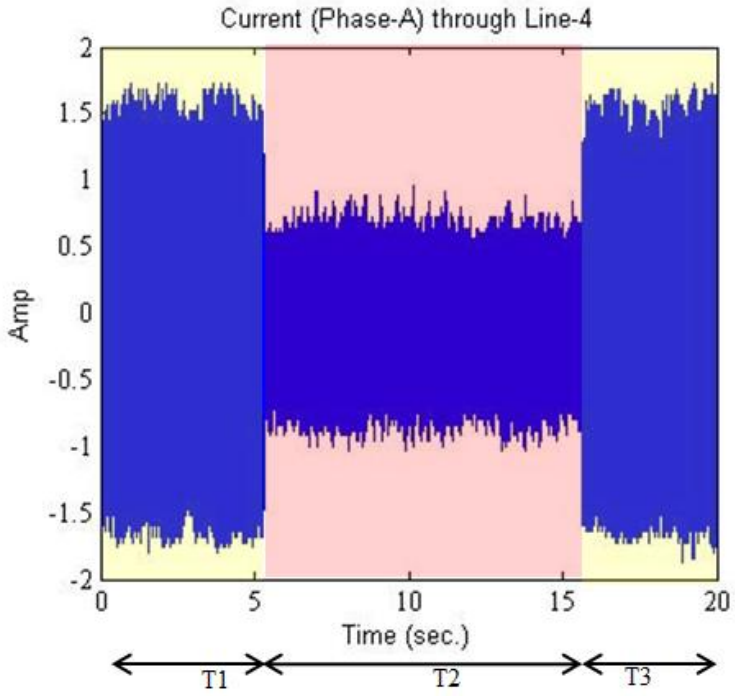

Figure 7.6: Change of current through line 4 for the change of network topology.

www.manaraa.com

Chapter 8

Future work and conclusion

This work reveals the impact of cooperative control strategies on the modernization of future microgrids. Microgrids provide the opportunity to integrate a variety of renewable energy sources and conventional fossil-fuel sources in a local energy network to significantly boost efficiency. Therefore, they have the potential to be the basic core technology that will make up the entire future power grid.

Future Work:

A possible future for a smart power grid, could be the combination of clusters of micro-grids. Many studies have been performed on the stand-alone and grid-tied micro-grids, which prove that these systems tend to work well independently. However, when they are combined to form clusters of micro-grid systems, many unexpected behaviors can occur. Creating a resilient, reliable, and safe smart grid thus requires the capability to test how systems perform and interact prior to deployment in practical operating environments. Realistic test environments can fill this role.

Testbeds are essentially platforms for the demanding and replicable testing of theories, computational tools, new technologies, and systems. The micro-grid testbed

www.manaraa.com

provides a development environment without the potential hazards or consequences present when testing in a real scale production environment. A testbed can be used to demonstrate new components or entire systems, and can include software and hardware /physical equipment as well as networking components.

As mentioned earlier, during this project a laboratory setup for a typical AC/DC microgrid system was developed. Although this setup has been used to study some control aspects and issues related to power management of the microgrid systems, there is still more to investigate. Some of the limitations of the P-MG systems can be summarized as follows:

- Uni-direction power flow between the AC and DC part of the hybrid AC/DC microgrid.
- Grid connectivity has been neglected in this study. Therefore, the system is always operating off the grid.
- The grid size is limited to 4-bus system in both AC and DC system.

Hence, improving these limitations could be the potential tasks for future researchers to be addressed. Additionally, the other aspects of the power grid to be studied are as follows:

i. Islanding in microgrid: In an islanded microgrid operation, DGs continue to power the loads located in the microgrid without requiring to obtain power from the utility grid.

ii. Cyber security analysis: The U.S. Department of Homeland Security (DHS) reports that cyber-attacks on the electric power grid are enormously increasing.

www.manaraa.com

Concern over the possibility of hacking into power grid software and disruption in the electrical supply system is growing because such an attack could be one of the quickest ways to mark irreversible economic and environmental impacts.

iii. Reliability analysis and evaluation of microgrids: For microgrid owners, there are insurers who will cover losses for some types of equipment and systems. But there are currently no insurance policies that will cover the mis-performance of the entire microgrid. That suggests a need to uncover some of the complexities associated with the resilience of microgrids.

iv. Data visualization and management using the phasor measurement units (PMU): Due to recent installation of the PMUs in the power grids, one major component of this research is management and analysis of big data.

v. Construction and development of clusters of microgrids: Development of clusters of microgrids shared between multiple universities and research centers will provide a platform to develop a practical solution for uncertainties, components' failure and cyber-attacks in a typical smart grid.

vi. Stability analysis of microgrid: Stability of microgrid is of paramount interest as microgrids will serve critical loads when employed in real world. Especially the stability is a big concern when several microgrids are connected together to from cluster of microgrid.

vii. Energy storage systems (ESS): ESSs are one of the key components of microgrid operations. In order to effectively manage the intermittent characteristics of RESs, ESSs are required to provide support to the microgrid.

www.manaraa.com

Conclusion

In this study, the performance of droop-based cooperative methodology has been studied and verified through simulation and experiments. These experiments have been done on a standalone AC microgrid, DC microgrid and hybrid AC/DC microgrid systems. The results have proven that the application of the designed methodology provides a promising solution to the realization of the resilient and intelligent microgrids. Since the term "microgrid" has still a vague definition in the vocabulary of power systems engineering and the standards are yet to be fully developed, further improvement of this approach can drive the microgrid evolution one step forward.

www.manaraa.com

References

[1] R. H. Lasseter, "MicroGrids," in *2002 IEEE Power Engineering Society Winter Meeting. Conference Proceedings (Cat. No.02CH37309)*, vol. 1, pp. 305–308, 2002.

[2] S. M. Ashabani and Y. A. I. Mohamed, "New Family of Microgrid Control and Management Strategies in Smart Distribution Grids—Analysis, Comparison and Testing," *IEEE Trans. Power Syst.*, vol. 29, no. 5, pp. 2257–2269, Sep. 2014.

[3] A. Kwasinski, "Quantitative Evaluation of DC Microgrids Availability: Effects of System Architecture and Converter Topology Design Choices," *IEEE Trans. Power Electron.*, vol. 26, no. 3, pp. 835–851, Mar. 2011.

[4] T. Dragicevic, J. C. Vasquez, J. M. Guerrero, and D. Skrlec, "Advanced LVDC Electrical Power Architectures and Microgrids: A step toward a new generation of power distribution networks.," *IEEE Electrif. Mag.*, vol. 2, no. 1, pp. 54–65, Mar. 2014.

[5] S. Anand and B. G. Fernandes, "Optimal voltage level for DC microgrids," in *IECON - 36th Annual Conference on IEEE Industrial Electronics Society*, 2010, pp. 3034–3039, *2010*.

[6] J.-D. Park and J. Candelaria, "Fault Detection and Isolation in Low-Voltage DC-Bus Microgrid System," *IEEE Trans. Power Deliv.*, vol. 28, no. 2, pp. 779–787, Apr. 2013.

www.manaraa.com

[7] R. Salcedo, A. Bokhari, M. Diaz-Aguilo, N. Lin, T. Hong, F. de Leon, D. Czarkowski, S. Flank, A. McDonnell, and R. E. Uosef, "Benefits of a Nonsynchronous Microgrid on Dense-Load LV Secondary Networks," *IEEE Trans. Power Deliv.*, vol. 31, no. 3, pp. 1076–1084, Jun. 2016.

[8] P. C. Loh and F. Blaabjerg, "Autonomous operation of hybrid microgrid with AC and DC sub-grids," pp. 1–10.

[9] X. Liu, P. Wang, and P. C. Loh, "A Hybrid AC/DC Microgrid and Its Coordination Control," *IEEE Trans. Smart Grid*, vol. 2, no. 2, pp. 278–286, Jun. 2011.

[10] T.-P. Chen, "Zero-Sequence Circulating Current Reduction Method for Parallel HEPWM Inverters Between AC Bus and DC Bus," *IEEE Trans. Ind. Electron.*, vol. 59, no. 1, pp. 290–300, Jan. 2012.

[11] Z. Jiang and Xunwei Yu, "Power electronics interfaces for hybrid DC and AC-linked microgrids," in *2009 IEEE 6th International Power Electronics and Motion Control Conference*, 2009, pp. 730–736.

[12] J. M. Guerrero, J. C. Vasquez, J. Matas, L. G. de Vicuna, and M. Castilla, "Hierarchical Control of Droop-Controlled AC and DC Microgrids—A General Approach Toward Standardization," *IEEE Trans. Ind. Electron.*, vol. 58, no. 1, pp. 158–172, Jan. 2011.

[13] V. Nasirian, S. Moayedi, A. Davoudi, and F. L. Lewis, "Distributed Cooperative Control of DC Microgrids," *IEEE Trans. Power Electron.*, vol. 30, no. 4, pp. 2288–2303, Apr. 2015.

المنارة للاستشارات
www.manaraa.com

[14] S. Anand and B. G. Fernandes, "Optimal voltage level for DC microgrids," in *IECON 2010 - 36th Annual Conference on IEEE Industrial Electronics Society*, 2010, pp. 3034–3039.

[15] S. Anand, B. G. Fernandes, and J. Guerrero, "Distributed Control to Ensure Proportional Load Sharing and Improve Voltage Regulation in Low-Voltage DC Microgrids," *IEEE Trans. Power Electron.*, vol. 28, no. 4, pp. 1900–1913, Apr. 2013.

[16] K. Mets, T. Verschueren, F. De Turck, and C. Develder, "Exploiting V2G to optimize residential energy consumption with electrical vehicle (dis)charging," in *2011 IEEE First International Workshop on Smart Grid Modeling and Simulation (SGMS)*, 2011, pp. 7–12.

[17] R. Yu, J. Ding, W. Zhong, Y. Liu, and S. Xie, "PHEV Charging and Discharging Cooperation in V2G Networks: A Coalition Game Approach," *IEEE Internet Things J.*, vol. 1, no. 6, pp. 578–589, Dec. 2014.

[18] S. W. Hadley, "Evaluating the impact of Plug-in Hybrid Electric Vehicles on regional electricity supplies," in *2007 iREP Symposium - Bulk Power System Dynamics and Control - VII. Revitalizing Operational Reliability*, 2007, pp. 1–12.

[19] T. Ma, S. Member, and O. A. Mohammed, "Optimal Charging of Plug-in Electric Vehicles for a Car-Park Infrastructure," vol. 50, no. 4, pp. 2323–2330, 2014.

[20] C. Chen and S. Duan, "Optimal Integration of Plug-In Hybrid Electric Vehicles in Microgrids," *IEEE Trans. Ind. Informatics*, vol. 10, no. 3, pp. 1917–1926, Aug. 2014.

www.manaraa.com

[21] V. Nasirian, A. Davoudi, F. L. Lewis, and J. M. Guerrero, "Distributed Adaptive Droop Control for DC Distribution Systems," *IEEE Trans. Energy Convers.*, vol. 29, no. 4, pp. 944–956, Dec. 2014.

[22] S. Bashash, S. J. Moura, J. C. Forman, and H. K. Fathy, "Plug-in hybrid electric vehicle charge pattern optimization for energy cost and battery longevity," *J. Power Sources*, vol. 196, no. 1, pp. 541–549, Jan. 2011.

[23] S. Chen, T. Mount, and L. Tong, "Optimizing Operations for Large Scale Charging of Electric Vehicles," in *2013 46th Hawaii International Conference on System Sciences*, 2013, pp. 2319–2326.

[24] W. Su and M.-Y. Chow, "Performance evaluation of a PHEV parking station using Particle Swarm Optimization," in *2011 IEEE Power and Energy Society General Meeting*, 2011, pp. 1–6.

[25] Y. Gu, X. Xiang, W. Li, and X. He, "Mode-Adaptive Decentralized Control for Renewable DC Microgrid With Enhanced Reliability and Flexibility," *IEEE Trans. Power Electron.*, vol. 29, no. 9, pp. 5072–5080, Sep. 2014.

[26] X. Lu, K. Sun, J. M. Guerrero, J. C. Vasquez, and L. Huang, "Double-Quadrant State-of-Charge-Based Droop Control Method for Distributed Energy Storage Systems in Autonomous DC Microgrids," *IEEE Trans. Smart Grid*, vol. 6, no. 1, pp. 147–157, Jan. 2015.

[27] N. Rahbari-Asr and M.-Y. Chow, "Cooperative Distributed Demand Management for Community Charging of PHEV/PEVs Based on KKT Conditions and Consensus Networks," *IEEE Trans. Ind. Informatics*, vol. PP, no. 3, pp. 1–1, 2014.

www.manaraa.com

[28] D. C. Link, V. Sensing, P. Goli, S. Member, W. Shireen, and S. Member, "PV Integrated Smart Charging of PHEVs Based on," vol. 5, no. 3, pp. 1421–1428, 2014.

[29] Y. Xu, "Optimal Distributed Charging Rate Control of Plug-In Electric Vehicles for Demand Management," *IEEE Trans. Power Syst.*, vol. PP, no. 99, pp. 1–10, 2014.

[30] X. Lu, J. M. Guerrero, K. Sun, J. C. Vasquez, R. Teodorescu, and L. Huang, "Hierarchical Control of Parallel AC-DC Converter Interfaces for Hybrid Microgrids," *IEEE Trans. Smart Grid*, vol. 5, no. 2, pp. 683–692, Mar. 2014.

[31] J. M. Carrasco, L. G. Franquelo, J. T. Bialasiewicz, E. Galvan, R. C. PortilloGuisado, M. A. M. Prats, J. I. Leon, and N. Moreno-Alfonso, "Power-Electronic Systems for the Grid Integration of Renewable Energy Sources: A Survey," *IEEE Trans. Ind. Electron.*, vol. 53, no. 4, pp. 1002–1016, Jun. 2006.

[32] B. S. Hartono and R. Setiabudy, "Review of microgrid technology," in *2013 International Conference on QiR*, 2013, pp. 127–132.

[33] F. Blaabjerg, Z. Chen, and S. B. Kjaer, "Power Electronics as Efficient Interface in Dispersed Power Generation Systems," *IEEE Trans. Power Electron.*, vol. 19, no. 5, pp. 1184–1194, Sep. 2004.

[34] A. P. Martins, A. S. Carvalho, and A. S. Araujo, "Design and implementation of a current controller for the parallel operation of standard UPSs," in *Proceedings of IECON '95 - 21st Annual Conference on IEEE Industrial Electronics*, 1995, vol. 1, pp. 584–589.

www.manaraa.com

[35] R. A. Kaushik and N. M. Pindoriya, "Power flow control of hybrid AC-DC microgrid using master-slave technique," in *2014 IEEE Conference on Energy Conversion (CENCON)*, 2014, pp. 389–394.

[36] S. T. Cady, A. D. Dominguez-Garcia, and C. N. Hadjicostis, "A Distributed Generation Control Architecture for Islanded AC Microgrids," *IEEE Trans. Control Syst. Technol.*, vol. PP, no. 99, pp. 1–1, 2015.

[37] F. Katiraei and M. R. Iravani, "Power Management Strategies for a Microgrid With Multiple Distributed Generation Units," *IEEE Trans. Power Syst.*, vol. 21, no. 4, pp. 1821–1831, Nov. 2006.

[38] A. G. Tsikalakis and N. D. Hatziargyriou, "Centralized Control for Optimizing Microgrids Operation," *IEEE Trans. Energy Convers.*, vol. 23, no. 1, pp. 241–248, Mar. 2008.

[39] A. N. Venkat, I. A. Hiskens, J. B. Rawlings, and S. J. Wright, "Distributed MPC Strategies With Application to Power System Automatic Generation Control," *IEEE Trans. Control Syst. Technol.*, vol. 16, no. 6, pp. 1192–1206, Nov. 2008.

[40] S. Bolognani and S. Zampieri, "A Distributed Control Strategy for Reactive Power Compensation in Smart Microgrids," *IEEE Trans. Automat. Contr.*, vol. 58, no. 11, pp. 2818–2833, Nov. 2013.

[41] A. Bidram and A. Davoudi, "Hierarchical Structure of Microgrids Control System," *IEEE Trans. Smart Grid*, vol. 3, no. 4, pp. 1963–1976, Dec. 2012.

www.manaraa.com

[42] S. Liu, X. Wang, and P. X. Liu, "Impact of Communication Delays on Secondary Frequency Control in an Islanded Microgrid," *IEEE Trans. Ind. Electron.*, vol. 62, no. 4, pp. 2021–2031, Apr. 2015.

[43] M. Savaghebi, A. Jalilian, J. C. Vasquez, and J. M. Guerrero, "Secondary Control Scheme for Voltage Unbalance Compensation in an Islanded Droop-Controlled Microgrid," *IEEE Trans. Smart Grid*, vol. 3, no. 2, pp. 797–807, Jun. 2012.

[44] B. Dong, Y. Li, Z. Zheng, and L. Xu, "Control strategies of microgrid with Hybrid DC and AC Buses," in *Power Electronics and Applications (EPE 2011), Proceedings of the 2011-14th European Conference on*, 2011, pp. 1–8.

[45] P. Wang, S. Member, C. Jin, D. Zhu, S. Member, Y. Tang, P. C. Loh, and F. H. Choo, "Distributed Control for Autonomous Operation of a Three-Port AC / DC / DS Hybrid Microgrid," vol. 62, no. 2, pp. 1279–1290, 2015.

[46] N. Eghtedarpour and E. Farjah, "Power control and management in a Hybrid AC/DC microgrid," *IEEE Trans. Smart Grid*, vol. 5, no. 3, pp. 1494–1505, 2014.

[47] P. C. Loh, D. Li, Y. K. Chai, and F. Blaabjerg, "Autonomous control of interlinking converter with energy storage in hybrid AC-DC microgrid," *IEEE Trans. Ind. Appl.*, vol. 49, no. 3, pp. 1374–1382, 2013.

[48] C. Wang, X. Li, L. Guo, and Y. W. Li, "A nonlinear-disturbance-observer-based DC-Bus voltage control for a hybrid AC/DC microgrid," *IEEE Trans. Power Electron.*, vol. 29, no. 11, pp. 6162–6177, 2014.

www.manaraa.com

[49] T. S. Ustun, C. Ozansoy, and A. Zayegh, "Recent developments in microgrids and example cases around the world—A review," *Renew. Sustain. Energy Rev.*, vol. 15, no. 8, pp. 4030–4041, Oct. 2011.

[50] C. E. Commission, "Certs microgrid laboratory test bed," *Energy*, vol. 26, no. February, pp. 1–8, 2009.

[51] L. Meng, A. Luna, E. Diaz, B. Sun, T. Dragicevic, M. Savaghebi, J. Vasquez, J. Guerrero, and M. Graells, "Flexible System Integration and Advanced Hierarchical Control Architectures in the Microgrid Research Laboratory of Aalborg University," *IEEE Trans. Ind. Appl.*, vol. 52, no. 2, pp. 1–1, 2015.

[52] B. Zhao, X. Zhang, and J. Chen, "Integrated microgrid laboratory system," *IEEE Trans. Power Syst.*, vol. 27, no. 4, pp. 2175–2185, 2012.

[53] V. Salehi, A. Mohamed, A. Mazloomzadeh, and O. A. Mohammed, "Laboratory-based smart power system, part I: Design and system development," *IEEE Trans. Smart Grid*, vol. 3, no. 3, pp. 1394–1404, 2012.

[54] C. Wang, X. Yang, Z. Wu, Y. Che, L. Guo, S. Zhang, and Y. Liu, "A Highly Integrated and Reconfigurable Microgrid Testbed with Hybrid Distributed Energy Sources," *IEEE Trans. Smart Grid*, vol. 7, no. 1, pp. 451–459, 2014.

[55] S. S. Thale, R. G. Wandhare, and V. Agarwal, "A Novel Reconfigurable Microgrid Architecture With Renewable Energy Sources and Storage," *IEEE Trans. Ind. Appl.*, vol. 51, no. 2, pp. 1805–1816, 2015.

www.manaraa.com

[56] G. Turner, J. P. Kelley, C. L. Storm, D. A. Wetz, and W. J. Lee, "Design and active control of a microgrid testbed," *IEEE Trans. Smart Grid*, vol. 6, no. 1, pp. 73–81, 2015.

[57] F. Guo, L. Herrera, M. Alsolami, H. Li, P. Xu, X. Lu, A. Lang, J. Wang, and Z. Long, "Design and development of a reconfigurable hybrid Microgrid testbed," in *2013 IEEE Energy Conversion Congress and Exposition*, 2013, pp. 1350–1356.

[58] A. Vukojevic, S. Laval, and J. Handley, "An integrated utility microgrid test site ecosystem optimized by an open interoperable distributed intelligence platform," in *2015 IEEE Power & Energy Society Innovative Smart Grid Technologies Conference (ISGT)*, 2015, pp. 1–5.

[59] S. Bracco, F. Delfino, F. Pampararo, M. Robba, and M. Rossi, "The University of Genoa smart polygeneration microgrid test-bed facility: The overall system, the technologies and the research challenges," *Renew. Sustain. Energy Rev.*, vol. 18, pp. 442–459, Feb. 2013.

[60] D. De and S. K. Das, "A wireless smart grid testbed in lab," *IEEE Wirel. Commun.*, vol. 19, no. 3, pp. 58–64, Jun. 2012.

[61] R. Olfati-Saber, J. A. Fax, and R. M. Murray, "Consensus and Cooperation in Networked Multi-Agent Systems," *Proc. IEEE*, vol. 95, no. 1, pp. 215–233, Jan. 2007.

[62] N. Rotering and M. Ilic, "Optimal Charge Control of Plug-In Hybrid Electric Vehicles in Deregulated Electricity Markets," *IEEE Trans. Power Syst.*, vol. 26, no. 3, pp. 1021–1029, Aug. 2011.

www.manaraa.com

[63] J. Kim, J. M. Guerrero, P. Rodriguez, R. Teodorescu, and K. Nam, "Mode adaptive droop control with virtual output impedances for an inverter-based flexible AC microgrid," *IEEE Trans. Power Electron.*, vol. 26, no. 3, pp. 689–701, Mar. 2011.

[64] R. Majumder, G. Ledwich, A. Ghosh, S. Chakrabarti, and F. Zare, "Droop Control of Converter-Interfaced Microsources in Rural Distributed Generation," *IEEE Trans. Power Deliv.*, vol. 25, no. 4, pp. 2768–2778, Oct. 2010.

[65] S. M. Ashabani and Y. A.-R. I. Mohamed, "General Interface for Power Management of Micro-Grids Using Nonlinear Cooperative Droop Control," *IEEE Trans. Power Syst.*, vol. 28, no. 3, pp. 2929–2941, Aug. 2013.

[66] Y. Mohamed and E. F. El-Saadany, "Adaptive Decentralized Droop Controller to Preserve Power Sharing Stability of Paralleled Inverters in Distributed Generation Microgrids," *IEEE Trans. Power Electron.*, vol. 23, no. 6, pp. 2806–2816, Nov. 2008.

[67] R. Majumder, A. Ghosh, G. Ledwich, and F. Zare, "Angle droop versus frequency droop in a voltage source converter based autonomous microgrid," in *2009 IEEE Power & Energy Society General Meeting*, 2009, pp. 1–8.

[68] N. Pogaku, M. Prodanovic, and T. C. Green, "Modeling, Analysis and Testing of Autonomous Operation of an Inverter-Based Microgrid," *IEEE Trans. Power Electron.*, vol. 22, no. 2, pp. 613–625, Mar. 2007.

www.manaraa.com

[69] A. Bidram, A. Davoudi, F. L. Lewis, and J. M. Guerrero, "Distributed Cooperative Secondary Control of Microgrids Using Feedback Linearization," *IEEE Trans. Power Syst.*, vol. 28, no. 3, pp. 3462–3470, Aug. 2013.

[70] L. Che, M. Shahidehpour, A. Alabdulwahab, and Y. Al-Turki, "Hierarchical Coordination of a Community Microgrid With AC and DC Microgrids," *IEEE Trans. Smart Grid*, vol. PP, no. 99, pp. 1–1, 2015.

[71] V. Nasirian, Q. Shafiee, J. M. Guerrero, F. L. Lewis, and A. Davoudi, "Droop-Free Distributed Control for AC Microgrids," *IEEE Trans. Power Electron.*, vol. 31, no. 2, pp. 1600–1617, 2016.

[72] "DC Power Supply Products - High Voltage and High Current | Magna-Power." [Online]. Available: http://www.magna-power.com/products. [Accessed: 18-May-2016].

[73] "XDC 6000 Watt and 12000 Watt Series Digital Programmable DC Power Supply."[Online].Available:http://www.programmablepower.com/products/XDC/downloads/XDC_6kW_12kW_User_Guide_XDOP-01XN.pdf. [Accessed: 18-May-2016].

[74] "Programmable AC Power Source Model 61511/61512/61611/61612 ." [Online]. Available: http://www.chromausa.com/pdf/Br-61611+61612-acsource-022011.pdf. [Accessed: 18-May-2016].

[75] A. Koran and K. Sano, "Design of a Photovoltaic Simulator With a Novel Reference Signal Generator and Two-Stage LC Output Filter," *IEEE Trans. Power Electron.*, vol. 25, no. 5, pp. 1331–1338, May 2010.

www.manaraa.com

[76] Qingrong Zeng, Pinggang Song, and Liuchen Chang, "A photovoltaic simulator based on DC chopper," in *IEEE CCECE2002. Canadian Conference on Electrical and Computer Engineering. Conference Proceedings (Cat. No.02CH37373)*, 2002, vol. 1, pp. 257–261.

[77] M. Park and I.-K. Yu, "A Novel Real-Time Simulation Technique of Photovoltaic Generation Systems Using RTDS," *IEEE Trans. Energy Convers.*, vol. 19, no. 1, pp. 164–169, Mar. 2004.

[78] E. Koutroulis, K. Kalaitzakis, and V. Tzitzilonis, "Development of an FPGA-based System for Real-Time Simulation of Photovoltaic Modules," in *Seventeenth IEEE International Workshop on Rapid System Prototyping (RSP'06)*, 2006, pp. 200–208.

[79] M. G. Villalva, J. R. Gazoli, and E. R. Filho, "Comprehensive Approach to Modeling and Simulation of Photovoltaic Arrays," *IEEE Trans. Power Electron.*, vol. 24, no. 5, pp. 1198–1208, May 2009.

[80] S. Farag, C. Lerman, S. Lineykin, and A. Kuperman, "Off-the-shelf-Power-Supply-based Battery-Supercapacitor Emulator for Charger Functionality Testing," *IEEE Trans. Transp. Electrif.*, vol. 2, no. 99, pp. 1–1, 2016.

[81] T. Kim and W. Qiao, "A Hybrid Battery Model Capable of Capturing Dynamic Circuit Characteristics and Nonlinear Capacity Effects," *IEEE Trans. Energy Convers.*, vol. 26, no. 4, pp. 1172–1180, Dec. 2011.

www.manaraa.com

[82] K. Nguyen-Duy, A. Knott, and M. A. E. Andersen, "High Dynamic Performance Nonlinear Source Emulator," *IEEE Trans. Power Electron.*, vol. 31, no. 3, pp. 2562–2574, Mar. 2016.

[83] L. H.-W. L. J.-G. K. S.-H. S. Eun-Kyung, "Implementation of Fuel Cell Dynamic Simulator," in *37th IEEE Power Electronics Specialists Conference*, 2006, pp. 1–5.

[84] linkchain. t. co., "Chroma ATE Inc. | English," Jan. 2012.

[85] "SEMIKRON Online Shop | SEMITEACH B6U+E1CIF+B6CI | Buy Power Modules online!" [Online]. Available: http://shop.semikron.com/en/Products-and-Shop/Product-Groups/STACKs/SEMITEACH/SEMITEACH-B6U-E1CIF-B6CI.html. [Accessed: 19-May-2016].

[86] K. Jalili and S. Bernet, "Design of LCL Filters of Active-Front-End Two-Level Voltage-Source Converters," *IEEE Trans. Ind. Electron.*, vol. 56, no. 5, pp. 1674–1689, May 2009.

[87] A. Reznik, M. G. Simoes, A. Al-Durra, and S. M. Muyeen, "LCL Filter design and performance analysis for grid-interconnected systems," *IEEE Trans. Ind. Appl.*, vol. 50, no. 2, pp. 1225–1232, 2014.

[88] "Jantzen Audio 1.0mH 18 AWG Air Core Inductor Crossover Coil." [Online]. Available: http://www.parts-express.com/jantzen-audio-10mh-18-awg-air-core-inductor-crossover-coil--255-250. [Accessed: 19-May-2016].

www.manaraa.com

[89] X. Yang, S. P. Carullo, K. Miu, and C. O. Nwankpa, "Reconfigurable Distribution Automation and Control Laboratory: Multiphase, Radial Power Flow Experiment," *IEEE Trans. Power Syst.*, vol. 20, no. 3, pp. 1207–1214, Aug. 2005.

[90] "PROGRAMMABLE AC&DC ELECTRONIC LOAD MODEL 63800 SERIES." [Online]. Available: http://www.chromausa.com/pdf/63800-E.pdf. [Accessed: 02-May-2016].

[91] "DS1103 PPC Controller Board Powerful controller board for rapid control prototyping."[Online].Available:https://www.dspace.com/shared/data/pdf/2014/DS1103.pdf. [Accessed: 03-May-2016].

[92] "LEM Website - Search ."[Online]. Available: http://www. lem. com/hq/en/ component/ option,com_catalog/ task,displaymodel/id,90.08.19.000.0/. [Accessed: 03-May-2016].

[93] "LEM Website - Search." [Online]. Available: http://www.lem.com/ hq/en/component/ option,com_catalog/ task,displaymodel/ id,90.27.19.000.0/ [Accessed: 03-May-2016].

[94] "NI PCI-6024E (Legacy) - National Instruments." [Online]. Available: http://sine.ni.com/nips/cds/view/p/lang/en/nid/10968. [Accessed: 04-May-2016].

[95] "LabVIEW System Design Software - National Instruments." [Online]. Available: http://www.ni.com/labview/. [Accessed: 04-May-2016].

www.manaraa.com

[96] "Software, Drivers, Manuals for Programmable DC Power Supplies | Magna-Power." [Online]. Available: http://www.magna-power.com/support/download-center. [Accessed: 04-May-2016].

[97] "Chroma ATE chr616xx Power Supply - IEEE 488.2 (GPIB) Driver for LabVIEW - National Instruments." [Online]. Available: http://sine.ni.com/apps/utf8/niid_web_display.download_page?p_id_guid=E3B19B3E9172659CE034080020E74861. [Accessed: 04-May-2016].

[98] "ControlDesk Next Generation - dSPACE." [Online]. Available: https://www.dspace.com/en/inc/home/products/sw/experimentandvisualization/controldesk.cfm. [Accessed: 04-May-2016].

[99] T. Dragiˇ and J. M. Guerrero, "DC Microgrids — Part II : A Review of Power Architectures , Applications , and," *IEEE Trans. Power Electron.*, vol. 31, no. 5, pp. 3528–3549, 2016.

[100] G. Pepermans, J. Driesen, D. Haeseldonckx, R. Belmans, and W. D'haeseleer, "Distributed generation: definition, benefits and issues," *Energy Policy*, vol. 33, no. 6, pp. 787–798, Apr. 2005.

[101] T. C. Green and M. Prodanović, "Control of inverter-based micro-grids," *Electr. Power Syst. Res.*, vol. 77, no. 9, pp. 1204–1213, Jul. 2007.

[102] "IEEE Std 1547.4-2011," *IEEE Std 1547.4-2011*. pp. 1–54, 2011.

www.manaraa.com

[103] J. Rocabert, A. Luna, F. Blaabjerg, and P. Rodríguez, "Control of Power Converters in AC Microgrids," *IEEE Trans. Power Electron.*, vol. 27, no. 11, pp. 4734–4749, Nov. 2012.

[104] P. Piagi and R. H. Lasseter, "Autonomous control of microgrids," *2006 IEEE Power Eng. Soc. Gen. Meet.*, no. June, p. 8 pp., 2006.

[105] T. L. Vandoorn, B. Meersman, and L. Vandevelde, "Transition From Islanded to Grid-Connected Mode of Microgrids With Voltage-Based Droop Control," *IEEE Trans. Power Syst.*, vol. 28, no. 3, pp. 2545–2553, Aug. 2013.

www.manaraa.com